2006

The Roles of daf-6 and Cell-Cell Interactions in Sensory Organ Morphogenesis

Elliot A. Perens

THE ROLES OF *daf-6* AND CELL-CELL INTERACTIONS IN SENSORY ORGAN MORPHOGENESIS

A Thesis Presented to the Faculty of

The Rockefeller University

in Partial Fulfillment of the Requirements for

the degree of Doctor of Philosophy

by

Elliot A. Perens

June 2006

Abstract

The roles of *daf-6* and cell-cell interactions in sensory organ morphogenesis

Elliot A. Perens, PhD.
The Rockefeller University 2006

The development of multicellular organs depends on the regulation of cell shape, position, and orientation. The genetic regulation of these morphogenetic processes is poorly understood. As a model for organ morphogenesis, I studied the development of the *Caenorhabditis elegans* amphid sensory organ. Sensory organs in diverse species are often composed of neuronal sensory endings accommodated in a lumen formed by ensheathing epithelia or glia. The generation of this structure may require cell-autonomous factors that control lumen formation, as well as cell non-autonomous factors that coordinate the morphogenesis of the lumen with the resident neuronal processes. Understanding these processes would provide insight into lumen formation, glia morphogenesis, and cell-cell interactions during development, especially neuronal regulation of glia morphogenesis.

In this thesis, I identify and characterize genes required for lumen formation in the amphid sensory organ. First, the gene *daf-6* is required cell autonomously during amphid lumen formation. *daf-6* encodes a Patched-related protein that is a member of a previously uncharacterized sub-family of sterol-sensing domain containing proteins. Interestingly, *daf-6* is expressed and required in several tubular structures, such as the excretory system and vulva. Thus, a similar genetic pathway is required for the formation of different lumens. Secondly, I conducted a forward genetic screen and identified and characterized mutations that suppress the lumen formation defects in *daf-6* mutants. Finally,

by examining mutants defective in sensory neuron process formation, I showed that amphid lumen shape is determined by its resident sensory endings.

Acknowledgements

First I must thank my graduate advisor Shai Shaham. Shai provided help, input, and advice on all aspects of my graduate work. At the same time he respected my input and demonstrated great patience. He shared his vast scientific knowledge, especially his encyclopedic *C. elegans* knowledge, and perhaps more importantly, his appreciation and enthusiasm for science.

I've been grateful and honored to have my thesis committee members- Drs. Kathryn Anderson, Mary Beth Hatten, Oliver Hobert, and Hermann Steller- provide their time and insight during the completion of this thesis. Also, the administrative staffs in the Rockefeller Dean's office and the MD-PhD program (especially Dr. Olaf Andersen) have been very helpful guiding me through bureaucratic issues, both real and imagined.

I thank the students and post-docs of the Shaham lab- Carine, Carl, Grigorios, Margherita, Mary, Max, Maya, Satoshi, and Taulant- as well as the early days Shaham lab north rotation students- Graeme, Kenta, Erica, Beth, and Kevin. I must especially thank our outstanding tech's Allison, Angelo, Dana, and Limor, as well as our lab aide Sharon. They did a great job of keeping the lab running smoothly at all times.

Several people provided help in completing the work for this thesis. There were numerous members of the "*daf-6* Electron Microscopy Consortium" and I especially thank Erika Hartwieg and Yun Lu. Also, each chapter had a spark provided by others at the work's initiation; so thanks to Mark Schroeder (Chapter 2), Simi Hinden (Chapter 3), and Kenta Asahina (Appendix I).

I also need to thank some early teachers- Yip, Wayne #2, Sally, Kupperman, Jon, Jeremy, Emily, DYS, Debbie, Wayne #1, Renee, Paul, Nancy, Kate, Garriga, Fred, and Dianne.

Thank-you to my parents and bro.

And finally, thanks to the worms.

Table of Contents

LIST OF FIGURES

LIST OF TABLES

Chapter 1

Introduction

Sensory Organ Morphogenesis:
Lumen Formation, Neuron-Glia Interactions, and Sterol-Sensing Domain Containing Proteins

Elliot A. Perens

The development of complex multicellular organs depends on several coordinated phenomena. Cell division and growth determines the number and size of individual cells; differentiation generates diverse cell types; and morphogenesis controls the shape, position, and orientation of cells.

The genetic regulation of morphogenesis is poorly understood. To gain insight into organ morphogenesis, I have been studying the development of sensory organs. Sensory organs sit at the interface between the environment and cognition. Advances in molecular genetics and electrophysiology have provided insight into sensory organ function. For example, receptors and ion channels mediating olfaction, taste, hearing, and thermosensation have been cloned (Corey et al., 2004; Mombaerts, 1999; Montell, 2003; Scott, 2005). Also, studies in experimental organisms have provided insight into sensory neuron development; factors that control their differentiation and generate their specialized sensory endings have been isolated (Scholey et al., 2004; Schweisguth et al., 1996). Less, however, is known about sensory organ morphogenesis.

Sensory organs from diverse species share certain morphological features. In most cases, a sensory neuron or group of sensory neurons extend their specialized dendritic ending through a lumen formed by closely associated glia or ensheathing epithelia (Figure 1.1). Because factors controlling sensory organ function and differentiation have been conserved throughout evolution, genes required for sensory organ morphogenesis are likely to be conserved as well.

Importantly, understanding sensory organ morphogenesis will provide insight not only into sensory organ morphogenesis, but also into numerous basic morphogenesis paradigms. Sensory organ glia or ensheathing epithelia cells form a lumen for the sensory neuron dendrites. Lumens are a fundamental

component of most organ systems, so understanding this aspect of sensory organ formation may provide insight into a general feature of most organs systems. Secondly, the morphology of this lumen is physically coupled to the shape of the sensory endings that reside in it. Presumably, the morphogenesis of these two cell types is coordinated. Coupling the shapes of different cell types is a fundamental concept during organogenesis. Thus, understanding this aspect of sensory organ morphogenesis may provide insight into cell-to-cell communication during organ morphogenesis. Finally, and more specifically, sensory organs, like other parts of the peripheral and central nervous systems, are composed of neurons and glia. Thus understanding sensory organ morphogenesis may provide insight into glia morphogenesis and neuron-glia interactions during development.

In this thesis, I identify and characterize several genes, including a sterol-sensing domain containing gene, involved in sensory organ lumen morphogenesis and demonstrate a role for sensory neuron processes in regulating glia morphogenesis. In this chapter, I will first review sensory organ morphologies in different species. Then I will review several components of sensory organ morphogenesis identified in this thesis: lumen formation, neuronal regulation of glia morphogenesis, and sterol-sensing domain containing genes.

A Comparative Analysis of Sensory Organ Morphologies

Sensory organs in different species share a common structure. A sensory neuron dendrite extends through a lumen generated by specialized glia or ensheathing epithelia (Figure 1.1). Here I will review the structure and

development of sensory organs from three species- *Caenorhabditis elegans*, *Drosophila melanogaster*, and humans. In particular I will focus on mechanosensation and chemosensory organs.

C. elegans Sensory Organ Stucture

The nematode *C. elegans* contains six types of sensory organs. All six types of sensory organs share a basic structure- one or more sensory neurons extend the ciliated ending of its dendrite into or through a lumen generated by two ensheathing glia cells (Figure 1.1A) (Ward et al., 1975). The two bilaterally symmetric amphids, located at the anterior tip of the animal, are the primary sensory organs of the worm. Each amphid consists of twelve sensory neurons and two ensheathing glia cells, the sheath and socket cells. Amphid neuron cell bodies are located near the posterior bulb of the pharynx and have two projections: an axon that extends into the nerve ring, and a dendrite that extends to the anterior tip of the animal. The sheath cell body is near the amphid neuronal cell bodies while the socket cell body is more anterior, near the anterior bulb of the pharynx. Amphid sheath and socket glia also extend anterior processes that contact amphid neuron dendritic projections. At the anterior tip all neuronal sensory endings are ensheathed by the sheath glia. Four of the amphid neurons, which mediate chemotaxis to volatile chemicals and thermotaxis (Bargmann, 1993; Mori and Ohshima, 1995) have dendritic endings that are fully embedded within the amphid sheath glia. These endings are lodged within tightly fitting channels in which the neurons are surrounded by an undefined matrix material secreted by the sheath cell. The remaining eight neurons end in sensory cilia that house sensory receptors and signal transduction

molecules (Troemel, 1999), and gain access to the outside environment by extending through the main amphid channel: a bipartite channel, formed anteriorly by the socket glia and continued posteriorly by the sheath glia (Ward et al., 1975). This channel, which is also filled with a sheath cell derived matrix, is open to the outside environment and is supported by an array of cytoskeletal elements (Ward et al., 1975). Each dendrite enters the sheath cell through an individual lumen before joining together in a common lumen. The sheath cell lumen is an intracellular lumen lacking an autocellular junction. The socket cell lumen, on the other hand, requires an autocellular junction as the socket cell membrane wraps around the lumen and cilia. The sheath cell forms junctions with both the socket cell and neurons. These amphid channel neurons are required for avoidance of high osmolarity solutions, chemosensation of water-soluble solutes, mechanosensation, and sensation of dauer pheromone (Bargmann, 1997; Driscoll, 1997; Riddle, 1997).

Drosophila melanogaster Sensory Organ Stucture

Drosophila sensory organs share many features with worm sensory organs, suggesting common mechanisms for constructing these organs. Patterning, cell division, and differentiation of *Drosophila* sensory organs have been well studied (Schweisguth et al., 1996). On the other hand, while electron microscopy studies have revealed the detailed structure of the different sensory organs, the morphogenetic events and genes controlling these processes are poorly understood.

Drosophila external mechanosensory organ development has been studied extensively (Hartenstein and Posakony, 1989; Schweisguth et al., 1996). Lateral

inhibition mediated by Notch signaling selects a sensory organ precursor cell out of a group of equivalent ectodermal cells. Several rounds of asymmetric cell division give rise to the cells of the organ. The neuron cell body resides below the epidermis and extends a dendrite apically to the surface epithelium where it ends in an outer ciliary segment (Figure 1.1B). Three accessory cells form concentric sheaths around the dendrite. The thecogen (or sheath cell), whose cell body is near the neuron's cell body, forms an inner cylindrical sheath and secretes an electron dense extracellular matrix (the dendritic cap) around the tip. The thecogen lumen is junctionless. The outer two layers are formed by the tricogen (or bristle cell) and the tormogen (or socket cell). Unlike the thecogen, their cell bodies are located closer to the dendrite. Also, unlike the thecogen, they ensheath the dendrite with a mesaxon-like structure- they wrap around the neuronal process and form autocellular junctions. Finally, these cells are connected to each other, the dendrites, and surrounding epidermal cells by belt desmosomes.

Hartenstein and Posakony attempted to observe the morphogenesis of these organs (Hartenstein and Posakony, 1989). They observed that the neuron first migrated interiorly and then extended its dendrite and axon. To generate the association between the dendrite and the accessory cells, the dendrite was described as growing through or "invading" the thecogen cell. On the other hand, the trichogen and tormogen "wrap" mesaxon-like processes around the dendrite. Thus, formation of the lumens in the different accessory cells appears to be initiated by different mechanisms.

Drosophila olfactory organs share many structural features with the mechanosensory organs (Pollack and Balakrishnan, 1997; Shanbhag 1999;

Shanbhag 2000). The neuron and thecogen cell bodies are located internally while the tricogen and tormogen cell bodies are more superficial. The accessory cell bodies connect to the ensheathing/ dendritic portion by a thin process that does not contact other cells in the sensillum. In this case, only the tricogen forms a lumen with a mesaxon-like autojunction while both the thecogen and the tricogen are "perforated" by the dendrite.

Human Sensory Organ Structure

As might be expected, human sensory organs are more complex in structure than worm or fly sensilla. Nevertheless, they still share some basic features (Burkitt, 1993; Ross, 1995). Temperature, touch, and pain sensation are sensed by neurons with dendritic endings that penetrate the basal lamina of the epidermis and remain as simple free nerve endings. But even these nerve endings, like worm temperature sensitive nerve endings that are ensheathed by the sheath cell but fail to penetrate it, are sometimes associated with specialized epithelial cells, called Merkel cells. Merkel cells lie in close apposition to the terminal of a nerve fiber and, like other sensory organ accessory cells, contain electron-dense granules.

Other nerve endings mediating touch, on the other hand, do reside in a lumen. Neuronal endings in Pacinian corpuscles, for example, are encapsulated in elaborate concentric lamellae of specialized cells that wrap around the nerve endings. These cells are proposed to be modified Schwann glia.

More complex sensory organs also feature dendrites that extend through a lumen in a modified epithelium. For example, the olfactory epithelium is composed mostly of supporting or sustenticular columnar cells. Olfactory

neurons reside between these sustenticular cells and extend their dendrite between and above these cells. Olfactory dendrites, which end in non-motile cilia, join to the sustenticular cells by adherens junctions. Sustenticular cell bodies are located more superficially than the neuron's, and the cells contain numerous mitochorndria and endoplasmic reticulum. Meanwhile, in the retina, rod and cone photoreceptors are intimately associated with Mueller cells (Figure 1.1C). Mueller cells fill most of the extracellular space in the retina and send out cytoplasmic extensions that surround and sometimes ensheath the rod and cone photoreceptor cilia.

Conclusions

In sum, most sensory organs from these diverse species contain several morphological features in common. First, all are composed of sensory neurons and closely associated glia or specialized epithelia. These glia or epithelia, whose cell bodies are located more superficially than the neuronal cell bodies, often form a lumen around the neuronal dendrite. Finally, the glia or epithelia form junctions with the neurons and often secrete a matrix material around the dendrite. It is unknown how this structure is formed. Specifically, how the lumen forms in the glia or epithelia and how this structure is coupled to the resident neuronal processes is unknown.

Lumen Formation

As described above, lumens are a fundamental component of many sensory organs. In fact, lumens are a fundamental component of most organ systems. Tubular structures are found in the excretory, digestive, respiratory,

and circulatory systems. Recent studies are beginning to shed light on lumen morphogenesis and the genes regulating this process (Hogan and Kolodziej, 2002; Lubarsky and Krasnow, 2003). At first glance, many biological tubes have little in common as they vary in shape, size and complexity. Some are multicellular, others are unicellular with an autocellular junction, while others are a junctionless intracellular tubes (Figure 1.2). Furthermore, some are extensively branched while others are unbranched. Yet there appears to be some similar underlying events required to make these different lumens.

A review of lumen formation studies in different experimental systems suggests some common mechanisms for generating lumens. First, cells composing the tube must get into the proper position. This step is the most diverse step in lumen formation. Several different morphogenetic events can get the cells into place: wrapping up an epithelial sheet, as seen in the neural tube formation; budding outgrowth from an epithelial sheet or pre-exisiting tubes, as occurs during the *Drosophila* trachea formation; and cavitation, the removal of cells in a cluster of cells by apoptosis, as occurs during vertebrate intestine formation.

Also, the apico-basolateral polarity of the cells composing the tube must be established. Epithelial polarity is determined in invertebrates and vertebrates by a conserved set of molecules (Wodarz, 2002). Briefly, Par-6, Par-3/Bazooka, and atypical protein kinase C (αPCK) are apical determinants that promote the apical distribution of additional factors Crumbs, Stardust, and Discs lost. This complex inhibits the apical distribution of Scibble, Disk large and Lethal giant larvae, which collect at the basolateral surfaces. Also, at the basal surface,

integrins attach to the extracellular matrix (ECM). Finally, junctional complexes separate the basolateral and apical surfaces.

Once polarity is established, vesicles coalesce to generate and elaborate the luminal surface and thus the luminal space (Figure 1.2). If the tube is multicellular, then the cells' apical surfaces face the lumen, and the vesicles coalesce at that surface. If the lumen is made by one cell, then the vesicles coalesce at the center of the cell, away from the surface contacting the extracellular matrix or other cells. Once a lumen is generated, it may be stabilized by a secreted substance.

Because many of these morphogenetic features are shared during lumen formation in different systems, studying sensory organ lumen formation may provide insight into lumen formation in other systems, such as the excretory or digestive systems. Conversely, understanding lumen formation in other systems may provide insight into sensory organ lumen formation. Thus in this section I will review lumen formation in several well-studied experimental systems, focusing on common features. These systems include capillary forming endothelial cells, the *C. elegans* excretory canal cell, cultured Madin-Darby Canine Kidney (MDCK) cells, and *Drosophila* trachea and salivary glands.

Capillary lumen formation

Perhaps the simplest system for studying lumen formation is capillary lumen formation. These tubes are simple unicellular tubes without autocellular junctions. Cloned endothelial cells grown in culture form lumens. Observations of this process and recent molecular studies have provided insight into this lumen formation.

First, specific interactions with the ECM are necessary for the formation of a lumen. Lumen formation requires endothelial cell $\alpha_2\beta_1$ integrin expression in a collagen ECM and $\alpha_5\beta_3$ or $\alpha_5\beta_3$ integrins in a fibrin 3D matrix (Bayless et al., 2000; Davis and Camarillo, 1996). Apparently, the endothelial cells must be able to determine their orientation to allow the intracellular lumen to form.

Under the correct conditions, many researchers have observed the appearance of intracellular vacuoles in capillary forming endothelial cells (Davis and Camarillo, 1996; Dyson et al., 1976; Folkman and Haudenschild, 1980; Wolff and Bar, 1972). Wolff et al. and Dyson et al. noticed that while the lumen formed in these cells, the vacuole disappeared, suggesting that the vacuole contributed to the lumen formation. Davis and collegues demonstrated that the vacuole is created from a pinocytic event (Davis and Camarillo, 1996). When the plasma membrane was labeled, the vacuole also contained this label. Also, the vacuole membrane contained cell-surface markers (CD31 and β_1 integrin) as well as phagosome markers (such as F-actin). Finally, if fluorescent tracers were added to the extracellular space, the vauole contained this marker. Thus the vacuole appears to be the result of a phagocytic event. They also observed multiple

vacuoles of variable size and number per cell, and these vesicles would coalesce to generate the lumen. The generation of the vacuoles depended on the GTPases Rac1 and Cdc42, which localized to the vacuole membrane (Bayless and Davis, 2002). Finally, Folkman and Haudenschild also observed that the lumen was transiently filled with an amorphous material, which was later removed (Folkman and Haudenschild, 1980).

C. elegans excretory canal cell lumen formation

Like capillaries, the *C. elegans* excretory canal cell features a unicellular lumen lacking an autocellular junction. The single excretory canal cell is shaped like an "H". It extends long processes that run along both sides of the animal. Electron microscopy reconstruction of *in vivo* lumen formation in this cell shares features with lumen formation in cultured epithelial cells (Berry et al., 2003). First, one or two vacuoles appear in the cell shortly after its birth. These vacuoles appear to be the result of pincytosis- the vacuole has inclusions and dark membrane staining and is continuous with the plasma membrane. The vacuole then extends tubular arms through the cytoplasm. These arms then collapse and remodel to form the mature lumen with electron dense apical cytoskeletal material. Also, during embryogenesis, material is observed in the lumen, but this material disappears by hatching (Buechner, 2002). Thus, canal lumen formation, like capillary lumen formation, is dependent on vacuole formation follow by a transient secretion into the lumen.

Genetic studies have provided insight into the mechanisms of excretory canal lumen formation and maintenance. First, extension of the cytoplasmic arms is dependent on the same cues and mechanisms that guide the migration

and outgrowth of other cells, such as integrin components (INA-1 and PAT-3) and UNC-6 netrin and the netrin receptor UNC-5 (Baum and Garriga, 1997; Gettner et al., 1995; Hedgecock et al., 1987). This outgrowth appears to be the result of interactions between the basal, non-luminal surface and the surrounding cells and ECM. Importantly, this outgrowth can be uncoupled from apical/ luminal growth (Gettner et al., 1995). Thus the mechanisms used to generate the cell shape must be different than those used to generate the lumen.

A genetic screen identified worms with enlarged, cystic canal lumens (Buechner et al., 1999). Some of the genes identified in this screen have been cloned, and all appear to function in regulating the apical/ luminal surface. *sma-1*, for example, encodes the cytoskeletal protein β_H-spectrin, which localizes to the apical surface of cells (McKeown et al., 1998). In *sma-1* mutants, the actin-based apical terminal web in the canal cell is separated from the lumen. Thus β_H-spectrin stabilizes the lumen by connecting the actin cytoskeleton to the apical membrane. *exc-7* (for excretory canal abnormal) mutants have the same subcellular defects as *sma-1* mutants. *exc-7* encodes the mRNA binding protein ELAV which binds *sma-1* 3' UTR and presumably regulates *sma-1* translation (Fujita et al., 2003). Furthermore, the ERM-1 (for ezrin, radixin, moesin) cytoskeleton membrane linker localizes to the apical surface and interacts functionally with *sma-1* and *act-5*/ cytoplasmic actin to regulate apical membrane morphogenesis (Gobel et al., 2004). e*xc-5*, which encodes a GDP-GTP exchange factor that activates CDC42, coordinates apical/luminal versus basal growth (Gao et al., 2001; Suzuki et al., 2001). In *exc-5* mutants the apical surface extends too far (cyts accumulate at the distal tips of the canals), and when *exc-5* is

overexpressed the basal surface fails to extend while the luminal surface growth appears normal. Finally, several *exc* genes encode ion channels. For example, *exc-4* encodes a CLIC chloride ion channel that localizes to the apical surface of numerous luminal surfaces in the worm (Berry et al., 2003). *exc-4* is required before or during the extension of the tubular arms as well as for the maintenance of the tubular structure. In sum, studies on excretory canal cell lumen formation demonstrate the importance of the regulation of the apical surface and vacuole generation during lumen formation and maintenance.

Madin-Darby canine kidney cell lumen formation

Under certain conditions, cultured Madin-Darby canine kidney (MDCK) cells form lumens. Unlike cultured capillary endothelial cells or the *C. elegans* excretory canal cell, however, these lumens are multicellular. Nevertheless, specification of the apical surface and vesicles appear to be required for lumen formation in this seemingly unrelated system.

MDCK cells are derived from the kidney distal tubule and collecting duct. When grown in two-dimensional cultures, the cells form an epithelial sheet with defined apical and basolateral surfaces separated by tight junctions (Mostov et al., 2000). When the cells are grown in three-dimensional gels of ECM, they organize into a spherical cyst. Once again the cells are polarized. In this case, the apical surface faces the lumen. Mostov and collegues propose this arrangement is driven by a "drive for three surfaces"; the cells need to have lateral surface touching other cells, and free apical surface and a basal surface in contact with the ECM (O'Brien et al., 2002). Interestingly, cells at the center of the cyst, which fail to contact the ECM undergo apoptosis, suggesting a mechanism

for removing cells during the cavitation of the developing vertebrate intestine. Rac1 is required for cyst formation; dominant negative Rac1 inhibits lumen formation (O'Brien et al., 2001). O'Brien et al. suggest that this effect is due to inhibition of laminin secretion at the basement membrane and mislocalization of the apical markers Par3, Par6, and αPKC. Thus apico-basolateral specification appears to be essential for cyst formation.

Cultured MDCK cells can form a second type of tube, providing further insight into lumen formation. In the presence of hepatocyte growth factor (HGF) branches grow out of the cysts, and these branches contain a lumen (Montesano et al., 1991). To form these branches, some cells in the cyst extend pseudopodia from their basolateral surface and then migrate out from the cyst. To form a lumen, these cells first lose their apico-basolateral polarity; apical markers are lost and basolateral markers spread around the cell (Pollack et al., 1998; Yu et al., 2003). After the cells divide to form a cord of cells two cells wide, the cells in this bilayer reestablish their polarity with the apical surface facing inward. At this point, a potential lumen is present between the apical surfaces. The lumen is generated by the addition of membrane to the apical surfaces. Cytoplasmic vesicles called the vacuolar apical compartment (VAC) are found in isolated MDCK cells and contain apical surface markers (Vega-Salas et al., 1987). Exocytosis of the VACs occurs at points of cell-cell contact to add membrane to the apical surface (Figure 1.2C) (Vega-Salas et al., 1988).

In sum, like in unicellular tubes, these multicellular tubes first require specification of the apoico-basolateral polarity. Vesicles then add membrane to generate the luminal surface. The vesicles coalesce and add membrane to a

pinocytic vacuole in unicellular tubes, while they add to the apical/ luminal surface in multicululular tubes.

Drosophila trachea and salivary gland lumen formation

The *Drosophila* trachea and salivary glands provide unique advantages for studying lumen formation. The cytological events that generate the tubes have been described, and the ease of genetic manipulation allows insight into the genetic regulation of these phenomena. Both tubes are initiated in the same manner and require similar genes, but the trachea has several added levels of complexity; the trachea, unlike the salivary glands, is branched, has unicellular tubes (both with autocellular junctions and seamless intracellular lumens), and requires anastamoses between different tubes.

In both organs, the cells acquire their polarity from the epithelium from which they originate. Then, like the outgrowth of the *C. elegans* excretory canal cell arms, and the outgrowth of lumens from cultured MDCK cells, positioning the cells that make up the fly trachea and salivary glands requires a unique set of morphological changes. Initiation of lumen formation in both organs begins with the invagination of ectodermal epithelial placodes (Samakovlis et al., 1996). The cells' apical surfaces contract to change the cells' shape from columnar to pyramidal. This step requires the bHLH-PAS transcription factor *trachealess* in the trachea and salivary duct and the transcription *forkhead* for the remainder of the salivary gland (Isaac and Andrew, 1996; Kuo et al., 1996; Wilk et al., 1996). These cell shape changes alone distort the epithelium so that it bulges inward and a pocket forms with the apical surfaces of the cells facing the inner/ luminal

region. Interestingly, similar cell shape changes are observed in vertebrate embryos at the initiation of neural tube formation (Schoenwolf and Smith, 1990).

Once this invagination occurs, the cells migrate out in a well-coordinated fashion. Chemoattractants, such as the FGF-like ligand Branchless (Bnl) and Slit, orient the migration of cells at the tip of the invaginated pocket (Englund et al., 2002; Sutherland et al., 1996). The force generated by the migrating cells pulls the other invaginated cells and, in turn, elongates the tube. This migration, like the migration of other cells, is dependent on integrin function and the formation of filopodia and lamelapodia at the basal surface. The alternaing expression pattern of Bnl during trachea development causes the different cells to migrate out, resulting in a branched structure (Sutherland et al., 1996).

With the cells in place and a primitive lumen formed, the lumen is expanded. Lumen formation in both organs requires the transcription factor *ribbon* (Bradley and Andrew, 2001; Shim et al., 2001). *Ribbon* mutant tracheas, for example, have decreased luminal space. Importantly, the basal surface of the migrating cells still responds to the guidance chemoattractants in these mutants, but the apical/ luminal surfaces fail to follow. Thus, like in the *C. elegans* excretory canal cell, migration and positioning the cells of the tube is independent from lumen formation and extension. Conversely, flies mutant for the transcripition factor *grainyhead* have excessive apical/ luminal membrane, and overexpression of *grainyhead* results in decreased apical surface and narrow lumens (Hemphala et al., 2003). The targets of these transcription factors have not been identified.

Additional transcription factors have been shown to regulate vesicle transport during lumen membrane elaboration (Myat and Andrew, 2002). Myat

and Andrew demonstrated that the transcription factor *hariy* (*h*) restricts apical membrane growth; *h* mutants have enlarged lumens. On the other hand, *huckebein* (*hkb*) mutants have decreased apical membrane growth and narrow lumens, while overexpression of *hkb* results in increased apical growth. Genetic epistasis experiments suggest that these factors act in the same genetic pathway; *hairy* represses *hkb*.

Hkb regulates vesicle transport. Vesicles have been observed in developing salivary gland cells, and an apical marker labels these vesicles (Figure 1.2C). These vesicles may be analogous to the VACs seen in MDCK cells. *Hkb* overexpression causes a decrease in these vesicles; presumably the vesicles have added to the enlarged plasma membrane. On the other hand, these vesicles accumulate within cells in *hkb* mutants. Thus, *hkb* promotes vesicle addition to the apical luminal membrane

These researchers identified targets of *hkb*, and these targets suggest a mechanism for *hkb* regulation of vesicle dynamics. *Klarsicht* (*klar*) and *Crumbs* (*crb*) are expressed in the developing salivary gland, and their expression is dependent on *hkb*. *Klar* encodes a putative regulator of the microtubule motor dynein, which carries cargo to the negative end of microtubules (Mosley-Bishop et al., 1999). *Crb*, as discussed above, is an apical membrane determinant. Like *hkb* and *klar*, *crb* mutant salivary glands have reduced lumens, while overexpression results in enlarged lumens. *Klar* may promote dynein-mediated transport of vesicles along microtubules to the apical surface. Consistent with this model, microtubules in the salivary gland cells are oriented with their minus ends toward the luminal surface. Meanwhile, *crb* may stabilize the growing apical membrane. *Crb* functions in a complex with β_H-spectrin, and spectrin

inhibits endocytosis (Izaddoost et al., 2002; Pellikka et al., 2002). Thus *crb* may stabilize spectrin and inhibit endocytosis, a necessity for the net addition of membrane to the apical surface.

Apical membrane growth is also required during trachea lumen expansion as the animal grows. Surprisingly, genes required for this growth encode components of the fly septate junctions (Wu and Beitel, 2004). *Drosophila* septate junctions are functionally equivalent to vertebrate tight junctions; they form a diffusion barrier between adjacent epithelial cells. Unlike tight junctions, however, septate junctions are located basal to adherens junctions. There are two models for why septate junctions are required for lumen growth. One possibility is that loss of the diffusion barrier results in lumen growth regulation defects. However, there is no correlation between diffusion defects and lumen size defects. For example, some flies with diffusion barrier defects have no lumen size defects (Paul et al., 2003). An alternative model proposes that the septate junctions, which contain the basal promoting factors Lgl, Dlg, and Scribble (Scrib), influence the distribution of apico-basolateral polarity factors. Consistent with this model, these factors are mislocalized in septate junction mutants, and *scrib* mutants have excessive lumen growth defects similar to septate junction mutants (Behr et al., 2003; Paul et al., 2003; Wu and Beitel, 2004). Thus, as in the salivary gland, where the apical promoting factor *crb* promoted lumen growth, lumen expansion in the trachea depends on regulating the apical surface.

As described above, the trachea has several additional levels of complexity not seen in the salivary glands. More specifically, in addition to multicellular tubes, the trachea contains unicellular tubes with autojunctions, unicellular tubes with an intracellular lumen, and anastamoses between different

tubes. Tracheal tubes with autocellular junctions don't form by wrapping. Instead the tubes begin as a multicellular tube- two cells surrounding a central lumen (Ribeiro et al., 2004). These two cells are then pulled apart, presumably due to the force generated by the migration outward of the tube at the tip. As this occurs, the intercellular adherens junctions transform into autocellular junctions. Expression of the transcription factor Spalt determines the decision to transform the multicellular tube into an autocellular tube (Ribeiro et al., 2004). Also, the zona pellucida domain proteins Piopio and Dumpy are required to maintain the contacts between the two cells after they have changed from facing one another to lying adjacent (Jazwinska et al., 2003). Thus this analysis of trachea lumen formation has provided insight into the morphogenetic changes and genetic regulation that may underlie the formation of some unicellular tubes with an autocellular junction.

The *Drosophila* trachea is also composed of unicellular tubes with an intracellular lumen lacking an autocellular junction. The terminal cells of the trachea have such an arrangement, and they form by first extending a cytoplasmic process (Guillemin et al., 1996; Samakovlis et al., 1996). Lumen is initiated by invasion from the neighboring cell. Then the majority of the intracellular lumen growth is due to addition of membrane to the luminal surface of the terminal cell. This growth is dependent on the *Drosophila* serum response factor *pruned*, but the downstream targets of *pruned* are unknown (Guillemin et al., 1996). This growth, however, has been proposed to be dependent on the fusion of vesicles to the growing luminal surface (Uv et al., 2003).

Fusion between two tracheal branches is also made by cells with lumens lacking an autocellular junction. Studies of this process provide insight into both tube anastamosis formation and intracellular lumen formation. First, the basal surface of cells from neighboring branches form a contact mediated by E-cadherin. Then a complex of microtubules, Short Stop (a plakin-like protein) and F-actin directs the formation of an F-actin tract that spans each cell from the basal E-cadherin contact site to the apical luminal surface. Apical membrane markers then accumulate along this track allowing for growth of the lumen through the cell. The actin tract appears to provide a scaffold for vesicles to add apical membrane to the growing luminal surface.

Conclusions

In sum, several common events occur during lumen formation. First, the cells get in position to form the tube and orient their polarity so that the apical surface forms the luminal surface. Then vesicles coalesce at the apical surface to generate and expand the luminal surface. Presumably, sensory organ lumen formation requires similar processes.

Neuronal Regulation of Glia Morphogenesis

Neurons and glia are intimately associated with one another during nervous system development and function. For example, reciprocal interactions between neurons and glia guide their migrations. Neurons migrate along radial glial cells in the developing forebrain or along Bergmann glia in the developing cerebellum (Hatten, 1999). On the other hand, migrating zebrafish peripheral nervous system glia follow axons; laser ablation of the neurons disrupts glial cell

migration, and in mutants with misdirected axons, the glial cells follow the path of the misrouted axons (Gilmour et al., 2002). Additionally, secretions and cell-cell contacts can regulate subcellular localization of proteins in these cells. Both a large protein complex and secreted factors from glia regulate the clustering of specific ion channels in axonal nodes of Ranvier (Bhat et al., 2001; Kaplan et al., 1997). Similarly, astrocyte-secreted cholesterol regulates synapse formation and function (Mauch et al., 2001). Finally, glial cells and neurons depend on one another for their survival (Hidalgo et al., 2001; Woldeyesus et al., 1999).

Presumably, similar interactions coordinate glia and neuron morphogenesis. In vertebrates, astrocytes project foot processes that ensheath the basement membranes of neurons and synapses. The other type of central nervous system glia, oligodendrocytes, wrap their cell membranes around the nerve axon to form myelin. In the peripheral nervous system, Schwann glia perform the functions of both oligodendrocytes and astrocytes. Like oligodendrocytes, they myelinate peripheral nerves, and like astrocytes, they ensheath and separate unmyelinated axons.

Similar associations between glia and neuronal processes are found in sensory organs. For example, in the retina, Mueller cells ensheath photoreceptor processes. Also, some *Drosophila* sensory organ accessory cells ensheath the associated neuronal process with a structure similar to an intermediate formed during myelin formation, called the mesaxon. Studying these sensory organ structures, therefore, may give insight into certain aspects of glia morphogenesis.

Some studies of myelination have shed light on the initial steps of glia morphogenesis. Briefly, the myelinating glial cell extends its plasma membrane around the neuronal process and forms a double membrane structure called the

mesaxon. Additional steps are then required to elongate the membrane as it spirals around the neurons. Finally, the glia must grow as the neuronal processes elongates during post-embryonic growth. Presumably, mechanisms controlling the initiation of myelination, the extension of the process to form the mesaxon, and the lengthening of the glia as the animal grows could be conserved among different types of glia.

Axon derived signals appear to be important for the initiation of myelination. For example, the neurotrophin nerve growth factor (NGF), in addition to its role in mediating trophism, promotes Schwann cell myelination and inhibits oligodendrocyte myelination (Chan et al., 2004). Surprisingly, NGF acts through axonal TrkA receptors, suggesting that the NGF signal affects glia morphogenesis through a neuron-derived intermediate. Also, neuronal activity influences the onset of myelination. For example, mice raised in the dark have diminished optic nerve myelination, while premature opening of rabbit eyelid accelerates myelination (Gyllensten and Malmfors, 1963; Tauber et al., 1980). Furthermore, *in vivo* and *in vitro* exposure of neurons to neurotoxins that increase or decrease neuronal electrical activity effect myelination (Demerens et al., 1996).

Thus, NGF and electrical activity may affect expression and production of neuronal derived secreted factors and cell surface markers that affect myelination initiation. Some of these factors have been identified. For example, neuronal activity results in the secretion of adenosine, which act through purinergic receptors on oligodendrocyte precursors to stimulate myelination (Stevens et al., 2002). Conversely, adenosine inhibits Schwann cell myelination (Stevens and Fields, 2000). Similarly, neuronal electrical activity affects neuronal expression of the neural cell adhesion protein L1, and antibody inhibition of L1 disrupts

myelination initiation (Itoh et al., 1995; Wood et al., 1990). On the other hand, antibody mediated inhibition of polysialic acid NCAM promotes myelination (Charles et al., 2000). Consistent with this finding, neuronal expression of this molecule decreases with myelination initiation. Finally, glia laminin deposition is required for myelination, and glia express laminin receptors (Podratz et al., 2001; Previtali et al., 2003). Integrins, one type of laminin receptor expressd by myelinating glia, are localized to the myelin membrane, and a Schwann cell specific knockout of the β1 integrin subunit disrupts Schwann cell interactions with axons (Feltri et al., 2002; Feltri et al., 1994).

Once myelination is initiatiated, the membrane must extend around the neuronal process. This event requires the generation of new membrane. Myelin membranes have a unique lipid and protein composition, so these factors must be selectively generated and delivered to the growing membrane. Cholesterol is a major constituent of the myelin membrane, and disruption of oligodendrocyte cholesterol synthesis delays myelin formation (Saher et al., 2005). Furthermore, polarized delivery of myelin membrane components, similar to that seen in polarized epithelial cells, has been identified in developing oligodendrocytes (de Vries et al., 1998). Selective localization of a protein component of myelin, myelin basic protein (MBP), is achived by localized mRNA translation of MBP near the growing membrane (Colman et al., 1982; Griffiths et al., 1989; Saher et al., 2005). Finally, the actin cytoskeleton is important for extension of the membrane. Cytochalasin D inhibition of actin polymerization results in the failure to extend the glia membrane and form the mesaxon (Fernandez-Valle et al., 1997). Thus, formation of the unique membrane that composes the myelin

sheath is dependent on the selective biogenesis and delivery of these components to the growing membrane.

Once melination is completed, the membrane must continue to grow as the animal and nerves elongate. Another laminin receptor, dystroglycan, is required for this step. Elongation of the glia fails in mice with a Schwann cell specific disruption of the periaxin–DRP2–dystroglycan complex (Fernandez-Valle et al., 1997; Saito et al., 2003; Sherman and Brophy, 2005; Sherman et al., 2001).

In sum, *in vitro* and *in vivo* studies have provided some insight into glia morphogenesis and the neuronal regulation of this process. Still, additional studies will be necessary to understand how glia morphogenesis is tightly coupled to the neuronal process it ensheaths.

Sterol-Sensing Domain containing proteins

The sterol-sensing domain (SSD) is an approximately 180 amino acid, five transmembrane protein motif found in seven proteins: the sterol regulatory element-binding protein (SREBP)-cleavage activating protein (SCAP), 3-hydroxy-3-methylglutaryl coenzyme A-reductase (HMGCR), 7-dehydrocholesterol reductase (7DHCR), Niemann–Pick disease type C1 protein (NPC1), Patched (Ptc), Dispatched (Disp), and Patched-related (Ptr) (Figure 1.3) (Kuwabara and Labouesse, 2002). As described below, these proteins perform very different functions. For example, HMGCR and 7DHCR function in the biosynthesis of cholesterol while Ptc is a component of a signal transduction pathway essential

during embryonic development. Why then do they all posses a SSD? In other words, what is the function of the SSD?

Mutational analysis described below has demonstrated that the SSD plays a unique, essential role in these proteins. Furthermore, a variety of analysises have demonstrated that the SSD plays a role independent from the enzymatic function of each protein. Thus, even though these proteins do perform different functions, the SSD may play a conserved role in each protein.

In this thesis, I provide the first analysis of a member of a previously uncharacterized sub-family of SSD containing proteins- the Ptr family. While I demonstrate that this protein, DAF-6, is required for lumen formation, the mechanism of DAF-6 function is poorly understood. Determining the conserved function of the SSD may provide insight into DAF-6 regulation or function. Here I will review the function of the SSD in each family of SSD containing proteins. Evidence suggests that the SSD couples sterol levels to protein conformation, subcellular localization, and stability.

SCAP

Sterol regulatory element-binding protein (SREBP)-cleavage activating protein (SCAP) was originally isolated based on a missense mutation in its SSD. When wildtype mammalian cells are given excessive amounts of sterols, cholesterol synthesis and uptake are suppressed. These changes are mediated by cleavage and activation of the transcription factors SREBP-1 and –2. The Brown and Goldstein laboritories screened for dominant mutations that rendered the cells resistant to sterol-mediated suppression of these changes (Hua et al., 1996).

From this screen, they isolated SCAP. The mutant protein had a dominant SSD D443N mutation.

SCAP is an eight transmembrane protein, and transmembranes two through six correspond to the SSD (Figure 1.3) (Nohturfft et al., 1998b). Work mainly from the Brown and Goldstein labs has elucidated the role of the SSD in SCAP function. The SSD directly binds cholesterol (Adams et al., 2004; Radhakrishnan et al., 2004). In the presence of excess sterols, SCAP changes its conformation (as revealed by changes in the trypsin cleavage pattern) (Brown et al., 2002) and binds INSIG-1 and –2, resident endoplamic reticulum (ER) proteins (Adams et al., 2003; Yabe et al., 2002; Yang et al., 2002). Finally, sterols, in an INSIG-dependent manner, also inhibit SCAP from binding the COPII proteins Sec 23/24 (Espenshade et al., 2002). When sterol levels are low, SCAP binds Sec 23/24 via its cytoplasmic loop, not its SSD, and tranlocates to the Golgi (Nohturfft et al., 1999). In turn, SCAP (which binds SREBP via its carboxy-terminus, not the SSD) and SREBP move to the Golgi, where SREBP is cleaved and activated (Nohturfft et al., 2000; Sakai et al., 1997).

Analysis of SCAP SSD mutants confirms this domain's role in coupling activity to sterol levels. Two SSD mutations (D443N and Y298C) render SCAP resistant to increased sterol levels (Hua et al., 1996; Nohturfft et al., 1998a; Nohturfft et al., 1996). These SCAP SSD mutants fail to alter their conformation or bind INSIG (Brown et al., 2002; Yang et al., 2002). They can, however, promote SREBP translocation to the Golgi. Additionally, expression of the first six transmembrane regions of SCAP in wildtype cells renders these cells resistant to sterol inhibition of wildtype SCAP movement to the Golgi; presumably, the SSD of this truncated SCAP binds all of the sterols, leaving the remaining

wildtype SCAP able to bind SREBP and Sec 23/24 (Yang et al., 2002). Furthermore, the Y298C mutation in this truncated SCAP blocks its dominant effect. On the other hand, a new SSD mutation (D428A in the fifth SSD transmembrane region) constitutively keeps SCAP in an INSIG bound conformation, even in the presence of low sterols (Feramisco et al., 2005). Thus, the SSD appears to couple SCAP conformation to sterol levels, in turn effecting its protein binding ability and subcellular localization. The SSD, however, does not play a direct role in the more specific function of SCAP, namely binding SREBP.

Cholesterol biosynthesis enzymes: HMGCR and 7DHCR

3-Hydroxy-3-methylglutaryl coenzyme A-reductase (HMGCR) and 7-dehydrocholesterol reductase (7DHCR) are required for the *de novo* biosynthesis of cholesterol. HMGCR catalyzes the conversion of 3-hydroxy-3-methyl-glutaryl CoA to mevalonate, the rate determining step in the synthesis of cholesterol. HMGCR levels decrease as cholesterol levels increase in part due to an increase in HMGCR degradation (Chin et al., 1985; Faust et al., 1982). The enzymatic function of HMGCR can be separated from this cholesterol-induced regulation.

HMGCR, like SCAP, has eight transmembrane domains, and domains two through six constitute the SSD (Figure 1.3) (Liscum et al., 1985; Olender and Simon, 1992). The enzymatic function is contained in the carboxy terminus. A truncated version lacking the amino-terminal transmembrane domains and containing only the carboxy terminus is still catalytically active (Gil et al., 1985). This mutant protein is found in the cytosol, rather than the ER membrane, and its degradation is not increased by increased sterol levels. Similarly, deletion of just

the third and fourth SSD transmembrane regions also leaves the protein catalytically active but insensitive to sterol-dependent degradation (Jingami et al., 1987). On the other hand, the HMGCR amino-terminal transmembrane domains alone are still properly localized to the ER and undergo sterol-dependent degradation (Kumagai et al., 1995; Skalnik et al., 1988). Interestingly, sea urchin HMGCR is not subject to sterol-dependent regulation, and by generating mammalian-sea urchin chimeric HMGCR Kumagai et al. demonstrated that the first SSD transmembrane domain can confer sterol-dependent degradation (Kumagai et al., 1995). Thus, like for SCAP, the SSD couples protein regulation to sterol levels but does not play a role in the unique catalytic activity.

In fact, the mechanism of HMGCR sterol regulation is conserved with SCAP. Increased sterol levels alter HMGCR conformation and promote its binding to INSIG (Sever et al., 2003a; Shearer and Hampton, 2005). The HMGCR-INSIG complex is then recognized by gp78, a membrane bound E3 ubiquitin ligase, which targets HMGCR for degradation (Song et al., 2005). The connection between HMGCR and SCAP SSD-mediated regulation was confirmed by an experiment in which overexpression of the SCAP SSD domain resulted in a decrease in the sterol induced degradation of HMGCR (Sever et al., 2003b).

In contrast to HMGCR and SCAP, the role of 7DHCR's SSD has not been elucidated. 7DHCR catalyzes the final step in cholesterol biosynthesis, and mutations in 7DHCR result in Smith-Lemli-Optiz Syndrome (SLOS). In patients with this syndrome, who have low serum cholesterol levels, morphogenetic defects, mental retardation, and failure to thrive, mutations are found thoughout

the 7DHCR gene, although substantial number of mutations are found in the SSD (Bae et al., 1999; Fitzky et al., 1999).

NPC1

Niemann-Pick type C disease is characterized by progressive neurodegeneration and hepatosplenomegaly (Vanier et al., 1991). The gene mutated in 95% of these patients- NPC1- was cloned and encodes a thirteen transmembrane protein (Carstea et al., 1997). The protein has an amino-terminal tail followed by a transmembrane domain, and then it has the twice repeated motif of one transmembrane domain, a large cytosolic loop, and then the five transmembrane SSD (Figure 1.3) (Davies and Ioannou, 2000).

Analysis of NPC1 mutant cells suggests that NPC1 is required for lipid transport. Cellular cholesterol derived from endocytosed LDL-cholesterol is modified by lipase in endosomes before being transported elsewhere in the cell. In NPC1 mutant cells, this cholesterol accumulates in late endosomes and lysosomes (Kobayashi et al., 1999; Mobius et al., 2003; Wojtanik and Liscum, 2003). Mammalian cells can also synthesize cholesterol *de novo*. In both normal and NPC1 mutant cells, newly synthesized cholesterol can be transported from the ER to caveolae in the plasma membrane. In mutant cells, however, this cholesterol accumulates in late endosomes and lysosomes after recycling from the plasma membrane (Cruz and Chang, 2000; Liscum et al., 1989). Consistent with these findings, cholesterol transport to and from the plasma membrane is delayed in mutant cells, and overexpression of NPC1 increases cholesterol transport to the plasma membrane (Millard et al., 2000). Consistent with a role

for NPC1 in cholesterol usage, *C. elegans* with mutations in worm NPC1 homologs are hypersensitive to cholesterol deprivation (Sym et al., 2000).

A variety of other defects have been identified in NPC1 mutant cells. For example, sphingomyelin, glucosylceramide, gangliosides, and lisobisphosphatidic acid all accumulate in these cells (Malathi et al., 2004; Neufeld et al., 1999; Zervas et al., 2001). Some evidence suggests that some of these defects may be secondary to the cholesterol accumulation defect (Puri et al., 1999). Specifically, excess cholesterol can result in the same glycosphingolipid mislocalization seen in NPC1 mutant cells. Further studies, however, are necessary to determine NPC1's role in trasporting other lipids.

Consistent with a role for NPC1 in mediating transport from late endosomes and lysosomes, NPC1 protein is found primarily in late endosomes and secondarily in lysosomes and the trans-Golgi network (Higgins et al., 1999; Neufeld et al., 1999; Zhang et al., 2001). Furthermore, cellular uptake of cholesterol enhances NPC1 localization to Rab7 positive late endosomes.

NPC1, like SCAP, was shown to directly bind cholesterol (Ohgami et al., 2004). Furthermore, two NPC1 SSD mutants, P692S and Y635C, fail to bind cholesterol or rescue the cholesterol trafficking defect in mutant cells (Ko et al., 2001; Watari et al., 1999). Interestingly, the Y635C mutation is analogous to the Y298C SCAP SSD mutation. (Proline 692 is not conserved in other SSDs.) While these two mutations result in decreased rates of cholesterol transport between the ER and plasma membrane, two other SSD mutations, L657F and D787N (the equivalent mutations of SCAP SSD mutation L315F and D443N) are functional and increase rates of cholesterol transport, revealing an unexplained level of complexity in SSD function (Millard et al., 2005).

Adding to the complexity, NPC1 has significant similarities with the resistance-nodulation-division (RND) family of prokaryotic permeases. These proteins are proton driven efflux antiporters (Nies and Silver, 1995; Tseng et al., 1999). They mediate the efflux of lipophilic drugs, detergents, bile salts, fatty acids, metal ions, and dyes (such as acriflavine) from the cytosol of gram-negative bacteria (Ma et al., 1995; Nikaido et al., 1998; Thanassi et al., 1997). The sequence and structure of these transporters is similar to NPC1. While these transporters lack the first transmembrane of NPC1, they have the same twice repeated structure of six transmembrane domains with a large loop between the first and second transmembrane domains (Gotoh et al., 1999). Ioannou and colleagues have reported several lines of evidence showing that NPC1 can function as a transporter (Davies et al., 2000). First, unlike wildtype cells, NPC1 mutant cells failed to remove acriflavine. Also, when ectopically expressed in *E. coli*, NPC1 promoted the cells' uptake of acriflavine and oleic acid, a long-chain fatty acid. It failed, however, to confer the ability to transport cholesterol. Therefore, like other SSD proteins, NPC1 may have an enzymatic function distinct from its cholesterol/ SSD interaction.

Hedgehog signal transduction proteins: Patched and Dispatched

Unlike, SCAP, HMGCR, 7DHCR, and NPC1, Patched and Dispatched are not involved in cholesterol synthesis and usage. Instead, in vertebrates and *Drosophila* Patched is required for the response to the morphogen Hedgehog while Dispatched is required for the release of Hedgehog from signaling cells. Both proteins have twelve transmembrane domains; like RND permeases, they have the repeated structure of one transmemebrane followed by a large

extracellular loop and the five transmemebrane SSD (Figure 1.3) (Burke et al., 1999; Hooper and Scott, 1989; Nakano et al., 1989).

Most studies have focused on Patched, which has been implicated in numerous aspects of development and disease (Ingham and McMahon, 2001; McMahon et al., 2003). In vertebrates and *Drosophila*, Patched represses the seven transmembrane G protein-coupled receptor-like protein Smoothened, in turn inhibiting signal transduction. When Hedgehog binds Patched, Patched is inhibited, relieving the repression of Smoothened. Determining the role of the SSD in Patched has focused on these two functions- responding to Hedgehog and inhibiting Smoothened.

Biochemical evidence suggests that Patched directly binds Hedgehog (Marigo et al., 1996). Interestingly, Hedgehog undergoes several post-translational modifications, including the addition of a cholesterol molecule (Mann and Beachy, 2004). Thus, one possible function for the Patched SSD is to bind or respond to cholesterol-modified Hedgehog. Two pieces of evidence counter this idea. First, in both vertebrates and *Drosophila*, use of a non-cholesterol modified Hedgehog only disrupts the range of Hedgehog signaling, but cells, and therefore Patched, are still able to respond to the signal (Lewis et al., 2001; Porter et al., 1996; Zeng et al., 2001). Secondly, as discussed below, mutations in the Patched SSD apparently do not alter the Hedgehog-Patched interaction (Martin et al., 2001; Strutt et al., 2001).

On the other hand, the Patched SSD may play a role in mediating the interaction between Patched and Smoothened. Initial experiments suggested that Patched might directly bind Smoothened (Stone et al., 1996), but these results could not be repeated and were apparently just due to the artificial

overexpression Patched and Smoothened during the experiements (Alcedo et al., 2000; Incardona et al., 2002; Johnson et al., 2000). Instead, Patched may alter the subcellular localization of Smoothened, which in turn undergoes alternative post-translational modification (Figure 1.4). Patched is normally found both at the plasma membrane and in endosomes (Capdevila et al., 1994; Martin et al., 2001; Strutt et al., 2001). Upon binding to Hedgehog, Patched is preferentially endocytosed along with Hedgehog (Figure 1.4) (Denef et al., 2000; Incardona et al., 2000; Strutt et al., 2001; Tabata and Kornberg, 1994). Conversely, exposure to Hedgehog or removal of Patched activity increases the amount of Smoothened found at the cell surface (Alcedo et al., 2000; Denef et al., 2000; Ingham et al., 2000), due to either increased transport or stability. Also, some experiments suggest that the overall amount of Smoothened is increased, while other suggest that the amount stays the same, but the Smoothened conformation changes. Exposure to Hedgehog or removal of Patched activity also increases Smoothened phosphorylation (Denef et al., 2000).

So how does Patched inhibit Smoothened? In other words, why does Hedghehog inhibition of Patched allow Smoothened to become phosphorylated and accumulate at the cell surface? Studies in cell culture suggest that in the absence of Hedgehog, Patched and Smoothened are internalized together first to endosomes and then to lysosomes where they are degraded (Figure 1.4) (Incardona et al., 2002). Consistent with this co-localization, both proteins are found in caveolae, cholesterol-rich microdomain rafts, even though only Patched directly binds caveolin (Karpen et al., 2001). In the presence of Hedgehog, on the other hand, while Patched, Smoothened, and Hedgehog are still internalized to late endosomes, only Patched and Hedgehog are sorted to lysososomes while

Smoothened is recycled to the cell surface (Figure 1.4). Thus the binding of Hedgehog to Patched influences the subcellular localization of Smoothened; Patched is no longer able to promote Smoothened sorting to the lysosome. This effect is somewhat analogous to the ability of SCAP to affect the movement of SREBP from the ER to the Golgi depending on sterol concentration.

Experiments with Patched SSD mutants suggest that this domain may mediate the regulation of Smoothened by Patched. These mutations were identified in genetic screens, and interestingly, one mutation is analogous to a mutation found in SSDs of SCAP and NPC1. ptc^{S2} results in D584N (the equivalent mutation as SCAP D443N and NPC1 D787N), while ptc^{34} results in G447R (Martin et al., 2001; Strutt et al., 2001). These SSD mutations have several properties different from other *ptc* alleles, suggesting a unique function for the Patched SSD. First, localization of these SSD mutant Patched proteins appears normal (Martin et al., 2001; Strutt et al., 2001). Second, genetic and co-localization experiments suggest that these SSD mutant Patched proteins can still bind Hedgehog (Chen and Struhl, 1996; Martin et al., 2001; Strutt et al., 2001). Third, while Patched SSD mutant and other Patched mutants have the same phenotype when homozygous (both are unable to repress Smoothened, resulting in ectopic activation of the Hedgehog signal transduction cascade), Patched SSD mutants have a dominant activity. For example, ectopic expression of the Patched SSD mutant protein results in ectopic activation of the signal transduction pathway. In other words, either these mutants can outcompete wildtype Patched to activate Smoothened or they can prevent wildtype Patched from inhibiting Smoothened. Similarly, when these mutants are placed in trans to a *patched* hypomorphic mutation, the *patched* SSD mutants result in a stronger

Hedgehog transduction derepression phenotype then when other *patched* loss-of-function mutations are used in the same assay. Finally, while overexpression of wildtype Patched decreases Smoothened levels, overexpression of SSD mutant Patched increases Smoothened. Thus SSD mutant Patched appears to protect Smoothened and allow it to activate downstream components. In sum, Patched affects Smoothened subcellular localization, in turn affecting Smoothened's stability, transport, and/or phosophorylation. The Patched SSD determines the ability of Patched to influence Smoothened.

The role of the SSD in Dispatched function is even less well understood. Dispatched is required in Hedgehog-secreting cells (Burke et al., 1999). Interestingly, Dispatched is only required for the long range signaling by cholesterol modified Hedgehog (Caspary et al., 2002; Kawakami et al., 2002; Tian et al., 2005). Signaling to cells immediately adjacent to the Hedgehog producing cells is unaffected in Dispatched mutants, and signaling by noncholesterol modified Hedgehog does not require Dispatched. While the role of the Dispatched SSD has not been elucidated, Dispatched appears to be required for secretion or release of the Hedgehog signal.

That Patched and Dispatched function in part to regulate intracellular trafficking is supported by analysis of the *C. elegans* homologs. It has been long assumed that worms lack conventional Hedgehog signaling. The genome lacks an apparent Smoothened homolog; while the genome encodes Hedgehog-like proteins, the signaling portion of these proteins is quite divergent from *Drosophila* and vertebrate Hedgehog; and mutations in the worm homolog of the family of transcription factors that mediate Hedgehog signaling, Gli/Ci, result in phenotypes different than Patched and Dispatched homolog mutant phenotypes

(Burglin, 1996; Zarkower and Hodgkin, 1992; Zugasti et al., 2005). Thus, in the absence of Hedgehog signalling, what do these proteins do? The Patched homolog, *ptc-1*, is required for germline cytokinesis, and the PTC-1 proteins localizes to vesicles at the growing cleavage furrow (Kuwabara et al., 2000). Thus *ptc-1* appears to be required for the sorting of vesicles to the growing cleavage furrow. Similarly, the Dispatched homolog, CHE-14, localizes to vesicles and the apical plasma membranes in several cells types (Michaux et al., 2000). Based on this localization and *che-14* mutant phenotypes, these authors suggest that *che-14* is required for exocytosis. For example, the secretion of the cuticle is defective in these mutant worms. Thus, in the apparent absence of classical Hedgehog signaling, worm Patched and Dispatched homologs appear to play roles in vesicle transport, perhaps reflecting a primitive role for the SSD in these proteins.

Conclusions

The SSD containing proteins are required for diverse processes. The SSD, however, appears to play a conserved function in these proteins. In each case, the proteins are affected by sterols. SCAP conformation, protein binding ability, and ultimately subcellular localization are affected by sterol concentrations. Similarly, HMGCR conformation, protein binding ability, and ultimately protein degradation are affected by sterol concentrations. Also, Patched subcellular localization and association with another protein, Smoothened, are affected upon binding to cholesterol modified Hedgehog.

A possible role for this five-transmembrane domain is to affect protein association with sterol-enriched membrane sub-domains. This association would

be dependent on sterol concentrations or the presence of a sterol-conjugated binding partner. This sub-membrane localization would affect the proteins' ability to associate with other proteins, such as SREBP, INSIGs, COPII proteins, or Smoothened.

In this thesis, I characterize the first member of a previously uncharacterized subfamily of SSD containing proteins, called Patched-related proteins. A model of Patched-related protein function should incorporate the apparent conserved function of the SSD. The Patched-related protein's subcellular localization and association with other proteins may be dependent on association with sterol-enriched membrane microdomains.

References

Adams, C. M., Goldstein, J. L., and Brown, M. S. (2003). Cholesterol-induced conformational change in SCAP enhanced by Insig proteins and mimicked by cationic amphiphiles. Proc Natl Acad Sci U S A *100*, 10647-10652.

Adams, C. M., Reitz, J., De Brabander, J. K., Feramisco, J. D., Li, L., Brown, M. S., and Goldstein, J. L. (2004). Cholesterol and 25-hydroxycholesterol inhibit activation of SREBPs by different mechanisms, both involving SCAP and Insigs. J Biol Chem *279*, 52772-52780.

Alcedo, J., Zou, Y., and Noll, M. (2000). Posttranscriptional regulation of smoothened is part of a self-correcting mechanism in the Hedgehog signaling system. Mol Cell *6*, 457-465.

Bae, S. H., Lee, J. N., Fitzky, B. U., Seong, J., and Paik, Y. K. (1999). Cholesterol biosynthesis from lanosterol. Molecular cloning, tissue distribution, expression, chromosomal localization, and regulation of rat 7-dehydrocholesterol reductase, a Smith-Lemli-Opitz syndrome-related protein. J Biol Chem *274*, 14624-14631.

Bargmann, C. I. (1993). Genetic and cellular analysis of behavior in C. elegans. Annu Rev Neurosci *16*, 47-71.

Bargmann, C. I., Mori, I., ed. (1997). Chemotaxis and thermotaxis. (Cold Spring Harbor, NY, Cold Spring Harbor Laboratory Press).

Baum, P. D., and Garriga, G. (1997). Neuronal migrations and axon fasciculation are disrupted in ina-1 integrin mutants. Neuron *19*, 51-62.

Bayless, K. J., and Davis, G. E. (2002). The Cdc42 and Rac1 GTPases are required for capillary lumen formation in three-dimensional extracellular matrices. J Cell Sci *115*, 1123-1136.

Bayless, K. J., Salazar, R., and Davis, G. E. (2000). RGD-dependent vacuolation and lumen formation observed during endothelial cell morphogenesis in three-dimensional fibrin matrices involves the alpha(v)beta(3) and alpha(5)beta(1) integrins. Am J Pathol *156*, 1673-1683.

Behr, M., Riedel, D., and Schuh, R. (2003). The claudin-like megatrachea is essential in septate junctions for the epithelial barrier function in Drosophila. Dev Cell *5*, 611-620.

Berry, K. L., Bulow, H. E., Hall, D. H., and Hobert, O. (2003). A C. elegans CLIC-like protein required for intracellular tube formation and maintenance. Science *302*, 2134-2137.

Bhat, M. A., Rios, J. C., Lu, Y., Garcia-Fresco, G. P., Ching, W., St Martin, M., Li, J., Einheber, S., Chesler, M., Rosenbluth, J., *et al.* (2001). Axon-glia interactions and the domain organization of myelinated axons requires neurexin IV/Caspr/Paranodin. Neuron *30*, 369-383.

Bradley, P. L., and Andrew, D. J. (2001). ribbon encodes a novel BTB/POZ protein required for directed cell migration in Drosophila melanogaster. Development *128*, 3001-3015.

Brown, A. J., Sun, L., Feramisco, J. D., Brown, M. S., and Goldstein, J. L. (2002). Cholesterol addition to ER membranes alters conformation of SCAP, the SREBP escort protein that regulates cholesterol metabolism. Mol Cell *10*, 237-245.

Buechner, M. (2002). Tubes and the single C. elegans excretory cell. Trends Cell Biol *12*, 479-484.

Buechner, M., Hall, D. H., Bhatt, H., and Hedgecock, E. M. (1999). Cystic canal mutants in Caenorhabditis elegans are defective in the apical membrane domain of the renal (excretory) cell. Dev Biol *214*, 227-241.

Burglin, T. R. (1996). Warthog and groundhog, novel families related to hedgehog. Curr Biol *6*, 1047-1050.

Burke, R., Nellen, D., Bellotto, M., Hafen, E., Senti, K. A., Dickson, B. J., and Basler, K. (1999). Dispatched, a novel sterol-sensing domain protein dedicated to the release of cholesterol-modified hedgehog from signaling cells. Cell *99*, 803-815.

Burkitt, H. G., Young, B., Heath, J.W. (1993). Wheater's Functional Histology (Edinburgh, UK, Churchill Livingstone Press).

Capdevila, J., Pariente, F., Sampedro, J., Alonso, J. L., and Guerrero, I. (1994). Subcellular localization of the segment polarity protein patched suggests an interaction with the wingless reception complex in Drosophila embryos. Development *120*, 987-998.

Carstea, E. D., Morris, J. A., Coleman, K. G., Loftus, S. K., Zhang, D., Cummings, C., Gu, J., Rosenfeld, M. A., Pavan, W. J., Krizman, D. B., *et al.* (1997). Niemann-Pick C1 disease gene: homology to mediators of cholesterol homeostasis. Science *277*, 228-231.

Caspary, T., Garcia-Garcia, M. J., Huangfu, D., Eggenschwiler, J. T., Wyler, M. R., Rakeman, A. S., Alcorn, H. L., and Anderson, K. V. (2002). Mouse Dispatched homolog1 is required for long-range, but not juxtacrine, Hh signaling. Curr Biol *12*, 1628-1632.

Chan, J. R., Watkins, T. A., Cosgaya, J. M., Zhang, C., Chen, L., Reichardt, L. F., Shooter, E. M., and Barres, B. A. (2004). NGF controls axonal receptivity to myelination by Schwann cells or oligodendrocytes. Neuron *43*, 183-191.

Charles, P., Hernandez, M. P., Stankoff, B., Aigrot, M. S., Colin, C., Rougon, G., Zalc, B., and Lubetzki, C. (2000). Negative regulation of central nervous system myelination by polysialylated-neural cell adhesion molecule. Proc Natl Acad Sci U S A *97*, 7585-7590.

Chen, Y., and Struhl, G. (1996). Dual roles for patched in sequestering and transducing Hedgehog. Cell *87*, 553-563.

Chin, D. J., Gil, G., Faust, J. R., Goldstein, J. L., Brown, M. S., and Luskey, K. L. (1985). Sterols accelerate degradation of hamster 3-hydroxy-3-methylglutaryl coenzyme A reductase encoded by a constitutively expressed cDNA. Mol Cell Biol *5*, 634-641.

Colman, D. R., Kreibich, G., Frey, A. B., and Sabatini, D. D. (1982). Synthesis and incorporation of myelin polypeptides into CNS myelin. J Cell Biol *95*, 598-608.

Corey, D. P., Garcia-Anoveros, J., Holt, J. R., Kwan, K. Y., Lin, S. Y., Vollrath, M. A., Amalfitano, A., Cheung, E. L., Derfler, B. H., Duggan, A., *et al.* (2004). TRPA1 is a candidate for the mechanosensitive transduction channel of vertebrate hair cells. Nature *432*, 723-730.

Cruz, J. C., and Chang, T. Y. (2000). Fate of endogenously synthesized cholesterol in Niemann-Pick type C1 cells. J Biol Chem *275*, 41309-41316.

Davies, J. P., Chen, F. W., and Ioannou, Y. A. (2000). Transmembrane molecular pump activity of Niemann-Pick C1 protein. Science *290*, 2295-2298.

Davies, J. P., and Ioannou, Y. A. (2000). Topological analysis of Niemann-Pick C1 protein reveals that the membrane orientation of the putative sterol-sensing domain is identical to those of 3-hydroxy-3-methylglutaryl-CoA reductase and sterol regulatory element binding protein cleavage-activating protein. J Biol Chem *275*, 24367-24374.

Davis, G. E., and Camarillo, C. W. (1996). An alpha 2 beta 1 integrin-dependent pinocytic mechanism involving intracellular vacuole formation and coalescence regulates capillary lumen and tube formation in three-dimensional collagen matrix. Exp Cell Res *224*, 39-51.

de Vries, H., Schrage, C., and Hoekstra, D. (1998). An apical-type trafficking pathway is present in cultured oligodendrocytes but the sphingolipid-enriched myelin membrane is the target of a basolateral-type pathway. Mol Biol Cell *9*, 599-609.

Demerens, C., Stankoff, B., Logak, M., Anglade, P., Allinquant, B., Couraud, F., Zalc, B., and Lubetzki, C. (1996). Induction of myelination in the central nervous system by electrical activity. Proc Natl Acad Sci U S A *93*, 9887-9892.

Denef, N., Neubuser, D., Perez, L., and Cohen, S. M. (2000). Hedgehog induces opposite changes in turnover and subcellular localization of patched and smoothened. Cell *102*, 521-531.

Driscoll, M. a. K., J. (1997). Mechanotransduction. In C. elegans II, B. J. M. a. J. R. P. D.L. Riddle, ed. (Cold Spring Harbor, NY, Cold Spring Harbor Laboratory Press), pp. 645-677.

Dyson, S. E., Jones, D. G., and Kendrick, W. L. (1976). Some observations on the ultrastructure of developing rat cerebral capillaries. Cell Tissue Res *173*, 529-542.

Englund, C., Steneberg, P., Falileeva, L., Xylourgidis, N., and Samakovlis, C. (2002). Attractive and repulsive functions of Slit are mediated by different receptors in the Drosophila trachea. Development *129*, 4941-4951.

Espenshade, P. J., Li, W. P., and Yabe, D. (2002). Sterols block binding of COPII proteins to SCAP, thereby controlling SCAP sorting in ER. Proc Natl Acad Sci U S A *99*, 11694-11699.

Faust, J. R., Luskey, K. L., Chin, D. J., Goldstein, J. L., and Brown, M. S. (1982). Regulation of synthesis and degradation of 3-hydroxy-3-methylglutaryl-coenzyme A reductase by low density lipoprotein and 25-hydroxycholesterol in UT-1 cells. Proc Natl Acad Sci U S A *79*, 5205-5209.

Feltri, M. L., Graus Porta, D., Previtali, S. C., Nodari, A., Migliavacca, B., Cassetti, A., Littlewood-Evans, A., Reichardt, L. F., Messing, A., Quattrini, A., *et al.* (2002). Conditional disruption of beta 1 integrin in Schwann cells impedes interactions with axons. J Cell Biol *156*, 199-209.

Feltri, M. L., Scherer, S. S., Nemni, R., Kamholz, J., Vogelbacker, H., Scott, M. O., Canal, N., Quaranta, V., and Wrabetz, L. (1994). Beta 4 integrin expression in myelinating Schwann cells is polarized, developmentally regulated and axonally dependent. Development *120*, 1287-1301.

Feramisco, J. D., Radhakrishnan, A., Ikeda, Y., Reitz, J., Brown, M. S., and Goldstein, J. L. (2005). Intramembrane aspartic acid in SCAP protein governs cholesterol-induced conformational change. Proc Natl Acad Sci U S A *102*, 3242-3247.

Fernandez-Valle, C., Gorman, D., Gomez, A. M., and Bunge, M. B. (1997). Actin plays a role in both changes in cell shape and gene-expression associated with Schwann cell myelination. J Neurosci *17*, 241-250.

Fitzky, B. U., Glossmann, H., Utermann, G., and Moebius, F. F. (1999). Molecular genetics of the Smith-Lemli-Opitz syndrome and postsqualene sterol metabolism. Curr Opin Lipidol *10*, 123-131.

Folkman, J., and Haudenschild, C. (1980). Angiogenesis in vitro. Nature *288*, 551-556.

Fujita, M., Hawkinson, D., King, K. V., Hall, D. H., Sakamoto, H., and Buechner, M. (2003). The role of the ELAV homologue EXC-7 in the development of the Caenorhabditis elegans excretory canals. Dev Biol *256*, 290-301.

Gao, J., Estrada, L., Cho, S., Ellis, R. E., and Gorski, J. L. (2001). The Caenorhabditis elegans homolog of FGD1, the human Cdc42 GEF gene

responsible for faciogenital dysplasia, is critical for excretory cell morphogenesis. Hum Mol Genet *10*, 3049-3062.

Gettner, S. N., Kenyon, C., and Reichardt, L. F. (1995). Characterization of beta pat-3 heterodimers, a family of essential integrin receptors in C. elegans. J Cell Biol *129*, 1127-1141.

Gil, G., Faust, J. R., Chin, D. J., Goldstein, J. L., and Brown, M. S. (1985). Membrane-bound domain of HMG CoA reductase is required for sterol-enhanced degradation of the enzyme. Cell *41*, 249-258.

Gilmour, D. T., Maischein, H. M., and Nusslein-Volhard, C. (2002). Migration and function of a glial subtype in the vertebrate peripheral nervous system. Neuron *34*, 577-588.

Gobel, V., Barrett, P. L., Hall, D. H., and Fleming, J. T. (2004). Lumen morphogenesis in C. elegans requires the membrane-cytoskeleton linker erm-1. Dev Cell *6*, 865-873.

Gotoh, N., Kusumi, T., Tsujimoto, H., Wada, T., and Nishino, T. (1999). Topological analysis of an RND family transporter, MexD of Pseudomonas aeruginosa. FEBS Lett *458*, 32-36.

Griffiths, I. R., Mitchell, L. S., McPhilemy, K., Morrison, S., Kyriakides, E., and Barrie, J. A. (1989). Expression of myelin protein genes in Schwann cells. J Neurocytol *18*, 345-352.

Guillemin, K., Groppe, J., Ducker, K., Treisman, R., Hafen, E., Affolter, M., and Krasnow, M. A. (1996). The pruned gene encodes the Drosophila serum response factor and regulates cytoplasmic outgrowth during terminal branching of the tracheal system. Development *122*, 1353-1362.

Gyllensten, L., and Malmfors, T. (1963). Myelinization of the optic nerve and its dependence on visual function--a quantitative investigation in mice. J Embryol Exp Morphol *11*, 255-266.

Hartenstein, V., and Posakony, J. W. (1989). Development of adult sensilla on the wing and notum of Drosophila melanogaster. Development *107*, 389-405.

Hatten, M. E. (1999). Central nervous system neuronal migration. Annu Rev Neurosci *22*, 511-539.

Hedgecock, E. M., Culotti, J. G., Hall, D. H., and Stern, B. D. (1987). Genetics of cell and axon migrations in Caenorhabditis elegans. Development *100*, 365-382.

Hemphala, J., Uv, A., Cantera, R., Bray, S., and Samakovlis, C. (2003). Grainy head controls apical membrane growth and tube elongation in response to Branchless/FGF signalling. Development *130*, 249-258.

Hidalgo, A., Kinrade, E. F., and Georgiou, M. (2001). The Drosophila neuregulin vein maintains glial survival during axon guidance in the CNS. Dev Cell *1*, 679-690.

Higgins, M. E., Davies, J. P., Chen, F. W., and Ioannou, Y. A. (1999). Niemann-Pick C1 is a late endosome-resident protein that transiently associates with lysosomes and the trans-Golgi network. Mol Genet Metab *68*, 1-13.

Hogan, B. L., and Kolodziej, P. A. (2002). Organogenesis: molecular mechanisms of tubulogenesis. Nat Rev Genet *3*, 513-523.

Hooper, J. E., and Scott, M. P. (1989). The Drosophila patched gene encodes a putative membrane protein required for segmental patterning. Cell *59*, 751-765.

Hua, X., Nohturfft, A., Goldstein, J. L., and Brown, M. S. (1996). Sterol resistance in CHO cells traced to point mutation in SREBP cleavage-activating protein. Cell *87*, 415-426.

Incardona, J. P., Gruenberg, J., and Roelink, H. (2002). Sonic hedgehog induces the segregation of patched and smoothened in endosomes. Curr Biol *12*, 983-995.

Incardona, J. P., Lee, J. H., Robertson, C. P., Enga, K., Kapur, R. P., and Roelink, H. (2000). Receptor-mediated endocytosis of soluble and membrane-tethered Sonic hedgehog by Patched-1. Proc Natl Acad Sci U S A *97*, 12044-12049.

Ingham, P. W., and McMahon, A. P. (2001). Hedgehog signaling in animal development: paradigms and principles. Genes Dev *15*, 3059-3087.

Ingham, P. W., Nystedt, S., Nakano, Y., Brown, W., Stark, D., van den Heuvel, M., and Taylor, A. M. (2000). Patched represses the Hedgehog signalling

pathway by promoting modification of the Smoothened protein. Curr Biol *10*, 1315-1318.

Isaac, D. D., and Andrew, D. J. (1996). Tubulogenesis in Drosophila: a requirement for the trachealess gene product. Genes Dev *10*, 103-117.

Itoh, K., Stevens, B., Schachner, M., and Fields, R. D. (1995). Regulated expression of the neural cell adhesion molecule L1 by specific patterns of neural impulses. Science *270*, 1369-1372.

Izaddoost, S., Nam, S. C., Bhat, M. A., Bellen, H. J., and Choi, K. W. (2002). Drosophila Crumbs is a positional cue in photoreceptor adherens junctions and rhabdomeres. Nature *416*, 178-183.

Jazwinska, A., Ribeiro, C., and Affolter, M. (2003). Epithelial tube morphogenesis during Drosophila tracheal development requires Piopio, a luminal ZP protein. Nat Cell Biol *5*, 895-901.

Jingami, H., Brown, M. S., Goldstein, J. L., Anderson, R. G., and Luskey, K. L. (1987). Partial deletion of membrane-bound domain of 3-hydroxy-3-methylglutaryl coenzyme A reductase eliminates sterol-enhanced degradation and prevents formation of crystalloid endoplasmic reticulum. J Cell Biol *104*, 1693-1704.

Johnson, R. L., Milenkovic, L., and Scott, M. P. (2000). In vivo functions of the patched protein: requirement of the C terminus for target gene inactivation but not Hedgehog sequestration. Mol Cell *6*, 467-478.

Kaplan, M. R., Meyer-Franke, A., Lambert, S., Bennett, V., Duncan, I. D., Levinson, S. R., and Barres, B. A. (1997). Induction of sodium channel clustering by oligodendrocytes. Nature *386*, 724-728.

Karpen, H. E., Bukowski, J. T., Hughes, T., Gratton, J. P., Sessa, W. C., and Gailani, M. R. (2001). The sonic hedgehog receptor patched associates with caveolin-1 in cholesterol-rich microdomains of the plasma membrane. J Biol Chem *276*, 19503-19511.

Kawakami, T., Kawcak, T., Li, Y. J., Zhang, W., Hu, Y., and Chuang, P. T. (2002). Mouse dispatched mutants fail to distribute hedgehog proteins and are defective in hedgehog signaling. Development *129*, 5753-5765.

Ko, D. C., Gordon, M. D., Jin, J. Y., and Scott, M. P. (2001). Dynamic movements of organelles containing Niemann-Pick C1 protein: NPC1 involvement in late endocytic events. Mol Biol Cell *12*, 601-614.

Kobayashi, T., Beuchat, M. H., Lindsay, M., Frias, S., Palmiter, R. D., Sakuraba, H., Parton, R. G., and Gruenberg, J. (1999). Late endosomal membranes rich in lysobisphosphatidic acid regulate cholesterol transport. Nat Cell Biol *1*, 113-118.

Kumagai, H., Chun, K. T., and Simoni, R. D. (1995). Molecular dissection of the role of the membrane domain in the regulated degradation of 3-hydroxy-3-methylglutaryl coenzyme A reductase. J Biol Chem *270*, 19107-19113.

Kuo, Y. M., Jones, N., Zhou, B., Panzer, S., Larson, V., and Beckendorf, S. K. (1996). Salivary duct determination in Drosophila: roles of the EGF receptor signalling pathway and the transcription factors fork head and trachealess. Development *122*, 1909-1917.

Kuwabara, P. E., and Labouesse, M. (2002). The sterol-sensing domain: multiple families, a unique role? Trends Genet *18*, 193-201.

Kuwabara, P. E., Lee, M. H., Schedl, T., and Jefferis, G. S. (2000). A C. elegans patched gene, ptc-1, functions in germ-line cytokinesis. Genes Dev *14*, 1933-1944.

Lewis, P. M., Dunn, M. P., McMahon, J. A., Logan, M., Martin, J. F., St-Jacques, B., and McMahon, A. P. (2001). Cholesterol modification of sonic hedgehog is required for long-range signaling activity and effective modulation of signaling by Ptc1. Cell *105*, 599-612.

Liscum, L., Finer-Moore, J., Stroud, R. M., Luskey, K. L., Brown, M. S., and Goldstein, J. L. (1985). Domain structure of 3-hydroxy-3-methylglutaryl coenzyme A reductase, a glycoprotein of the endoplasmic reticulum. J Biol Chem *260*, 522-530.

Liscum, L., Ruggiero, R. M., and Faust, J. R. (1989). The intracellular transport of low density lipoprotein-derived cholesterol is defective in Niemann-Pick type C fibroblasts. J Cell Biol *108*, 1625-1636.

Lubarsky, B., and Krasnow, M. A. (2003). Tube morphogenesis: making and shaping biological tubes. Cell *112*, 19-28.

Ma, D., Cook, D. N., Alberti, M., Pon, N. G., Nikaido, H., and Hearst, J. E. (1995). Genes acrA and acrB encode a stress-induced efflux system of Escherichia coli. Mol Microbiol *16*, 45-55.

Malathi, K., Higaki, K., Tinkelenberg, A. H., Balderes, D. A., Almanzar-Paramio, D., Wilcox, L. J., Erdeniz, N., Redican, F., Padamsee, M., Liu, Y., *et al.* (2004). Mutagenesis of the putative sterol-sensing domain of yeast Niemann Pick C-related protein reveals a primordial role in subcellular sphingolipid distribution. J Cell Biol *164*, 547-556.

Mann, R. K., and Beachy, P. A. (2004). Novel lipid modifications of secreted protein signals. Annu Rev Biochem *73*, 891-923.

Marigo, V., Davey, R. A., Zuo, Y., Cunningham, J. M., and Tabin, C. J. (1996). Biochemical evidence that patched is the Hedgehog receptor. Nature *384*, 176-179.

Martin, V., Carrillo, G., Torroja, C., and Guerrero, I. (2001). The sterol-sensing domain of Patched protein seems to control Smoothened activity through Patched vesicular trafficking. Curr Biol *11*, 601-607.

Mauch, D. H., Nagler, K., Schumacher, S., Goritz, C., Muller, E. C., Otto, A., and Pfrieger, F. W. (2001). CNS synaptogenesis promoted by glia-derived cholesterol. Science *294*, 1354-1357.

McKeown, C., Praitis, V., and Austin, J. (1998). sma-1 encodes a betaH-spectrin homolog required for Caenorhabditis elegans morphogenesis. Development *125*, 2087-2098.

McMahon, A. P., Ingham, P. W., and Tabin, C. J. (2003). Developmental roles and clinical significance of hedgehog signaling. Curr Top Dev Biol *53*, 1-114.

Michaux, G., Gansmuller, A., Hindelang, C., and Labouesse, M. (2000). CHE-14, a protein with a sterol-sensing domain, is required for apical sorting in C. elegans ectodermal epithelial cells. Curr Biol *10*, 1098-1107.

Millard, E. E., Gale, S. E., Dudley, N., Zhang, J., Schaffer, J. E., and Ory, D. S. (2005). The sterol-sensing domain of the Niemann-Pick C1 (NPC1) protein regulates trafficking of low density lipoprotein cholesterol. J Biol Chem *280*, 28581-28590.

Millard, E. E., Srivastava, K., Traub, L. M., Schaffer, J. E., and Ory, D. S. (2000). Niemann-pick type C1 (NPC1) overexpression alters cellular cholesterol homeostasis. J Biol Chem *275*, 38445-38451.

Mobius, W., van Donselaar, E., Ohno-Iwashita, Y., Shimada, Y., Heijnen, H. F., Slot, J. W., and Geuze, H. J. (2003). Recycling compartments and the internal vesicles of multivesicular bodies harbor most of the cholesterol found in the endocytic pathway. Traffic *4*, 222-231.

Mombaerts, P. (1999). Seven-transmembrane proteins as odorant and chemosensory receptors. Science *286*, 707-711.

Montell, C. (2003). Thermosensation: hot findings make TRPNs very cool. Curr Biol *13*, R476-478.

Montesano, R., Schaller, G., and Orci, L. (1991). Induction of epithelial tubular morphogenesis in vitro by fibroblast-derived soluble factors. Cell *66*, 697-711.

Mori, I., and Ohshima, Y. (1995). Neural regulation of thermotaxis in Caenorhabditis elegans. Nature *376*, 344-348.

Mosley-Bishop, K. L., Li, Q., Patterson, L., and Fischer, J. A. (1999). Molecular analysis of the klarsicht gene and its role in nuclear migration within differentiating cells of the Drosophila eye. Curr Biol *9*, 1211-1220.

Mostov, K. E., Verges, M., and Altschuler, Y. (2000). Membrane traffic in polarized epithelial cells. Curr Opin Cell Biol *12*, 483-490.

Myat, M. M., and Andrew, D. J. (2002). Epithelial tube morphology is determined by the polarized growth and delivery of apical membrane. Cell *111*, 879-891.

Nakano, Y., Guerrero, I., Hidalgo, A., Taylor, A., Whittle, J. R., and Ingham, P. W. (1989). A protein with several possible membrane-spanning domains encoded by the Drosophila segment polarity gene patched. Nature *341*, 508-513.

Neufeld, E. B., Wastney, M., Patel, S., Suresh, S., Cooney, A. M., Dwyer, N. K., Roff, C. F., Ohno, K., Morris, J. A., Carstea, E. D., *et al.* (1999). The Niemann-Pick C1 protein resides in a vesicular compartment linked to retrograde transport of multiple lysosomal cargo. J Biol Chem *274*, 9627-9635.

Nies, D. H., and Silver, S. (1995). Ion efflux systems involved in bacterial metal resistances. J Ind Microbiol *14*, 186-199.

Nikaido, H., Basina, M., Nguyen, V., and Rosenberg, E. Y. (1998). Multidrug efflux pump AcrAB of Salmonella typhimurium excretes only those beta-lactam antibiotics containing lipophilic side chains. J Bacteriol *180*, 4686-4692.

Nohturfft, A., Brown, M. S., and Goldstein, J. L. (1998a). Sterols regulate processing of carbohydrate chains of wild-type SREBP cleavage-activating protein (SCAP), but not sterol-resistant mutants Y298C or D443N. Proc Natl Acad Sci U S A *95*, 12848-12853.

Nohturfft, A., Brown, M. S., and Goldstein, J. L. (1998b). Topology of SREBP cleavage-activating protein, a polytopic membrane protein with a sterol-sensing domain. J Biol Chem *273*, 17243-17250.

Nohturfft, A., DeBose-Boyd, R. A., Scheek, S., Goldstein, J. L., and Brown, M. S. (1999). Sterols regulate cycling of SREBP cleavage-activating protein (SCAP) between endoplasmic reticulum and Golgi. Proc Natl Acad Sci U S A *96*, 11235-11240.

Nohturfft, A., Hua, X., Brown, M. S., and Goldstein, J. L. (1996). Recurrent G-to-A substitution in a single codon of SREBP cleavage-activating protein causes sterol resistance in three mutant Chinese hamster ovary cell lines. Proc Natl Acad Sci U S A *93*, 13709-13714.

Nohturfft, A., Yabe, D., Goldstein, J. L., Brown, M. S., and Espenshade, P. J. (2000). Regulated step in cholesterol feedback localized to budding of SCAP from ER membranes. Cell *102*, 315-323.

O'Brien, L. E., Jou, T. S., Pollack, A. L., Zhang, Q., Hansen, S. H., Yurchenco, P., and Mostov, K. E. (2001). Rac1 orientates epithelial apical polarity through effects on basolateral laminin assembly. Nat Cell Biol *3*, 831-838.

O'Brien, L. E., Zegers, M. M., and Mostov, K. E. (2002). Opinion: Building epithelial architecture: insights from three-dimensional culture models. Nat Rev Mol Cell Biol *3*, 531-537.

Ohgami, N., Ko, D. C., Thomas, M., Scott, M. P., Chang, C. C., and Chang, T. Y. (2004). Binding between the Niemann-Pick C1 protein and a photoactivatable

cholesterol analog requires a functional sterol-sensing domain. Proc Natl Acad Sci U S A *101*, 12473-12478.

Olender, E. H., and Simon, R. D. (1992). The intracellular targeting and membrane topology of 3-hydroxy-3-methylglutaryl-CoA reductase. J Biol Chem *267*, 4223-4235.

Paul, S. M., Ternet, M., Salvaterra, P. M., and Beitel, G. J. (2003). The Na+/K+ ATPase is required for septate junction function and epithelial tube-size control in the Drosophila tracheal system. Development *130*, 4963-4974.

Pellikka, M., Tanentzapf, G., Pinto, M., Smith, C., McGlade, C. J., Ready, D. F., and Tepass, U. (2002). Crumbs, the Drosophila homologue of human CRB1/RP12, is essential for photoreceptor morphogenesis. Nature *416*, 143-149.

Podratz, J. L., Rodriguez, E., and Windebank, A. J. (2001). Role of the extracellular matrix in myelination of peripheral nerve. Glia *35*, 35-40.

Pollack, A. L., Runyan, R. B., and Mostov, K. E. (1998). Morphogenetic mechanisms of epithelial tubulogenesis: MDCK cell polarity is transiently rearranged without loss of cell-cell contact during scatter factor/hepatocyte growth factor-induced tubulogenesis. Dev Biol *204*, 64-79.

Pollack, G. S., and Balakrishnan, R. (1997). Taste sensilla of flies: function, central neuronal projections, and development. Microsc Res Tech *39*, 532-546.

Porter, J. A., Young, K. E., and Beachy, P. A. (1996). Cholesterol modification of hedgehog signaling proteins in animal development. Science *274*, 255-259.

Previtali, S. C., Nodari, A., Taveggia, C., Pardini, C., Dina, G., Villa, A., Wrabetz, L., Quattrini, A., and Feltri, M. L. (2003). Expression of laminin receptors in schwann cell differentiation: evidence for distinct roles. J Neurosci *23*, 5520-5530.

Puri, V., Watanabe, R., Dominguez, M., Sun, X., Wheatley, C. L., Marks, D. L., and Pagano, R. E. (1999). Cholesterol modulates membrane traffic along the endocytic pathway in sphingolipid-storage diseases. Nat Cell Biol *1*, 386-388.

Radhakrishnan, A., Sun, L. P., Kwon, H. J., Brown, M. S., and Goldstein, J. L. (2004). Direct binding of cholesterol to the purified membrane region of SCAP: mechanism for a sterol-sensing domain. Mol Cell *15*, 259-268.

Ribeiro, C., Neumann, M., and Affolter, M. (2004). Genetic control of cell intercalation during tracheal morphogenesis in Drosophila. Curr Biol *14*, 2197-2207.

Riddle, D. L., Albert. P.S., ed. (1997). Genetic and environmental regulation of dauer larva development. (Cold Spring Harbor, NY, Cold Spring Harbor Laboratory Press).

Ross, M. H. R., L.J.; Kaye, I.K. (1995). Histology: A text and atlas, 3rd edn (baltimore, williams & Wilkins).

Saher, G., Brugger, B., Lappe-Siefke, C., Mobius, W., Tozawa, R., Wehr, M. C., Wieland, F., Ishibashi, S., and Nave, K. A. (2005). High cholesterol level is essential for myelin membrane growth. Nat Neurosci *8*, 468-475.

Saito, F., Moore, S. A., Barresi, R., Henry, M. D., Messing, A., Ross-Barta, S. E., Cohn, R. D., Williamson, R. A., Sluka, K. A., Sherman, D. L., *et al.* (2003). Unique role of dystroglycan in peripheral nerve myelination, nodal structure, and sodium channel stabilization. Neuron *38*, 747-758.

Sakai, J., Nohturfft, A., Cheng, D., Ho, Y. K., Brown, M. S., and Goldstein, J. L. (1997). Identification of complexes between the COOH-terminal domains of sterol regulatory element-binding proteins (SREBPs) and SREBP cleavage-activating protein. J Biol Chem *272*, 20213-20221.

Samakovlis, C., Hacohen, N., Manning, G., Sutherland, D. C., Guillemin, K., and Krasnow, M. A. (1996). Development of the Drosophila tracheal system occurs by a series of morphologically distinct but genetically coupled branching events. Development *122*, 1395-1407.

Schoenwolf, G. C., and Smith, J. L. (1990). Mechanisms of neurulation: traditional viewpoint and recent advances. Development *109*, 243-270.

Scholey, J. M., Ou, G., Snow, J., and Gunnarson, A. (2004). Intraflagellar transport motors in Caenorhabditis elegans neurons. Biochem Soc Trans *32*, 682-684.

Schweisguth, F., Gho, M., and Lecourtois, M. (1996). Control of cell fate choices by lateral signaling in the adult peripheral nervous system of Drosophila melanogaster. Dev Genet *18*, 28-39.

Scott, K. (2005). Taste recognition: food for thought. Neuron *48*, 455-464.

Sever, N., Song, B. L., Yabe, D., Goldstein, J. L., Brown, M. S., and DeBose-Boyd, R. A. (2003a). Insig-dependent ubiquitination and degradation of mammalian 3-hydroxy-3-methylglutaryl-CoA reductase stimulated by sterols and geranylgeraniol. J Biol Chem *278*, 52479-52490.

Sever, N., Yang, T., Brown, M. S., Goldstein, J. L., and DeBose-Boyd, R. A. (2003b). Accelerated degradation of HMG CoA reductase mediated by binding of insig-1 to its sterol-sensing domain. Mol Cell *11*, 25-33.

Shanbhag , S. R., Müller, B., Steinbrecht, R.A (1999). Atlas of olfactory organs of Drosophila melanogaster 1. Types, external organization, innervation and distribution of
olfactory sensilla. International Journal of Insect Morphology and Embryology *28*, 377-397.

Shanbhag , S. R., Müller, B., Steinbrecht, R.A (2000). Atlas of olfactory organs of Drosophila melanogaster 2. Internal organization and cellular architecture of olfactory sensilla. Arthropod Structure & Development *29*, 211-229.

Shearer, A. G., and Hampton, R. Y. (2005). Lipid-mediated, reversible misfolding of a sterol-sensing domain protein. Embo J *24*, 149-159.

Sherman, D. L., and Brophy, P. J. (2005). Mechanisms of axon ensheathment and myelin growth. Nat Rev Neurosci *6*, 683-690.

Sherman, D. L., Fabrizi, C., Gillespie, C. S., and Brophy, P. J. (2001). Specific disruption of a schwann cell dystrophin-related protein complex in a demyelinating neuropathy. Neuron *30*, 677-687.

Shim, K., Blake, K. J., Jack, J., and Krasnow, M. A. (2001). The Drosophila ribbon gene encodes a nuclear BTB domain protein that promotes epithelial migration and morphogenesis. Development *128*, 4923-4933.

Skalnik, D. G., Narita, H., Kent, C., and Simoni, R. D. (1988). The membrane domain of 3-hydroxy-3-methylglutaryl-coenzyme A reductase confers endoplasmic reticulum localization and sterol-regulated degradation onto beta-galactosidase. J Biol Chem *263*, 6836-6841.

Song, B. L., Javitt, N. B., and DeBose-Boyd, R. A. (2005). Insig-mediated degradation of HMG CoA reductase stimulated by lanosterol, an intermediate in the synthesis of cholesterol. Cell Metab *1*, 179-189.

Stevens, B., and Fields, R. D. (2000). Response of Schwann cells to action potentials in development. Science *287*, 2267-2271.

Stevens, B., Porta, S., Haak, L. L., Gallo, V., and Fields, R. D. (2002). Adenosine: a neuron-glial transmitter promoting myelination in the CNS in response to action potentials. Neuron *36*, 855-868.

Stone, D. M., Hynes, M., Armanini, M., Swanson, T. A., Gu, Q., Johnson, R. L., Scott, M. P., Pennica, D., Goddard, A., Phillips, H., *et al.* (1996). The tumour-suppressor gene patched encodes a candidate receptor for Sonic hedgehog. Nature *384*, 129-134.

Strutt, H., Thomas, C., Nakano, Y., Stark, D., Neave, B., Taylor, A. M., and Ingham, P. W. (2001). Mutations in the sterol-sensing domain of Patched suggest a role for vesicular trafficking in Smoothened regulation. Curr Biol *11*, 608-613.

Sutherland, D., Samakovlis, C., and Krasnow, M. A. (1996). branchless encodes a Drosophila FGF homolog that controls tracheal cell migration and the pattern of branching. Cell *87*, 1091-1101.

Suzuki, N., Buechner, M., Nishiwaki, K., Hall, D. H., Nakanishi, H., Takai, Y., Hisamoto, N., and Matsumoto, K. (2001). A putative GDP-GTP exchange factor is required for development of the excretory cell in Caenorhabditis elegans. EMBO Rep *2*, 530-535.

Sym, M., Basson, M., and Johnson, C. (2000). A model for niemann-pick type C disease in the nematode Caenorhabditis elegans. Curr Biol *10*, 527-530.

Tabata, T., and Kornberg, T. B. (1994). Hedgehog is a signaling protein with a key role in patterning Drosophila imaginal discs. Cell *76*, 89-102.

Tauber, H., Waehneldt, T. V., and Neuhoff, V. (1980). Myelination in rabbit optic nerves is accelerated by artificial eye opening. Neurosci Lett *16*, 235-238.

Thanassi, D. G., Cheng, L. W., and Nikaido, H. (1997). Active efflux of bile salts by Escherichia coli. J Bacteriol *179*, 2512-2518.

Tian, H., Jeong, J., Harfe, B. D., Tabin, C. J., and McMahon, A. P. (2005). Mouse Disp1 is required in sonic hedgehog-expressing cells for paracrine activity of the cholesterol-modified ligand. Development *132*, 133-142.

Troemel, E. R. (1999). Chemosensory signaling in C. elegans. Bioessays *21*, 1011-1020.

Tseng, T. T., Gratwick, K. S., Kollman, J., Park, D., Nies, D. H., Goffeau, A., and Saier, M. H., Jr. (1999). The RND permease superfamily: an ancient, ubiquitous and diverse family that includes human disease and development proteins. J Mol Microbiol Biotechnol *1*, 107-125.

Uv, A., Cantera, R., and Samakovlis, C. (2003). Drosophila tracheal morphogenesis: intricate cellular solutions to basic plumbing problems. Trends Cell Biol *13*, 301-309.

Vanier, M. T., Rodriguez-Lafrasse, C., Rousson, R., Duthel, S., Harzer, K., Pentchev, P. G., Revol, A., and Louisot, P. (1991). Type C Niemann-Pick disease: biochemical aspects and phenotypic heterogeneity. Dev Neurosci *13*, 307-314.

Vega-Salas, D. E., Salas, P. J., and Rodriguez-Boulan, E. (1987). Modulation of the expression of an apical plasma membrane protein of Madin-Darby canine kidney epithelial cells: cell-cell interactions control the appearance of a novel intracellular storage compartment. J Cell Biol *104*, 1249-1259.

Vega-Salas, D. E., Salas, P. J., and Rodriguez-Boulan, E. (1988). Exocytosis of vacuolar apical compartment (VAC): a cell-cell contact controlled mechanism for the establishment of the apical plasma membrane domain in epithelial cells. J Cell Biol *107*, 1717-1728.

Ward, S., Thomson, N., White, J. G., and Brenner, S. (1975). Electron microscopical reconstruction of the anterior sensory anatomy of the nematode Caenorhabditis elegans.?2UU. J Comp Neurol *160*, 313-337.

Watari, H., Blanchette-Mackie, E. J., Dwyer, N. K., Watari, M., Neufeld, E. B., Patel, S., Pentchev, P. G., and Strauss, J. F., 3rd (1999). Mutations in the leucine zipper motif and sterol-sensing domain inactivate the Niemann-Pick C1 glycoprotein. J Biol Chem *274*, 21861-21866.

Wilk, R., Weizman, I., and Shilo, B. Z. (1996). trachealess encodes a bHLH-PAS protein that is an inducer of tracheal cell fates in Drosophila. Genes Dev *10*, 93-102.

Wodarz, A. (2002). Establishing cell polarity in development. Nat Cell Biol *4*, E39-44.

Wojtanik, K. M., and Liscum, L. (2003). The transport of low density lipoprotein-derived cholesterol to the plasma membrane is defective in NPC1 cells. J Biol Chem *278*, 14850-14856.

Woldeyesus, M. T., Britsch, S., Riethmacher, D., Xu, L., Sonnenberg-Riethmacher, E., Abou-Rebyeh, F., Harvey, R., Caroni, P., and Birchmeier, C. (1999). Peripheral nervous system defects in erbB2 mutants following genetic rescue of heart development. Genes Dev *13*, 2538-2548.

Wolff, J. R., and Bar, T. (1972). 'Seamless' endothelia in brain capillaries during development of the rat's cerebral cortex. Brain Res *41*, 17-24.

Wood, P. M., Schachner, M., and Bunge, R. P. (1990). Inhibition of Schwann cell myelination in vitro by antibody to the L1 adhesion molecule. J Neurosci *10*, 3635-3645.

Wu, V. M., and Beitel, G. J. (2004). A junctional problem of apical proportions: epithelial tube-size control by septate junctions in the Drosophila tracheal system. Curr Opin Cell Biol *16*, 493-499.

Yabe, D., Brown, M. S., and Goldstein, J. L. (2002). Insig-2, a second endoplasmic reticulum protein that binds SCAP and blocks export of sterol regulatory element-binding proteins. Proc Natl Acad Sci U S A *99*, 12753-12758.

Yang, T., Espenshade, P. J., Wright, M. E., Yabe, D., Gong, Y., Aebersold, R., Goldstein, J. L., and Brown, M. S. (2002). Crucial step in cholesterol homeostasis: sterols promote binding of SCAP to INSIG-1, a membrane protein that facilitates retention of SREBPs in ER. Cell *110*, 489-500.

Yu, W., O'Brien, L. E., Wang, F., Bourne, H., Mostov, K. E., and Zegers, M. M. (2003). Hepatocyte growth factor switches orientation of polarity and mode of movement during morphogenesis of multicellular epithelial structures. Mol Biol Cell *14*, 748-763.

Zarkower, D., and Hodgkin, J. (1992). Molecular analysis of the C. elegans sex-determining gene tra-1: a gene encoding two zinc finger proteins. Cell *70*, 237-249.

Zeng, X., Goetz, J. A., Suber, L. M., Scott, W. J., Jr., Schreiner, C. M., and Robbins, D. J. (2001). A freely diffusible form of Sonic hedgehog mediates long-range signalling. Nature *411*, 716-720.

Zervas, M., Somers, K. L., Thrall, M. A., and Walkley, S. U. (2001). Critical role for glycosphingolipids in Niemann-Pick disease type C. Curr Biol *11*, 1283-1287.

Zhang, M., Dwyer, N. K., Neufeld, E. B., Love, D. C., Cooney, A., Comly, M., Patel, S., Watari, H., Strauss, J. F., 3rd, Pentchev, P. G., *et al.* (2001). Sterol-modulated glycolipid sorting occurs in niemann-pick C1 late endosomes. J Biol Chem *276*, 3417-3425.

Zugasti, O., Rajan, J., and Kuwabara, P. E. (2005). The function and expansion of the Patched- and Hedgehog-related homologs in C. elegans. Genome Res *15*, 1402-1410.

Figure 1.1

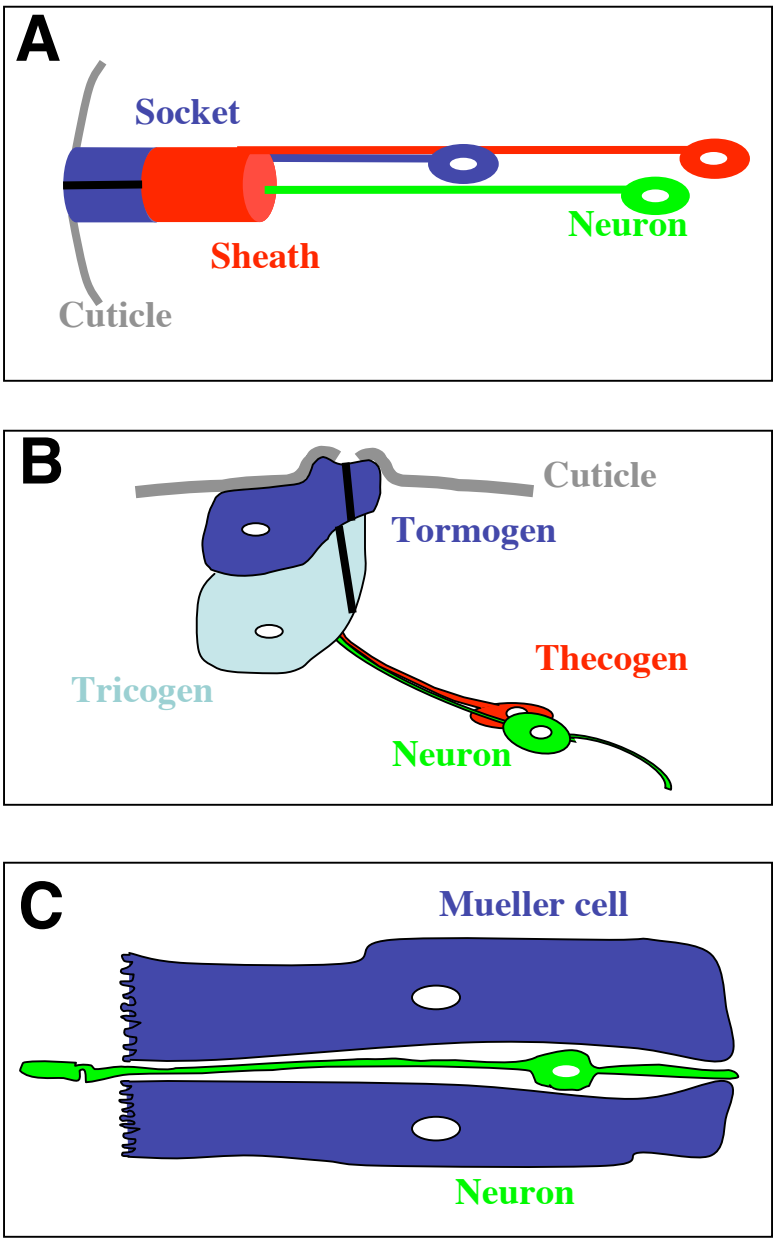
A
Socket
Neuron
Sheath
Cuticle
B
Cuticle
Tormogen
Thecogen
Tricogen
Neuron
C
Mueller cell
Neuron

Figure 1.1. Sensory Organ Morphologies. Cartoon representations of sensory organs from *C. elegans*, *Drosophila*, and humans. (A) Simplified representation of the *C. elegans* amphid sensory organ. Each amphid is composed of three cell types- the sheath, socket, and twelve neurons. Only one neuron is shown for simplicity. Anterior is to the left. (B) Representation of the four cell types of the *Drosophila* external mechanosensory organ. For simplicity, the bristle portion of the trichogen is not shown. (C) Relationship between Mueller cells and a photoreceptor neuron in the human retina. Mueller cells surround the photoreceptor neurons, except the distal portion of the dendrites, which extend beyond the Mueller cells.

Figure 1.2

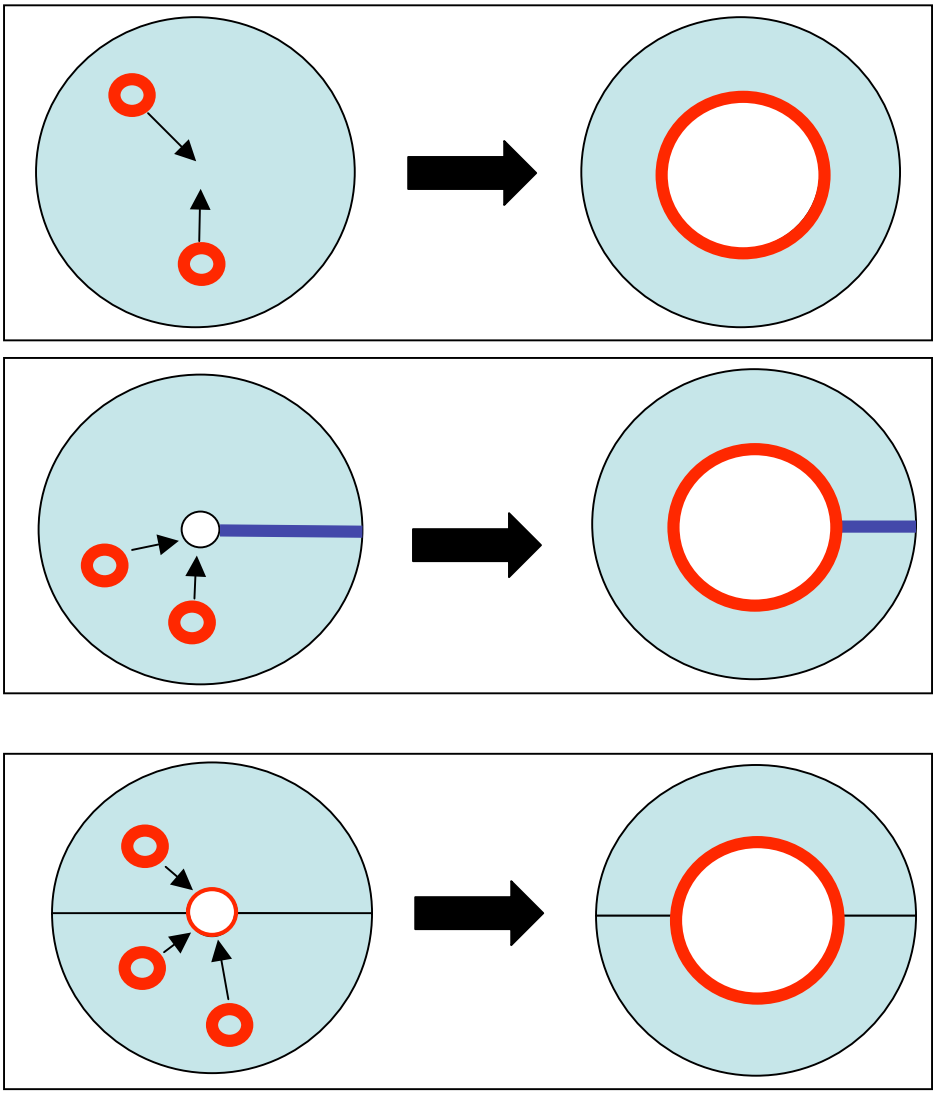

Figure 1.2. The role of vesicles during lumen formation. (A) Vesicles may coalesce inside cells to form a seamless intracellular lumen. The luminal membrane has a surface of apical character (red). This process may be required during lumen formation in capillary forming endothelial cells, the *C. elegans* excretory canal cell, and the *C. elegans* amphid sheath cell. (B) After autocellular junction (blue line) formation, vesicles may coalesce to form a lumen in tubes such as in the *C. elegans* socket cell and some branches of the *Drosophila* trachea. (C) The apical surfaces of two neighboring cells face one another, and this surface is increased by the addition of vesicles. This process may occur during lumen formation in the *Drosophila* salivary glands, the *C. elegans* vulva, cultured MDCK cells.

Figure 1.3

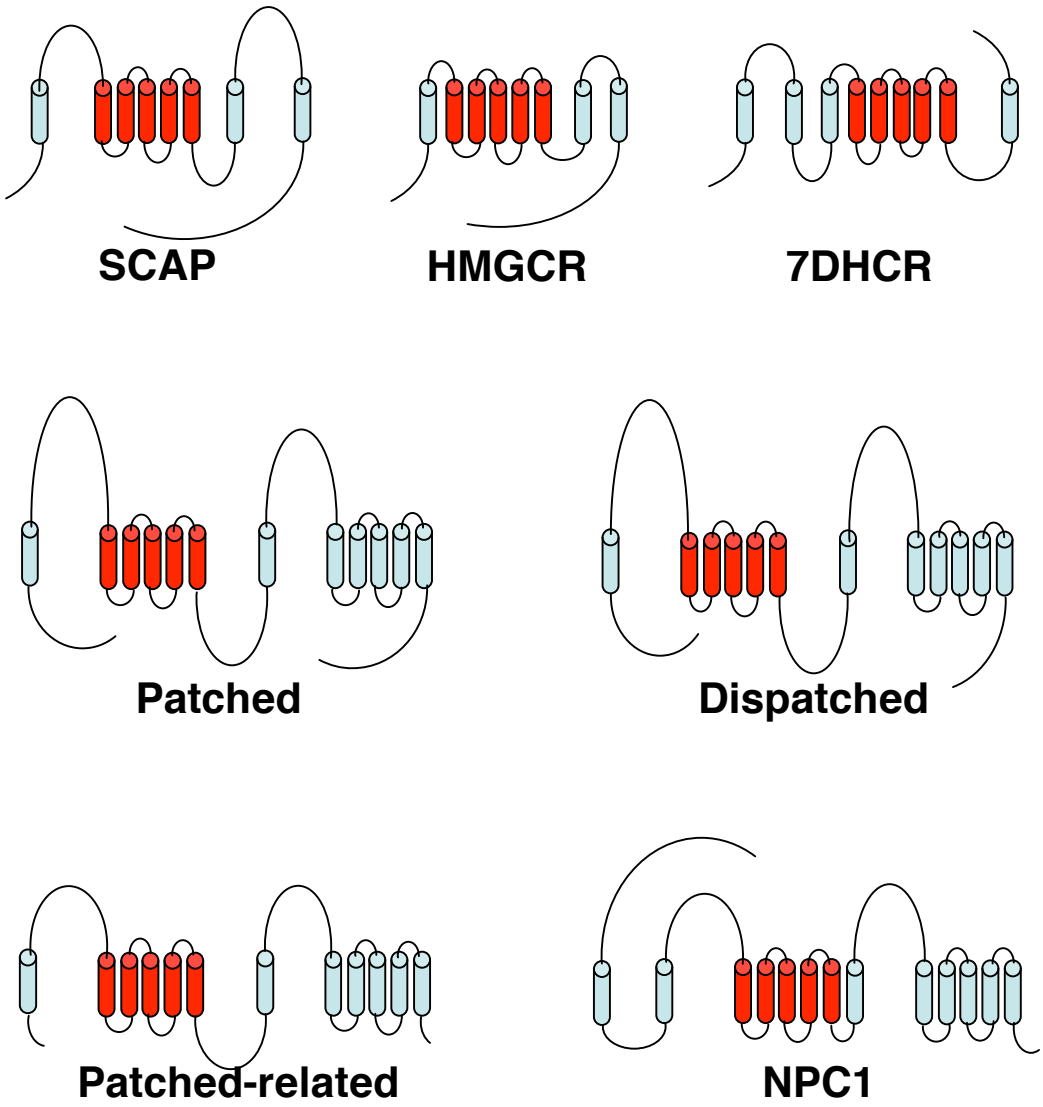

Figure 1.3. Sterol-Sensing Domain Containing Proteins. Schematic representations of the seven classes of sterol-sensing domain (SSD) containing proteins. The transmembrane domains are represented by cylinders, and the SSDs are in red.

Figure 1.4

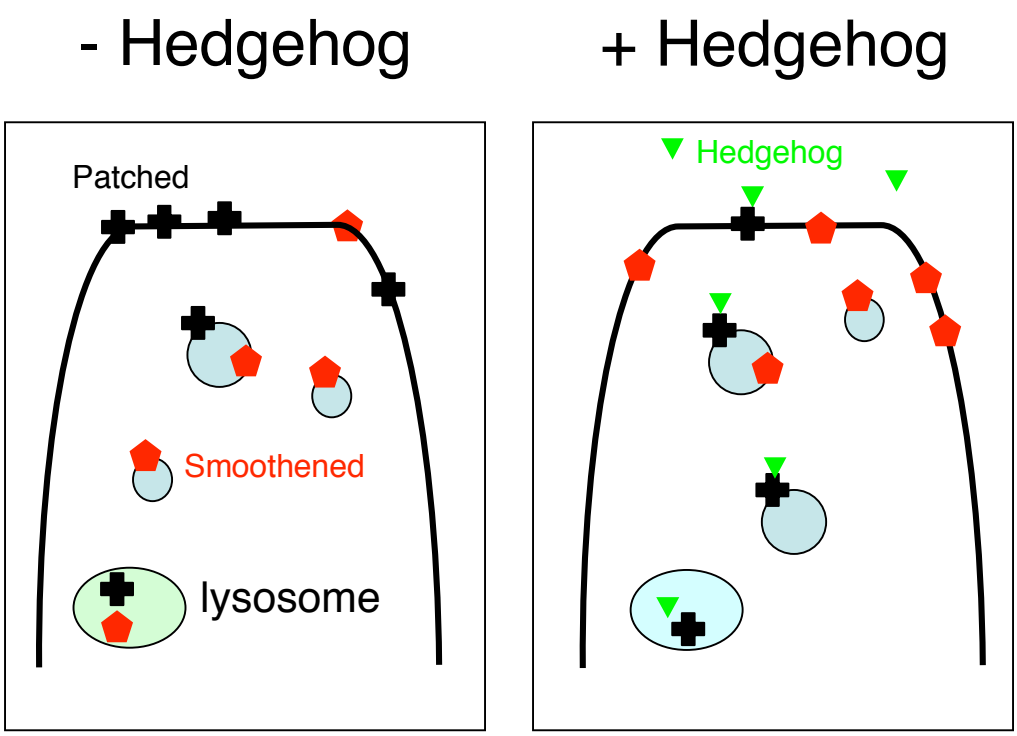

Figure 1.4. Patched and Smoothened localization during Hedgehog signaling. (A) In the absence of Hedgehog, Patched (black crosses) localizes to the plasma membrane and endosomes. Patched is internalized with Smoothened (red pentagons) to endosomes and lysosomes. (B) In the presence of Hedgehog (green triangles), Patched and Hedgehog are internalized together. Only Patched and Hedgehog appear to sort to lysosomes. Smoothened levels may increase at the cell surface, while Patched levels decrease. For simplicity, other components of the signal transduction pathaway, such as the transcription factor Gli/ Cubitus interruptus, are not shown.

Chapter 2

C. elegans daf-6 encodes a Patched-related protein required for lumen formation

Elliot A. Perens and Shai Shaham

Summary

Sensory organs are often composed of neuronal sensory endings accommodated in a lumen formed by ensheathing epithelia or glia. Here we show that lumen formation in the *C. elegans* amphid sensory organ requires the gene *daf-6*. *daf-6* encodes a Patched-related protein that localizes to the luminal surfaces of the amphid channel and other *C. elegans* tubes. While *daf-6* mutants display only amphid lumen defects, animals defective for both *daf-6* and the *Dispatched* gene *che-14* exhibit defects in all tubular structures that express *daf-6*. Furthermore, DAF-6 protein is mislocalized, and lumen morphogenesis is abnormal, in mutants with defective sensory neuron endings. We propose that amphid lumen morphogenesis is coordinated by neuron-derived cues and a DAF-6/CHE-14 system that regulates vesicle dynamics during tubulogenesis.

Introduction

Sensory structures in many organisms share a common morphology in which sensory neuron endings extend through a tubular channel formed by their associated glia or epithelia (Ward et al., 1975; Burkitt et al., 1993; Jan and Jan, 1993). The formation of all biological tubes, both unicellular and multicellular, has been proposed to occur by a common mechanism in which vesicles within the tube-forming cells coalesce at a luminal surface of apical character (Lubarsky and Krasnow, 2003). This process has been observed in cultured Madin-Darby canine kidney (MDCK) cells (Montesano et al., 1991), capillary forming endothelial cells (Folkman and Haudenschild, 1980; Davis and Camarillo, 1996), *Drosophila* salivary glands (Myat and Andrew, 2002), and the *C. elegans* excretory canal cell (Berry et al., 2003). Some of the molecular players controlling tube outgrowth and branching are known (Ghabrial et al., 2003), however, the initial steps of lumen formation and morphogenesis are poorly understood. Glia that ensheath sensory neuron endings, as well as glia that myelinate or ensheath neuronal projections, must regulate their lumen dimensions to accommodate precisely their resident neuronal processes. Little is known about how this is accomplished (Wegner, 2000), although it is reasonable to hypothesize that neuronal processes induce aspects of glial lumen formation.

To understand sensory organ morphogenesis and specifically glial lumen formation, we have been studying the *C. elegans* amphid sensory organ. *C. elegans* possesses two bilaterally symmetric amphids, located at the anterior tip of the animal (Ward et al., 1975). Each amphid consists of twelve sensory neurons and two ensheathing glial cells, the sheath and socket cells. Amphid neurons have two projections: an axon that extends into the nerve ring, and a dendrite

that extends to the anterior tip of the animal. Amphid sheath and socket glia also extend anterior processes that contact amphid neuron dendritic projections (Ward et al., 1975). At the tip of the nose all neuronal sensory endings are ensheathed by the sheath glia (Figure 2.1A, B). Four of the amphid neurons, which mediate chemotaxis to volatile chemicals and thermotaxis (Bargmann et al., 1993; Mori and Ohshima, 1995), have dendritic endings that are fully embedded within the amphid sheath glia. These endings are lodged within tightly fitting glial channels in which the neurons are surrounded by an undefined matrix material. The remaining eight neurons end in sensory cilia that house sensory receptors and signal transduction molecules (Troemel, 1999), and gain access to the outside environment by extending through the main amphid channel: a bipartite channel, formed anteriorly by the socket cell and continued posteriorly by the sheath cell (Figure 2.1A; Ward et al., 1975). This matrix-filled channel is open to the outside environment and is supported by an array of cytoskeletal elements (Ward et al., 1975). We will henceforth refer to this channel as the amphid channel. Amphid channel neurons are required for avoidance of high osmolarity solutions, chemosensation of water-soluble solutes, and mechanosensation (Bargmann and Mori, 1997; Driscoll and Kaplan, 1997). They also sense dauer pheromone (Riddle and Albert, 1997).

Animals defective in the *daf-6* gene (*daf*, dauer formation defective) were first isolated because of their inability to enter an alternative developmental state known as dauer (Riddle et al., 1981). Dauer animals exhibit prolonged life span and resistance to environmental insults, and entry into dauer is mediated by a continuously released pheromone (Riddle and Albert, 1997). Four previous observations suggest that *daf-6* mutants have amphid channel defects. First, *daf-6*

mutants are defective in sensory functions that require direct exposure of channel neurons to the outside environment (Albert et al., 1981; Perkins et al., 1986), but respond normally to volatile odorants, temperature changes, and mechanosensory stimuli (Albert et al., 1981; Bargmann et al., 1993; Perkins et al., 1986) that do not require direct access to the animal's surroundings. Second, in wild-type animals, channel neurons can take up lipophilic dyes such as DiO from the environment (Hedgecock et al., 1985), however, *daf-6* mutants are dye-filling defective (Starich et al., 1995). Third, Herman (1987) demonstrated by mosaic analysis that *daf-6* function is required in the amphid sheath glia and not in the amphid neurons for dye uptake. Fourth, using scanning electron microscopy, an open channel could not be found in the anterior tip of the amphid in *daf-6* mutants (Albert et al., 1981).

Here we describe our studies of *daf-6*. We show that although amphid channel neurons reside within a sheath cell channel in *daf-6* mutants, this channel fails to open anteriorly, consistent with a role for *daf-6* in lumen formation. We also demonstrate that *daf-6* function is required in the amphid around the time of lumen formation. We cloned *daf-6*, and showed that it encodes a novel, conserved, sterol-sensing domain (SSD) containing protein related to the vertebrate and *Drosophila* Hedgehog receptor Patched. A rescuing DAF-6::GFP fusion protein localized to the luminal surfaces of several tubular structures, including those of the amphid sheath glia. Studies of mutant forms of DAF-6 revealed crucial residues and domains required for DAF-6 localization, function, or both. *daf-6* interacted genetically with the *Dispatched* gene *che-14*, suggesting that both genes function in concert in the same cells to regulate lumen formation in multiple *C. elegans* tubes. Finally, we uncovered a requirement for ciliated

endings of amphid sensory neurons in regulating DAF-6 localization and morphogenesis of the amphid channel. Our results provide insights into the genetic basis of tube morphogenesis during sensory organ formation and during tubulogenesis in general. Furthermore, our results demonstrate a dedicated role for a member of a previously uncharacterized subfamily of SSD containing proteins in lumen formation.

Results

daf-6 Mutants Contain Abnormal Amphid Channels

To understand the cause of the sensory deficits in *daf-6* mutants, we examined in detail the structure of the amphids in these animals. Specifically, we examined animals that were homozygous for the strong loss-of-function allele *daf-6*(*e1377*), and that also harbored two transgenes: a P_{vap-1} DsRed transgene, expressing DsRed fluorescent protein in amphid sheath glia under control of the *vap-1* gene promoter (*vap*, venom allergen protein; B. Westlund, Cambria Biosciences, personal communication); and a P_{gcy-5}GFP transgene, expressing green fluorescent protein (GFP) in the right ASE (ASER) amphid channel neuron (Yu et al., 1997). We identified three major defects in these animals, all consistent with a failure of the sheath glia portion of the amphid channel to open to the outside environment.

First, whereas the sheath channel was open in wild-type animals (Figures 2.1C, D), this portion of the channel was not open in *daf-6(e1377)* animals (Figures 2.1E, F). Consistent with this observation, the ASER neuronal cilia of wild-type animals extended through the sheath channel (Figures 2.1C, D), but the ASER cilia of *daf-6(e1377)* animals did not penetrate this channel, and remained encased within the sheath cell (Figures 2.1E, F). A similar defect was observed for the ADF neurons in *daf-6*(*e1377*) animals (Figures 2.1G-J).

Second, whereas wild-type cilia were invariably straight (Figures 2.1C, G), the ASER cilia, as well as other cilia, in *daf-6*(*e1377*) animals tended to curve near the tip of the nose (Figures 2.1E, I), seemingly in response to the physical constraint of being embedded within the sheath cell.

Third, *daf-6*(*e1377*) adults contained vacuolar structures within the sheath cell (Figures 2.1E, F) that were not seen in wild-type adults (Figures 2.1C, D). These structures may correspond to the vacuoles seen previously in electron microscope (EM) sections of adult *daf-6*(*e1377*) animals (Albert et al., 1981). To determine the contents of these abnormal vacuoles, we examined *daf-6*(*e1377*) animals expressing the VAP-1::GFP protein in the sheath glia. VAP-1 is a component of the sheath glia matrix: an undefined matrix encased in large secretory vesicles that is secreted from the amphid sheath glia into the channel surrounding the sensory cilia (M. Heiman and S. Shaham, unpublished results; Figures 2.1B, K, L; Ward et al., 1975). VAP-1 can be released from animals to their surroundings (B. Westlund, Cambria Biosciences, personal communication), presumably through the amphid channel. As shown in Figures 1M and 1N, VAP-1::GFP accumulated within sheath cell vacuolar structures, suggesting that these vacuoles contained matrix material. Consistent with this observation, EM cross sections of *daf-6*(*e1377*) animals revealed that amphid cilia resided within a sheath cell pocket containing material similar in electron density to matrix material (Figure 1O). These findings are also consistent with a failure to open the sheath glia channel: failure in channel opening prevents matrix material from exiting the animal, causing this material to accumulate at the anterior tip of the sheath glia.

Our studies of *daf-6(e1377)* adults suggested that vacuole accumulation and bending of ciliated sensory endings may both be secondary manifestations of the closure of the sheath cell channel in these animals. If this were true, these defects might not be present early during channel development. Indeed, as shown in Table 2.1, young *daf-6*(*e1377*) larvae did not frequently contain bent

cilia or vacuolar structures. However, dye uptake was completely blocked at all stages, indicating that channel neurons always lacked access to the outside environment. Furthermore, animals at all stages observed also exhibited fully penetrant defects in cilia extension through the sheath channel into the socket channel (Table 2.1, Figures 2.1G-J).

These studies suggest that failure to generate an open sheath cell channel, and the resulting failure of the amphid cilia to gain exposure to the external environment, are the primary causes of the sensory deficits of *daf-6* mutants. Using EM and fluorescent microscopy we could not detect any major changes in the AWC sheath-embedded neuron or in the tight-fitting channel that surrounds this cell (data not shown; Albert et al., 1981), consistent with the ability of *daf-6*(*e1377*) animals to sense volatile odorants (Bargmann et al., 1993).

Sensory defects in *daf-6* mutants could be due not only to structural defects in the amphid channel, but also to defects in the sensory cilia themselves. To determine whether cilia components were misexpressed or mislocalized in *daf-6*(*e1377*) animals, we examined localization of the cilia resident protein CHE-2 (Fujiwara et al., 1999). Functional CHE-2::GFP protein was localized to amphid cilia in 20/20 *daf-6(e1377)* animals examined, even when these were severely bent, suggesting that at least one cilia component was properly localized in these mutants.

daf-6 Encodes a Patched-Related Protein

To understand how *daf-6* controls amphid channel opening, we cloned the gene. *daf-6* was previously mapped between the *unc-3* and *unc-7* genes on linkage group X (Herman, 1984). We established strains homozygous for the *daf-6*(*e1377*)

allele and containing extrachromosomal arrays of candidate cosmids from the genetic interval described above. The dye-filling defect of *daf-6(e1377)* animals was fully rescued by 2 extrachromosomal arrays containing cosmid F31F6 (data not shown). A predicted gene in this region, F31F6.5 (also named *ptr-7*; Kuwabara et al., 2000), encodes a protein related to the sterol-sensing domain (SSD) containing protein Patched. To determine whether *daf-6* is F31F6.5/*ptr*-7, we generated a 9 kb subclone of F31F6 that included 3 kb of sequence upstream of the predicted *ptr-7* ATG, and the full *ptr-7* genomic coding region fused to GFP. Four transmitted lines containing this subclone rescued the dye uptake defect of *daf-6(e1377)* animals as efficiently as the cosmid (data not shown; see also Figure 5).

To confirm that *daf-6* is F31F6.5/*ptr-7* and to determine the location and nature of molecular lesions associated with each of the seven known *daf-6* alleles, we determined the sequences of all exons and exon/intron boundaries of *ptr-7* in each *daf-6* allele (Figure 2.2A). Amphid neurons in animals homozygous for either the *e1377*, *n1543*, or *m506* alleles were completely defective in dye uptake (Figure 2.2B). *e1377* contains a nonsense mutation that is predicted to result in production of a severely truncated protein; *m506* appears to contain a deletion at the 5′ end of the gene; and *n1543* is a 23 bp deletion that shifts the coding region out of frame. The remaining four alleles still conferred some ability to take up dye from the environment, and their associated molecular lesions are consistent with the generation of some functional protein (Figures 2.2A, B).

A 2968 bp full-length *daf-6* cDNA clone was obtained from Yuji Kohara (DNA Data Bank of Japan). The *daf-6* intron/exon organization was determined by comparing the cDNA and genomic sequences (Figure 2.2A). Conceptual

translation of the *daf-6* cDNA suggested that *daf-6* encodes a 913 amino-acid protein similar to the Hedgehog receptor Patched, and is one of 24 such *ptr* (patched related) genes in the *C. elegans* genome (Kuwabara et al., 2000; Kuwabara and Labouesse, 2002). All PTR proteins contain a sterol-sensing domain (SSD), a conserved 180 amino-acid sequence predicted to form five transmembrane domains (Kuwabara and Labouesse, 2002). While other SSD containing proteins are important regulators of development or metabolic homeostasis, no function has been assigned to PTR proteins.

DAF-6 and other PTR proteins are most closely related to the Patched, Dispatched, and NPC1 SSD containing proteins, and the similarity to these proteins is greatest within the putative SSDs (Figure 2.2D, E). For example, DAF-6 SSD is 20.5% identical to the SSD of the *C. elegans* Patched protein PTC-1, 19.3% identical to the *C. elegans* NPC-1 SSD, and 21.1% identical to the SSD of the *C. elegans* Dispatched protein CHE-14. Like Patched and Dispatched, DAF-6 contains 12 predicted transmembrane domains with large extracellular loops between transmembrane segments 1 and 2, and 7 and 8 (Kuwabara et al., 2000).

DAF-6 has potential *Drosophila* and human orthologs (Figures 2.2C-E). Within their putative SSDs, DAF-6 is 36.8% identical to *Drosophila* AAF57274, 33.9% identical to human FLJ44037, and 24% identical to human FLJ30296. Sequence comparisons suggest that these proteins are more closely related to DAF-6 than to other SSD containing proteins (Figure 2.2C; Kuwabara et al., 2000). Thus, DAF-6 seems to belong to a conserved, previously uncharacterized, subfamily of SSD containing proteins.

daf-6 Is Required During Amphid Lumen Formation

To further characterize the role of *daf-6* in amphid lumen formation, we sought to determine when *daf-6* function was required during development. We attempted to rescue the dye uptake defect of *daf-6*(*e1377*) animals at specific stages of development using a heat-inducible promoter (P_{HS}) to drive expression of the *daf-6* cDNA. *daf-6*(*e1377*) animals harboring an extrachromosomal array bearing the P_{HS}*daf-6* transgene were incubated at 34ºC for 30 minutes and assayed for dye uptake four days later. As shown in Figure 3, expression of the *daf-6* cDNA at either the comma or 1.5-fold stages of embryogenesis corrected the dye uptake defect. Transgenic animals kept at 20ºC, as well as non-transgenic *daf-6*(*e1377*) animals subjected to a heat shock, remained dye-filling defective (Figure 2.3). These results demonstrate that *daf-6* functions around the comma and 1.5-fold stages of embryogenesis to promote amphid lumen formation. Embryos of similar stages (330 and 430 minutes post-fertilization) were previously sectioned for EM and photographed by N. Thompson, J. White, and J. Sulston (personal communication). In these sections we found that the amphid sheath glia channel was not present at 330 minutes, but was fully formed by 430 minutes (M. Heiman and S. Shaham, unpublished results). Therefore, *daf-6* functions in the amphid at the time of amphid lumen formation.

Heat-shock induced *daf-6* expression during comma stage still rescued the dye uptake defect of *daf-6*(*e1377*) animals eight days after induction (data not shown), suggesting that *daf-6* is not required for lumen maintenance. Two additional results support this conclusion. First, heat-induced expression of *daf-6* at the ball stage of embryogenesis (Figure 2.3) did not rescue *daf-6*(*e1377*) animals, even though expression induced at comma stage, approximately three

hours later, could rescue the defect. This experiment suggests that DAF-6 protein may be unstable. Second, as described below, expression of a rescuing DAF-6::GFP fusion protein was rarely observed in the amphid beyond the L1 larval stage. Thus, *daf-6* is probably required for lumen formation, and not maintenance.

DAF-6 Lines the Luminal Surfaces of Tubes

To determine in which cells *daf-6* was expressed, we examined wild-type animals containing a transgene expressing GFP under the control of a 3 kb *daf-6* promoter fragment. $P_{daf\text{-}6}$GFP was expressed in the amphid sheath glia (Figures 2.1G, I), consistent with previous mosaic analysis studies suggesting that *daf-6* functions cell autonomously in these cells (Herman, 1987). Expression was also seen in amphid socket glia (Figures 2.1G, I), the phasmid sensory organ sheath and socket cells, cells of the excretory system (the excretory canal, duct, pore, and gland cells), the vulval E and F cells, the K, K', F, and U rectal epithelial cells, and less frequently in posterior intestinal cells. These cells all form tubes, suggesting that *daf-6* might function not only in amphid channel opening, but also in lumen morphogenesis of a variety of different tubes.

We also determined the expression pattern and subcellular localization of a DAF-6::GFP fusion protein produced from a $P_{daf\text{-}6}$*daf-6*::GFP transgene able to rescue the dye uptake defects of *daf-6*(*e1377*) mutants. In the amphid, DAF-6::GFP fusion protein expression usually persisted only up to the L1 larval stage, and the protein localized to the region of the amphid channel formed by the sheath and socket cells (Figures 2.4A, B), supporting a role for DAF-6 in tube formation.

DAF-6::GFP fusion protein also localized to the luminal surfaces of tubes generated by the phasmid sheath and socket cells, excretory system cells, the vulval E and F cells, the K, K', F, and U rectal epithelial cells, and the posterior intestinal cells (Figures 2.4C-I). As in the amphid, expression in the phasmid sheath and socket cells usually did not persist beyond the L1 larval stage. Expression in vulval cells was usually restricted to the L4 larval stage, after the cells were generated and during or shortly after the vulval lumen was generated. Expression in the rectum and excretory system was observed throughout embryogenesis and larval development, but usually not during adulthood. These results suggest that DAF-6 protein may perform a dedicated function in tube formation.

Several SSD-containing proteins have been shown to associate with intracellular vesicles (Kuwabara and Labouesse, 2002). Interestingly, DAF-6::GFP protein was detected in punctate structures within the cytoplasm of expressing cells. This localization was best seen in the vulva and in the excretory canal cell (Figures 2.4D, F). Thus, DAF-6 may localize to vesicles as well.

DAF-6 Mutations Affect Function and Subcellular Localization

To define regions important for DAF-6 function and subcellular localization, we established transgenic lines expressing different mutant versions of the DAF-6::GFP rescuing protein. Patched, Dispatched, and NPC1 proteins, share sequence features with members of the resistance-nodulation-division (RND) family of prokaryotic permeases, which function as antiporters that confer resistance to drugs or heavy metals (Nies, 1995; Tseng et al., 1999). These proteins share an overall similarity in membrane topology, and contain a GxxxD

motif predicted to be important in permease function within their fourth and tenth transmembrane domains (Guan and Nakae, 2001; Ma et al., 2002; Taipale et al., 2002). Unlike Patched and Dispatched, DAF-6 protein contains only a single GxxxD motif in its putative tenth transmembrane region. Altering the conserved aspartate residue of this motif to either asparagine or alanine, as done previously for Dispatched (Ma et al., 2002) reduced but did not eliminate rescue. Intriguingly, localization of these mutant DAF-6 proteins was perturbed (most easily assessed in vulval cells; Figures 2.5B, C). These results suggest that DAF-6, and perhaps Patched and Dispatched as well, is not likely to function as an RND permease, but that the GxxxD motif may contribulte DAF-6 protein localization.

The SSD has also been suggested to regulate protein localization. For example, point mutations in the SSD disrupt the subcellular localization and function of mammalian SCAP and the function of *Drosophila* Patched (Hua et al., 1996; Martin et al, 2001; Strutt et al, 2001). To examine the role, if any, of the DAF-6 SSD, we established transgenic animals expressing DAF-6::GFP proteins containing mutations similar to those used to study the SCAP and Patched SSD. Surprisingly, these mutant proteins were still functional; however, the Gly321Arg mutation disrupted the subcellular localization of a fraction of the DAF-6::GFP proteins (Figures 2.5D and E). We had also identified a mutation in the putative signal sequence that similarly disrupted subcellular localization without disrupting function (Figure 2.5F). We determined whether the combination of this mutation with the SSD mutations would abolish function. As shown in Figures 2.5G and 2.5H, these double mutant proteins failed to rescue the *daf-6* dye-filling defect, confirming a functional role for the DAF-6 SSD in protein localization Interestingly, DAF-6 SSD alone was not sufficient to confer

appropriate DAF-6 function or subcellular localization, suggesting that function and localization are not determined entirely by this domain (Figure 2.5I).

Two of the mutants we examined demonstrated that the extracellular loops of DAF-6 protein are also essential for its function. First, deletion of the second extracellular loop (Figure 2.5J) abolished both DAF-6 function and localization. A similar deletion in *Drosophila* Patched resulted in a dominant, Hedgehog-insensitive allele (Briscoe et al., 2001). Second, the *daf-6*(*m176*) allele results in a missense mutation, converting asparagine96 to lysine in the first extracellular loop. We established transgenic animals expressing a DAF-6::GFP protein containing the identical mutation. As with the endogenous mutant protein, the mutant DAF-6::GFP protein was only able to rescue the dye-filling defect in a small percentage of expressing animals (Figure 2.5K). Surprisingly, however, subcellular localization of DAF-6::GFP was not disrupted by this mutation. This result suggests that proper DAF-6 localization is not sufficient for DAF-6 function, and that DAF-6 activity may be regulated by interaction with other proteins making contact with the first extracellular loop.

Our studies also suggest that DAF-6 protein makes specific contact with other proteins as it transits to the plasma membrane. Specifically, a DAF-6::DsRed fusion protein, which was restricted to a peri-nuclear structure, perhaps the Golgi, blocked amphid neuron dye-filling and caused amphid vacuole accumulation, as seen in *daf-6* mutants (Figure 2.5L, data not shown). These defects may have been caused by DsRed-induced aggregation of DAF-6, titrating factors with which the protein normally interacts.

Taken together, our mutagenesis studies have revealed important domains required for DAF-6 localization and function, have provided evidence

against a role for this protein (and perhaps other family members) as a permease, and have defined a specific extracellular residue that may contact other proteins required for DAF-6 activity.

daf-6 Functions with *che-14* to Regulate Lumen Formation

daf-6 has several features in common with the *C. elegans Dispatched* gene *che-14*. *daf-6* and *che-14* mutants display similar amphid defects: *che-14* mutants are dye-filling defective, dauer defective, chemotaxis defective, and osmotic avoidance defective (Perkins et al., 1986). *che-14* mutants also appear to have amphid channel defects, and amphid sheath cells in these mutants accumulate matrix-containing vacuoles (Perkins et al., 1986; Michaux et al., 2000). Furthermore, *che-14* is expressed in the amphid and phasmid sheath and socket cells, the excretory system, the vulva, and the rectum (Michaux et al., 2000). Finally, CHE-14 is a SSD containing protein.

Because of these similarities, and despite previous studies showing that Dispatched and Patched proteins function in different cell types, we surmised that *daf-6* and *che-14* might interact genetically within the same cells. To examine this possibility, we generated *che-14*(*e1960*); *daf-6(e1377)*, *che-14*(*ok193*); *daf-6(e1377*), and *che-14(e1960)*; *daf-6*(*m176*) double mutant animals. *che-14*(*ok193*) is a large deletion that, like *daf-6(e1377*), is likely to be a molecular null. *che-14*(*e1960*) is a splice-site mutant that is phenotypically indistinguishable from *che-14*(*ok193*). Double mutant animals remained defective in dye uptake, suggesting that the mutations did not suppress one another (data not shown). However, double mutants were severely egg-laying defective, often forming "bags of worms" as the embryos hatched inside the mother. For example, whereas 0/51 *daf-6*(*e1377*)

and 0/64 *che-14*(*e1960*) adults were egg-laying defective, 96/98 *che-14*(*e1960*); *daf-6*(*e1377*) adults were egg-laying defective (Figure 2.6A). Consistent with our dye filling studies, the egg-laying defect of *che-14*(*e1960*); *daf-6*(*e1377*) animals was more severe than that of *che-14*(*e1960*); *daf-6*(*m176*) animals (Figure 2.6A).

che-14; *daf-6* double mutants were also severely defective in excretory system function, exhibiting either a characteristic rod-like L1 larval lethal phenotype (Rod) or a distinctive clear (Clr) phenotype. These phenotypes are caused by an accumulation of fluid in the animal, giving it a translucent appearance. For example, whereas 0/143 *daf-6*(*e1377*) and 9/57*che-14*(*e1960*) animals displayed excretory defects, 78/86 *che-14*(*e1960*); *daf-6*(*e1377*) animals displayed such defects (Figure 2.6B). *che-14*; *daf-6* animals were also slightly more defecation defective than either single mutant alone, consistent with defects in the posterior intestine and in rectal cells (data not shown).

Taken together, these experiments suggest that *daf-6* and *che-14* interact genetically, perhaps functioning in concert to regulate lumen formation in a variety of tubular structures throughout the animal.

To examine lumen formation directly in double mutant animals, we examined the morphology of the excretory canal cell lumen in *che-14*(*e1960*); *daf-6*(*e1377*) animals containing a P_{vha-1}GFP reporter transgene. *vha-1* is expressed in the excretory canal cell (M. Buechner, personal communication). In wild-type animals, a continuous and uniform lumen extended within the two canal cell processes to the posterior tip of the animal (Figures 6C, D). *che-14(e1960); daf-6(e1377)* double mutants, however, had obvious lumen defects. While the canal cell extended two processes to the posterior tip of the animal, the lumen often only extended part way through these processes (Figures 2.6E-G). Thus, in these

double mutants, it appeared as though formation of the lumen had been initiated, but not completed. In some animals, pockets containing many vesicles were observed within the canal processes. Anterior to these pockets the lumen was generally intact, however, posterior to the pockets, regions lacking lumen were present. These results suggest that the abnormal vesicle accumulation may represent a lumen formation intermediate (Figure 2.6G).

In addition to lumen extension defects, excretory canals in some animals displayed regions with cystic features, reminiscent of a class of previously described *exc* (excretory canal abnormal) mutants (Buechner et al., 1999; Berry et al., 2003) and *erm-1* mutants (Gobel et al., 2004). Unlike *exc* and *erm-1* mutants, however, *daf-6*; *che-14* mutants predominantly exhibited lumen formation defects rather than cystic features. Thus, as in the amphid, where the sensory defects of *daf-6* mutants seemed to be due to a lumen formation defect in the sheath glia, the excretory dysfunction in *daf-6*; *che-14* double mutants appeared to result from a lumen formation defect in excretory system cells.

What is the nature of the genetic interaction between *daf-6* and *che-14*? Since both DAF-6 and CHE-14 are SSD containing proteins, it is possible that both perform identical functions. If this were the case, overexpression of *daf-6* should rescue the defects of animals homozygous for a loss-of-function mutation in *che-14*. To test this, we asked whether *che-14*(*1960*) animals carrying a P_{HS}*daf-6* transgene and subjected to a heat shock would remain defective for dye uptake. We found that overexpression of *daf-6* did not increase the frequency of amphid neuron dye-filling. Specifically, 39/43 *che-14*(*e1960*); P_{HS}*daf-6* animals heat-exposed at comma or 1.5-fold stages were dye-filling defective, and 69/91 *che-14*(*e1960*) non-transgenic heat-exposed comma or 1.5-fold embryos were

defective in dye uptake. Animals heat-shocked at other stages of development also remained dye-filling defective. Conversely, we asked whether *daf-6*(*e1377*) animals carrying a P_{HS}*che-14* transgene and subjected to a heat shock would remain defective for dye uptake. Overexpression of *che-14* did not rescue the amphid neuron dye-filling. Specifically, 66/66 *daf-6*(*e1377*); P_{HS}*che-14* animals heat-exposed at comma or 1.5-fold stages were dye-filling defective. Animals heat-shocked at other stages of development also remained dye-filling defective. (The transgene did rescue the *che-14* dye-filling defect. Specifically, 68/99 *che-14*(*e1960*) animals heat-exposed at comma or 1.5-fold stages were dye-filling defective, while only 8/28 *che-14*(*e1960*); P_{HS}*che-14* animals heat-exposed at comma or 1.5-fold stages were dye-filling defective). These results suggest that *daf-6* and *che-14* do not perform identical functions in the amphid.

We also examined whether DAF-6 was required for CHE-14 localization, and *vice versa*. We examined the subcellular localization of the proteins in the phasmid, because both *daf-6*(*e1377*) and *che-14*(*e1960*) were completely defective in dye uptake in this organ (Michaux et al., 2000). We found that DAF-6::GFP was still localized to the phasmid channel in *che-14*(*e1960*) mutants, and that CHE-14::GFP was properly localized in *daf-6*(*e1377*) mutants (data not shown). Thus, localization of either protein was independent of the other.

Neuronal Cilia Are Important for Amphid Channel Morphogenesis

Since DAF-6 protein localizes to the amphid channel lumen, we reasoned that neuronal cilia residing in this lumen might directly or indirectly regulate DAF-6 function or localization. To test this idea, we examined the amphid channels of L1 animals homozygous for mutations in the *daf-19* gene. *daf-19* encodes an RFX

transcription factor expressed in ciliated neurons (Swoboda et al., 2000). In *daf-19* mutants, neuronal sensory cilia fail to form, presumably because *daf-19* controls the expression of many cilia structural genes (Perkins et al., 1986, Swoboda et al., 2000, Li et al., 2004). We observed that, similar to *daf-6* mutants, *daf-19* mutants accumulated vacuoles containing VAP-1::GFP within the sheath glia (Figures 2.7A, B). Matrix-filled vacuoles were also previously seen in EM cross sections of *daf-19* mutants (Perkins et al., 1986). These results suggested that *daf-19* animals might harbor amphid channel defects that could, in part, be caused by abnormal DAF-6 function. To test this, we examined DAF-6::GFP localization in *daf-19* mutants. In wild-type animals, DAF-6::GFP localized to the lumen of the channel in 68/87 amphids (Figures 2.7C, D, G). In *daf-19*(*m86*) and *daf-19*(*m334*) mutants, however, DAF-6::GFP localized only to a punctate structure (Figures 2.7E, F), approximately at the location of the junction between the sheath and socket channels, in 30/37 and 59/62 amphids, respectively (Figure 2.7G). These defects were not due to a change in *daf-6* transcription within the sheath or socket glia (data not shown).

To confirm that altered DAF-6::GFP localization in *daf-19* mutants was indeed due to cilia defects, we also examined localization of this reporter protein in other cilia defective mutants (Figure 2.7G). As in *daf-19* mutants, DAF-6::GFP in the amphid localized to a punctate structure in the cilia defective mutants *che-3*, *che-11*, *che-13*, *daf-10*, and *osm-6*. Taken together, these results suggest that neuronal cilia regulate DAF-6::GFP localization in the amphid.

DAF-6::GFP appearance could be altered in cilia mutants either because cilia regulate DAF-6 localization or because cilia regulate sheath cell channel morphology. Previous EM analysis revealed no gross amphid channel defects in

mutants with cilia defects (Perkins et al., 1986). Nevertheless, because DAF-6 localization was disrupted in these mutants, minor channel abnormalities might exist. To address this issue more rigorously, we examined the morphology of the channel in *daf-19* mutants. We examined serial cross-sections of two *daf-19* (*m86*) and three wild-type animals by EM. In 2/2 *daf-19* (*m86*) animals, we found a continuous lumen between the sheath and socket channels (four channels observed), and channel length was only mildly affected, if at all. Strikingly, however, the sheath channel lumen was irregular in shape, with branching outpockets (Figures 2.7H–J). In addition, the distance from the anterior end of the dendrite to the anterior end of the sheath glia lumen was reduced in *daf-19* (*m86*) mutants (Figure 2.7J). Thus, altered DAF-6 localization in cilia-defective mutants may indeed lead to channel alterations. Alternatively, the absence of cilia in *daf-19* mutants may cause channel morphology defects independently of the DAF-6 localization defects.

Discussion

daf-6 Is Required for Lumen Morphogenesis

Several lines of evidence suggest that *daf-6* is required for lumen morphogenesis. Scanning EM (Albert et al., 1981), transmission EM, and fluorescent microscopy all revealed that *daf-6* sensory defects are due to a failure to generate a normal channel within the amphid sheath glia. In addition, *daf-6* functions cell-autonomously in the sheath glia (Herman, 1987), and is required in the amphid during a narrow window of embryogenesis when the amphid sheath lumen forms. DAF-6::GFP localizes to the luminal surfaces of many tube-forming cells in *C. elegans*, including the amphid and phasmid sheath and socket cells, the excretory system, the vulva, the rectum, and the posterior intestine. Finally, all tubes containing DAF-6 protein are disrupted in *daf-6*; *che-14* double mutants.

What might be the role of *daf-6* in lumen formation? Vesicle fusion has been proposed to be a key step in lumen formation (Lubarsky and Krasnow, 2003). Whether a tube is unicellular or multicellular, luminal membrane surface is thought to be elaborated when vesicles fuse with this membrane. DAF-6::GFP was seen in punctate, vesicle-like structures (Figures 2.4D, F). Furthermore, *che-14*; *daf-6* double mutants accumulated unfused vesicles, instead of a lumen, in certain regions of the excretory canal (Figure 2.6G). Thus, DAF-6, may be involved in vesicle trafficking, and may be specifically utilized to shuttle vesicles to or from growing lumina. Interestingly, lumen formation is topologically similar to cleavage furrow formation during cytokinesis. Specifically, generation and elongation of the cleavage furrow requires vesicle fusion with the plasma membrane (Straight and Field, 2000). The *C. elegans* Patched ortholog PTC-1, which is similar in sequence to DAF-6, may be required for vesicle transport

during germ cell cytokinesis (Kuwabara et. al., 2000). Thus, DAF-6, like PTC-1, may regulate vesicle dynamics during plasma membrane growth.

DAF-6-related proteins may be required for lumen formation during angiogenesis in human beings. Tumor growth requires the creation of new vasculature (Hanahan and Folkman, 1996). Thus, DAF-6-related proteins may represent a novel target for preventing tumor proliferation.

DAF-6 Is a Sterol-Sensing Domain Containing Protein

Sequence comparisons suggest that DAF-6 is a member of a previously uncharacterized group of sterol-sensing domain (SSD) containing proteins. How might this observation explain the role of DAF-6 in lumen morphogenesis?

Seven protein subfamilies harbor SSDs (Kuwabara and Labouesse, 2002). Representatives of each subfamily include 7-Dehydrocholesterol reductase (Fitzky et al., 1998), HMG CoA reductase (HMGCR) (Gil et al., 1985), SREBP cleavage activating protein (SCAP) (Hua et al., 1996), Neimann-Pick type C1 disease protein (NPC1) (Carstea et al., 1997), Dispatched (Burke et al., 1999), Patched (Hooper et al., 1989), and Patched-related (PTR) (Kuwabara et al., 2000) proteins. While these proteins have different activities, they can all be associated with vesicles, and the subcellular localizations of some, and perhaps all, are regulated through the SSD by sterol levels or by sterol-conjugated proteins. For example, SCAP shuttles from the endoplasmic reticulum to the Golgi when cell sterol levels are low, or independently of sterol levels when the SSD is mutated (Hua et al., 1996; Nohturfft et al., 1999). Thus, the possible association of DAF-6 with vesicles is consistent with the localization of other SSD containing proteins.

Furthermore, our mutagenesis studies suggest that the DAF-6 SSD may determine preferential DAF-6 localization to the plasma membrane.

Since PTR proteins are most closely related to Patched, could DAF-6, like Patched, function in a Hedgehog signal transduction pathway to generate tubes? In this pathway, Hedgehog protein inhibits the function of its receptor, Patched, resulting in activation of the membrane protein Smoothened. Smoothened activation allows nuclear entry of and transcription by the Gli/Ci transcription factor (Nybakken and Perrimon, 2002). It has been assumed that the Hedgehog signal transduction pathway does not exist in *C. elegans* (Kuwabara et al., 2000) because proteins similar in sequence to Smoothened have not been identified, and because the *C. elegans* single Gli/ Ci ortholog, *tra-1*, seems only to be involved in sex determination (Zarkower and Hodgkin, 1992). Furthermore, the *C. elegans* Patched homolog, PTC-1, localizes to vesicles and to growing cell membranes during germ-line cytokinesis, and *ptc-1* mutants accumulate multinucleate germ cells (Kuwabara et al., 2000). Thus, *ptc-1* functions in germline cytokinesis and probably does not function in a Hedgehog signal transduction pathway. Nonetheless, our mutagenesis studies suggest that aspartate 96 of DAF-6, located in the first extracellular loop of the protein, is critical for DAF-6 function but not for localization, suggesting that this residue may interact with an extracellular protein to regulate lumen morphogenesis. There are several Hedgehog-like proteins encoded in the genome (Aspock et al., 1999), and although their amino-terminal signaling domains do not resemble Hedgehog, these proteins share the autoprocessing carboxy-terminal domain with Hedgehog. Intriguingly, some of these Hedgehog-related proteins are

expressed in tube forming cells (Aspock et al., 1999). Thus, a rudimentary Hedgehog pathway might exist in *C. elegans* to control tube morphogenesis.

Our studies do not support the notion that DAF-6 acts as a permease for two reasons. First, DAF-6 only harbors a single GxxxD motif, unlike the two motifs present in the RND permeases. Second, mutations of this single GxxxD motif in DAF-6 did not fully block DAF-6 function, but did affect protein localization, suggesting that reduced activity of these mutant proteins was due to mislocalization. Similarly, we suggest that mutations of the GxxxD in mammalian Patched and Dispatched, although interpreted as providing support for the permease hypothesis (Ma et al., 2002), may, in fact, block proper localization of these proteins. Extensive structure-function-subcellular localization studies have not been done on Patched in *Drosophila*, and have proven challenging in mammalian systems. Because DAF-6 is similar to Patched, however, we believe that our conclusions may be generalizable to other members of this family.

A Model for Amphid Lumen Formation

Our studies suggest that *daf-6* and *che-14* act in concert to regulate lumen formation in *C. elegans*. *che-14* is most similar to Dispatched, a protein required for the secretion of cholesterol modified Hedgehog (Burke et al., 1999). Furthermore, previous studies suggested a role for CHE-14 in exocytosis (Michaux et al., 2000). *che-14* may, therefore, promote exocytosis during lumen formation. *daf-6* is similar to *Drosophila* and vertebrate Patched, and binding of the Hedgehog ligand to Patched triggers endocytosis of the complex (Denef et al., 2000; Incardona et al., 2000; Martin et al., 2001; Strutt et al., 2001), an

observation that led Michaux et al. (2000) to speculate that Patched-like proteins may be involved in endocytosis. One possible, although non-conventional, interpretation of this result is that the normal function of Patched is to inhibit endocytosis rather than promote it. Binding of Hedgehog to Patched would inhibit Patched activity, allowing endocytosis to occur. By analogy, we hypothesize that DAF-6 might function to inhibit endocytosis during lumen growth. Thus, we speculate that during lumen growth, more membrane is added to the growing lumen than is removed, by both promotion of exocytosis (using CHE-14), and inhibition of endocytosis (using DAF-6) (Figure 2.8).

Why do the posterior amphid channel and the excretory canal lumen still form in *daf-6* mutants? One possibility is that loss of DAF-6 would reduce inhibition of endocytosis, however, exocytosis by CHE-14 would still allow a channel to be generated. Loss of both DAF-6 and CHE-14 would, however, be predicted to result in a severely diminished ability to extend a lumen, as observed in the excretory canal. The variable penetrance of the excretory canal defect in *che*-14(*null*); *daf-6*(*null*) mutants suggests that even in this genetic background, lumen formation can take place. There are 23 additional Patched-related genes, as well as two Dispatched and three Patched genes in the *C. elegans* genome (Kuwabara et al., 2000). Some or all of these may also function in lumen formation. Thus, redundancy in both the inhibition of endocytosis and the promotion of exocytosis may lead to the relatively mild lumen morphogenesis defects in *daf-6* and *che-14* mutants.

The situation may be different during amphid channel opening. This process is topologically different from intracellular lumen formation (as in the excretory canal or the posterior amphid channel) or the generation of a lumen

between two cells (as in the vulva and rectum). Amphid channel opening may require the generation of a hole within a cell, and this process may be more sensitive to disruption of vesicle dynamics. We would propose, therefore, that since both *daf-6* and *che-14* single mutants manifest defects in amphid channel opening, both exocytosis and a lack of endocytosis may be necessary for this event to take place. Furthermore, little genetic redundancy must exist in this process. The fusion of lumina of different tracheal branches in *Drosophila* may occur by generating a hole through the cells, and this process may also involve vesicle trafficking (Samakovlis et al., 1996). Thus, proteins similar to DAF-6 and CHE-14 may also function in this and similar processes.

Finally, how is amphid channel morphogenesis coordinated to accommodate the neuronal cilia it ensheaths? Our studies of channel defects in animals with mutant neuronal cilia revealed two interesting findings. First, DAF-6::GFP was confined to a punctate structure near the sheath-socket junction. Second, the sheath glia portion of the channel was present but was misshapen in *daf-19* mutants. These results support a model in which cilia signal to the sheath glia to regulate the localization of DAF-6::GFP, which, in turn, regulates channel morphology (Figure 2.8). We envision a carefully controlled interplay between the neuronal endings and their associated glia, resulting in a well-patterned channel of appropriate dimensions. These results suggest that the amphid of *C. elegans* could be used as an exciting system in which to study glia-neuron interactions during nervous system development.

Experimental Procedures

General Methods and Strains

C. elegans were cultured at 20°C as described by Brenner (1974), unless otherwise indicated. The wild-type strain used was *C. elegans* var. Bristol (N2). The following strains were used: LGI: *che-3*(*e1124*), *che-13*(*e1805*), *che-14*(*e1960*, *ok193*); LGII: *daf-19*(*m86*, *m344*); LGIV: *daf-10*(*e1387*), *osm-3*(*p802*); LGV: *che-11*(*e1810*), *osm-6*(*p811*), *ntIs1* ($P_{gcy\text{-}5}$GFP); LGX: *daf-6*(*e1377*, *m176*, *m186*, *m197*, *m205*, *m506*, *n1543*). *Is*[$P_{T08G3.3}$DsRed ADF] is unmapped. *mcEx178* ($P_{che\text{-}14}$*che-14*::GFP), *nsEx42* ($P_{daf\text{-}6}$GFP), *nsEx71* ($P_{vap\text{-}1}$ DsRed), *nsEx75* (P_{HS}*daf-6*), *nsEx85* ($P_{daf\text{-}6}$*daf-6*::GFP), *nsEx94* ($P_{daf\text{-}6}$*daf-6*::GFP), *nsEx105* ($P_{vap\text{-}1}$ *vap-1*::GFP), *nsEx110* ($P_{daf\text{-}6}$*daf-6*::GFP), *nsEx131* (P_{HS}*daf-6*), *nsEx164* ($P_{daf\text{-}6}$*daf-6*::GFP), *qpEx*[$P_{vha\text{-}1}$GFP], and *utEx*[$P_{che\text{-}2}$ *che-2*::GFP].

Dye Uptake and Heat Shock Assays

Dye uptake: Animals were washed off NGM plates with M9 medium (Sulston and Hodgkin, 1988) and spun down briefly in a picofuge. The supernatant was removed, and the lipophilic dye 1, 1'–dioctadecyl-3, methylindodicarbocyanine, 4-chlorobenzenesulfonate salt ('DiD' solid; $DiIC_{18}(5)$ solid) (Molecular Probes) was added at 10 μg/ml in M9. Animals were then soaked in dye for two hours in the dark and at room temperature. Animals were next placed on NGM plates seeded with *E. coli* strain OP50, and scored using a fluorescence dissecting microscope. Heat shock studies: animals were placed at 35°C for 30 minutes, allowed to recover at 20°C and scored for dye uptake four or eight days later.

Allele Sequence Determination

Coding region and intron/exon boundaries of *daf-6* were amplified by the polymerase chain reaction (PCR) from mutant animals using Amplitaq DNA polymerase (Roche) and appropriate primers. Amplicons were sequenced using an ABI sequencer.

Plasmid Constructions

$P_{daf\text{-}6}$GFP (pEP1): we amplified by PCR a 3 kb DNA fragment from cosmid F31F6 containing sequences upstream of the *daf-6* ATG as well as the coding sequence for the first four amino acids. The resulting amplicon was ligated to the GFP vector pPD95.69 (Miller et al., 1999) digested with XbaI and BamHI. $P_{daf\text{-}6}$*daf-6*::GFP (pEP3C): we amplified by PCR DNA containing the *daf-6* genomic coding region and 3 kb of upstream sequences from cosmid F31F6. The resulting amplicon was ligated to the GFP vector pPD95.75 (Miller et al., 1999) digested with XbaI and BamHI. $P_{vap\text{-}1}$ DsRed (pEP6): we amplified by PCR a 2.8 kb genomic DNA fragment containing sequences upstream of the *vap-1* ATG. The resulting amplicon was ligated to the DsRed gene (pEP5) digested with XbaI and BamHI. P_{HS}*daf-6* (pEP7): we amplified by PCR the *daf-6* cDNA in plasmid pBSKS (Stratagene) using the T3 and T7 primers. The resulting amplicon was digested with BamHI and KpnI and ligated into the BamHI and KpnI restriction sites of the heat shock construct pPD49.78 (Fire et al., 1990). P_{HS}*che-14* (pEP36): we amplified by PCR the *che-14* cDNA from a mixed stage cDNA library. The resulting amplicon was digested with EcoRV and NheI and ligated into the EcoRV and NheI restriction sites of the heat shock construct pPD49.78 (Fire et al., 1990). Point mutations in pEP3C were generated using QuikChange II XL Site-

Directed Mutagenesis Kit (Stratagene). The "SSD alone" construct (pEP29) was generated by PCR, and included 3kb of genomic sequence upstream of the *daf-6* ATG, the coding region for the first 24 amino acids of DAF-6 (including the putative signal sequence), and the coding region for amino acids 264-439 (amplified from the *daf-6* cDNA) cloned into pPD95.75. The "Δloop2" construct (pEP33) was generated by amplifying pEP3C by PCR except for the region coding for amino acids 564-735, and inserting sequence encoding amino acids LDL in its place.

Germline Transformation

Germ-line transformations were carried out using standard protocols (Mello and Fire, 1995). Constructs were injected together with either plasmid pRF4, containing the dominant marker *rol-6*(*su1006*) (Mello et al., 1991), or plasmid pJM23 containing wild-type *lin-15* (Huang et al., 1994).

Microscopy

Animals were examined by epifluorescence using either a fluorescence dissecting microscope (Leica) or an Axioplan II compound microscope (Zeiss). Images were captured using an AxioCam CCD camera (Zeiss) and analyzed using the Axiovision software (Zeiss).

Electron microscopy

Animals were fixed in 0.8% glutaraldehyde, 0.7% OsO_4, 0.1 M cacodylate buffer for 1 hour on ice. Samples were postfixed in 2% OsO_4, 0.1 M cacodylate buffer, mounted into agar blocks, dehydrated in a series of alcohols and embedded in a

mixture of Epon-Araldite. Thin sections (50nm) were cut on an Ultracut E microtome, contrasted with 2% Uranyl Acetate and 1% Lead Citrate, and pictures were taken with a JEOL100 CX TEM at 80 kV.

Acknowledgements

We thank Ann Baren, Dana Cruz, Glenn Gold, Dave Hall, Erika Hartwieg, Bob Horvitz and Helen Shio for EM assistance; Matthew Buechner, Oliver Hobert, Isao Katsura, Michel Labouesse, Don Riddle, Piali Sengupta, and the *Caenorhabditis* Genetics Center for strains; Max Heiman for the $P_{vap\text{-}1}$ *vap-1*::GFP construct; Yuji Kohara for the *daf-6* cDNA; Marie-Anne Felix for vulval cell identification; Mark Schroeder and Simi Hinden for technical assistance; and Mary Abraham, Taulant Bacaj, Max Heiman, and Carine Waase for comments on the manuscript. This work was supported in part by funds from the Patterson Trust (to S.S.) and NIH MSTP grant GM07739 (to E.A.P.).

References

Albert, P.S., Brown, S.J., and Riddle, D.L. (1981). Sensory control of dauer larva formation in *Caenorhabditis elegans*. J. Comp. Neurol. *198*, 435-451.

Aspock, G., Kagoshima, H., Niklaus, G., and Burglin, T.R. (1999). *Caenorhabditis elegans* has scores of hedgehog-related genes: sequence and expression analysis. Genome Res. *9*, 909-923.

Bargmann, C.I., Hartwieg, E., and Horvitz, H.R. (1993). Odorant-selective genes and neurons mediate olfaction in *C. elegans*. Cell *74*, 515-527.

Bargmann, C.I., and Mori, I., (1997). Chemotaxis and Thermotaxis. In *C. elegans* II. Riddle, D.L., Meyer, B.J., and Priess, J.R. eds. (Cold Spring Harbor, NY: Cold Spring Harbor Laboratory Press.) pp. 717-737.

Berry, K.L., Bulow, H.E., Hall, D.H., and Hobert, O. (2003). A *C. elegans* CLIC-like protein required for intracellular tube formation and maintenance. Science *5653*, 2134-2137.

Brenner, S. (1974). The genetics of *Caenorhabditis elegans*. Genetics *77*, 71-94.

Briscoe, J., Chen, Y., Jessell, T.M., and Struhl, G. (2001). A Hedgehog-insensitive form of Patched provides evidence for direct long-range morphogen activity of Sonic Hedgehog in the Neural Tube. Molecular Cell *7*, 1279-1291.

Buechner, M., Hall, D.H., Bhatt, H., and Hedgecock, E.M. (1999). Cystic canal mutants in *Caenorhabditis elegans* are defective in the apical membrane domain of the renal (excretory) cell. Dev. Biol. *214*, 227-241.

Burke, R., Nellen, D., Bellotto, M., Hafen, E., Senti, K.A., Dickson, B.J., and Basler, K. (1999). Dispatched, a novel sterol-sensing domain protein dedicated to the release of cholesterol-modified hedgehog from signaling cells. Cell *99*, 803-815.

Burkitt, H.G., Young, B., and Heath, J.W. (1993). Wheater's Functional Histology (Edinburgh, UK: Churchill Livingstone Press). pp. 374-399.

Carstea, E.D., Morris, J.A., Coleman, K.G., Loftus, S.K., Zhang, D., Cummings, C., Gu, J., Rosenfeld, M.A., Pavan, W.J., Krizman, D.B., et al. (1997). Niemann-Pick C1 disease gene: homology to mediators of cholesterol homeostasis. Science *277*, 228-231.

Davis, G.E., and Camarillo, C.W. (1996). An alpha 2 beta 1 integrin-dependent pinocytic mechanism involving intracellular vacuole formation and coalescence regulates capillary lumen and tube formation in three-dimensional collagen matrix. Exp. Cell. Res. *224*, 39-51.

Denef, N., Neubuser, D., Perez, L., and Cohen, S.M. (2000). Hedgehog induces opposite changes in turnover and subcellular localization of patched and smoothened. Cell *102*, 521-531.

Driscoll, M., and Kaplan, J. (1997). Mechanotransduction. In *C. elegans* II. Riddle, D.L., Meyer, B.J., and Priess, J.R. eds. (Cold Spring Harbor, NY: Cold Spring Harbor Laboratory Press.) pp. 645-677.

Fire, A., Harrison, S.W., and Dixon, D. (1990). A modular set of *lacZ* fusion vectors for studying gene expression in *Caenorhabditis elegans*. Gene *93*, 189-198.

Fitzky, B.U., Witsch-Baumgartner, M., Erdel, M., Lee, J.N., Paik, Y.K., Glossmann, H., Utermann, G., and Moebius, F.F. (1998). Mutations in the Delta7-sterol reductase gene in patients with the Smith-Lemli-Opitz syndrome. Proc. Natl. Acad. Sci. U S A. *95*, 8181-8186.

Folkman, J., and Haudenschild, C. (1980). Angiogenesis in vitro. Nature *288*, 551-556.

Fujiwara, M., Ishihara, T., and Katsura, I. (1999). A novel WD40 protein, CHE-2, acts cell-autonomously in the formation of *C. elegans* sensory cilia. Development *126*, 4839-4848.

Ghabrial, A., Luschnig, S., Metzstein, M.M., and Krasnow, M.A. (2003). Branching morphogenesis of the Drosophila tracheal system. Annu. Rev. Cell Dev. Biol. *19*, 623-647.

Gil, G., Faust, J.R., Chin, D.J., Goldstein, J.L., and Brown, M.S. (1985). Membrane-bound domain of HMG CoA reductase is required for sterol-enhanced degradation of the enzyme. Cell *41*, 249-258.

Gobel, V., Barrett, P.L., Hall, D.H., and Fleming, J.T. (2004). Lumen morphogenesis in *C. elegans* requires the membrane-cytoskeleton linker *erm-1*. Dev. Cell *6*, 865-873.

Guan, L., and Nakae, T. (2001). Identification of essential charged residues in transmembrane segments of the multidrug transporter MexB of Pseudomonas aeruginosa. J Bacteriol. *183*, 1734-1739.

Hanahan, D., and Folkman, J. (1996). Patterns and Emerging Mechanisms of the Angiogenic Switch During Tumorigenesis. Cell *86*, 353-364.

Hedgecock, E.M., Culotti, J.G., Thomson, J.N., and Perkins, L.A. (1985). Axonal guidance mutants of *Caenorhabditis elegans* identified by filling sensory neurons with fluorescein dyes. Dev. Biol. *111*, 158-170.

Herman, R.K. (1984). Analysis of genetic mosaics of the nematode *Caneorhabditis elegans*. Genetics *108*, 165-180.

Herman, R.K. (1987). Mosaic analysis of two genes that affect nervous system structure in *Caenorhabditis elegans*. Genetics *116*, 377-388.

Hooper, J.E., and Scott, M.P. (1989). The Drosophila patched gene encodes a putative membrane protein required for segmental patterning. Cell *59*, 751-765.

Hua, X., Nohturfft, A., Goldstein, J.L., and Brown, M.S. (1996). Sterol resistance in CHO cells traced to point mutation in SREBP cleavage-activating protein. Cell *87*, 415-426.

Huang, L.S., Tzou, P., and Sternberg, P.W. (1994). The *lin-15* locus encodes two negative regulators of *Caenorhabditis elegans* vulval development. Mol. Biol. Cell *5*, 395-411.

Incardona, J.P., Lee, J.H., Robertson, C.P., Enga, K., Kapur, R.P., and Roelink, H. (2000). Receptor-mediated endocytosis of soluble and membrane-tethered Sonic hedgehog by Patched-1. Proc. Natl. Acad. Sci. U S A. *97*, 12044-12049.

Jan, Y.N., and Jan, L.Y. (1993). The Peripheral Nervous System. In The Development of *Drosophila melanogaster*, M. Bate and A. Martinez Arias, eds. (Cold Spring Harbor Laboratory Press). pp. 1207-1244.

Kuwabara, P.E., and Labouesse, M. (2002). The sterol-sensing domain: multiple families, a unique role? Trends Genet. *18*, 193-201.

Kuwabara, P.E., Lee, M.H., Schedl, T., and Jefferis, G.S. (2000). A *C. elegans* patched gene, *ptc-1*, functions in germ-line cytokinesis. Genes Dev. *14*,1933-1944.

Li, J.B., Gerdes, J.M., Haycraft, C.J., Fan, Y., Teslovich, T.M., et al. (2004). Comparative Genomics Identifies a Flagellar and Basal Body Proteome that Includes the *BBS5* Human Disease Gene. Cell *117*, 541-552.

Lubarsky, B., and Krasnow, M.A. (2003). Tube morphogenesis: making and shaping biological tubes. Cell *112*, 19-28.

Ma, Y., Erkner, A., Gong, R., Yao, S., Taipale, J., Basler, K., and Beachy, P.A. (2002). Hedgehog-mediated patterning of the mammalian embryo requires transporter-like function of dispatched. Cell *111*, 63-75.

Martin, V., Carrillo, G., Torroja, C., and Guerrero, I. (2001). The sterol-sensing domain of Patched protein seems to control Smoothened activity through Patched vesicular trafficking. Curr. Biol. *11*, 601-607.

Mello, C.C., Kramer, J.M., Stinchcomb, D., and Ambros, V. (1991). Efficient gene transfer in *C. elegans*: extrachromosomal maintenance and integration of transforming sequences. EMBO J. *10*, 3959-3970.

Mello, C., and Fire, A. (1995). DNA transformation. Methods Cell Biol. *48*, 451-482.

Michaux, G., Gansmuller, A., Hindelang, C., and Labouesse, M. (2000). CHE-14, a protein with a sterol-sensing domain, is required for apical sorting in *C. elegans* ectodermal epithelial cells. Curr. Biol. *10*, 1098-1107.

Miller, D.M., Desai, N.S., Hardin, D.C., Piston, D.W., Patterson, G.H., Fleenor, J., Xu, S., and Fire, A. (1999). Two-color GFP expression system for *C. elegans*. Biotechniques *26*, 914-918, 920-921.

Montesano, R., Schaller, G., and Orci, L. (1991). Induction of epithelial tubular morphogenesis in vitro by fibroblast-derived soluble factors. Cell *66*, 697-711.

Mori, I., and Ohshima, Y. (1995). Neural regulation of thermotaxis in *Caenorhabditis elegans*. Nature *376*, 344-348.

Myat, M.M., and Andrew, D.J. (2002). Epithelial tube morphology is determined by the polarized growth and delivery of apical membrane. Cell *111*, 879-891.

Nies, D.H. (1995). The cobalt, zinc, and cadmium efflux system CzcABC from Alcaligenes eutrophus functions as a cation-proton antiporter in *Escherichia coli*. J. Bacteriol*. 177*, 2707–2712.

Nohturfft, A., DeBose-Boyd, R.A., Scheek, S., Goldstein, J.L., and Brown, M.S. (1999). Sterols regulate cycling of SREBP cleavage-activating protein (SCAP) between endoplasmic reticulum and Golgi. Proc. Natl. Acad. Sci. U S A. *96*, 11235-11240.

Nybakken, K., and Perrimon, N. (2002). Hedgehog signal transduction: Recent findings. Curr. Opin. Genet. Dev. *12*, 503-511.

Perkins, L.A., Hedgecock, E.M., Thomson, J.N., and Culotti, J.G. (1986). Mutant sensory cilia in the nematode *Caenorhabditis elegans*. Dev. Biol. *117*, 456-487.

Riddle, D.L., Swanson, M.M., and Albert, P.S. (1981). Interacting genes in nematode dauer larva formation. Nature *290*, 668-671.

Riddle, D.L., and Albert, P.S. (1997). Genetic and Environmental Regulation of Dauer Larva Development. In *C. elegans* II. Riddle, D.L., Meyer, B.J., and Priess, J.R. eds. (Cold Spring Harbor, NY: Cold Spring Harbor Laboratory Press.) pp. 739-768.

Samakovlis, C., Manning, G., Steneberg, P., Hacohen, N., Cantera, R., and Krasnow, M.A. (1996). Genetic control of epithelial tube fusion during *Drosophila* tracheal development. Dev. *122*, 3531-3536.

Snow, J.J., Ou, G., Gunnarson, A.L., Walker, M.R.S., Zhou, H.M., Brust-Mascher, I., and Scholey, J.M. (2004). Two anterograde intraflagellar transport motors cooperate to build sensory cilia on *C. elegans* neurons. Nature Cell Biol. *6*, 1109-1113.

Starich, T.A., Herman, R.K., Kari, C.K., Yeh, W.H., Schackwitz, W.S., Schuyler, M.W., Collet, J., Thomas, J.H., and Riddle, D.L. (1995). Mutations affecting the chemosensory neurons of *Caenorhabditis elegans*. Genetics *139*, 171-188.

Straight, A.F., and Field, C.M. (2000). Microtubules, membranes and cytokinesis. Curr. Biol. *10*, 760-770

Strutt, H., Thomas, C., Nakano, Y., Stark, D., Neave, B., Taylor A.M., and Ingham, P.W. (2001). Mutations in the sterol-sensing domain of Patched suggest a role for vesicular trafficking in Smoothened regulation. Curr. Biol. *11*, 608-613.

Sulston, J., and Hodgkin, J. (1988). Methods. In The Nematode *Caenorhabditis elegans*. Wood, W.B. ed. (Cold Spring Harbor, NY: Cold Spring Harbor Laboratory Press.) pp. 587-606.

Swoboda, P., Adler, H.T., and Thomas, J.H. (2000). The RFX-type transcription factor DAF-19 regulates sensory neuron cilium formation in *C. elegans*. Mol. Cell *5*, 411-421.

Taipale, J., Cooper, M.K., Maiti, T., and Beachy, P.A. (2002). Patched acts catalytically to suppress the activity of Smoothened. Nature *418*, 892–896.

Troemel, E.R. (1999). Chemosensory signaling in *C. elegans*. Bioessays *21*, 1011-1020.

Tseng, T.T., Gratwick, K.S., Kollman, J., Park, D., Nies, D.H., Goffeau, A., and Saier Jr., M.H. (1999). The RND permease superfamily: an ancient, ubiquitous and diverse family that includes human disease and development proteins. J. Mol. Microbiol. Biotechnol. *1*, 107–125.

Ward, S., Thomson, N., White, J.G., and Brenner, S. (1975). Electron microscopical reconstruction of the anterior sensory anatomy of the nematode *Caenorhabditis elegans*. J Comp. Neurol. *160*, 313-337.

Wegner, M. (2000). Transcriptional control in myelinating glia: the basic recipe. Glia 29, 118-123.

Yu, S., Avery, L., Baude, E., and Garbers, D.L. (1997). Guanylyl cyclase expression in specific sensory neurons: a new family of chemosensory receptors. Proc. Natl. Acad. Sci. U S A *94*, 3384-3387.

Zarkower, D., and Hodgkin, J. (1992). Molecular analysis of the *C. elegans* sex-determining gene *tra-1*: a gene encoding two zinc finger proteins. Cell *70*, 237-249.

Figure 2.1

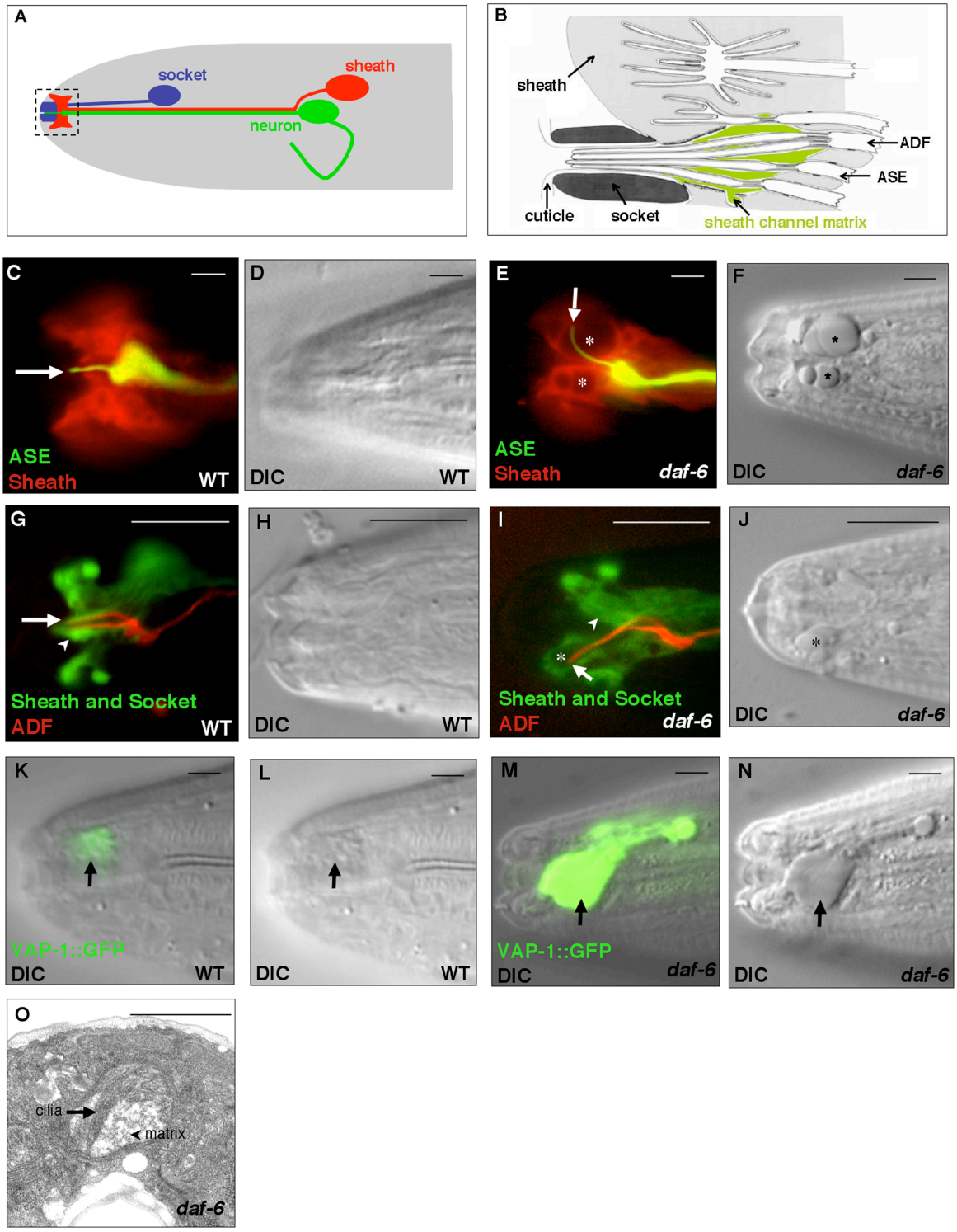
A
socket
sheath
neuron
B
sheath
ADF
ASE
cuticle
socket
sheath channel matrix
C
ASE
Sheath
WT
D
DIC
WT
E
ASE
Sheath
daf-6
F
DIC
daf-6
G
Sheath and Socket
ADF
WT
H
DIC
WT
I
Sheath and Socket
ADF
daf-6
J
DIC
daf-6
K
VAP-1::GFP
DIC
WT
L
DIC
WT
M
VAP-1::GFP
DIC
daf-6
N
DIC
daf-6
O
cilia
matrix
daf-6

Figure 2.1. The Amphid Sheath Cell Lumen Fails to Open in *daf-6* Mutants. (A) A schematic of the anterior of a worm with the three cell types of an amphid shown. Boxed region is area seen in C-N. (B) A schematic of the anterior end of an amphid (after Perkins et al., 1986). Cilia of ASE and ADF neurons extend through the amphid channel. Green, channel matrix. (C) Fluorescence image and (D) DIC image of a wild-type adult containing $P_{gcy\text{-}5}$GFP (ASER) and $P_{vap\text{-}1}$ DsRed (sheath) reporter transgenes. ASE cilium (arrow) extends through sheath cell lumen. (E, F) Same as (C, D), respectively, except that a *daf-6*(*e1377*) adult is shown. ASE cilium (arrow) fails to extend through the sheath cell. Asterisks, vacuoles. (G) Fluorescence image and (H) DIC image of a wild-type L2 containing $P_{T08G3.3}$DsRed (ADF) and $P_{daf\text{-}6}$GFP transgenes (socket (arrowhead) and sheath). ADF double cilium (arrow) extends through the sheath channel into the socket channel. (I, J) Same as (G, H), respectively, except that a *daf-6*(*e1377*) L2 is shown. ADF cilium (arrow) does not extend through the sheath channel into the socket channel (arrowhead). Asterisk, vacuole. (K) Merged DIC and fluorescence and (L) DIC image of a wild-type adult expressing $P_{vap\text{-}1}$*vap-1::*GFP. (M) Merged DIC and fluorescence and (N) DIC image of a *daf-6*(*e1377*) adult expressing $P_{vap\text{-}1}$*vap-1::*GFP. Arrows, sheath cell vacuoles. (O) Electron micrograph of a section through the amphid of a *daf-6*(*e1377*) L1. Neuronal cilia, which curve laterally, reside within a sheath pocket containing matrix material. A-N, anterior is left, dorsal is up. Scale bars, 5 μm, (except O, 1 μm).

Figure 2.2

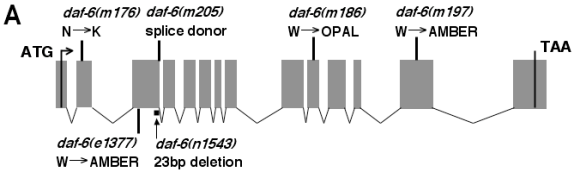

B

Allele	% Dyf	Lesion	Effect
e1377	100	G → A	W149 → amber
n1543	100	23bp deletion	deletion
m506	100	5' deletion	deletion
m186	97.5	G → A	W595 → opal
m197	97.0	G → A	W796 → amber
m205	95.5	G → A	splice donor
m176	93.0	C → A	N96 → K
wild-type	0.0	NA	NA

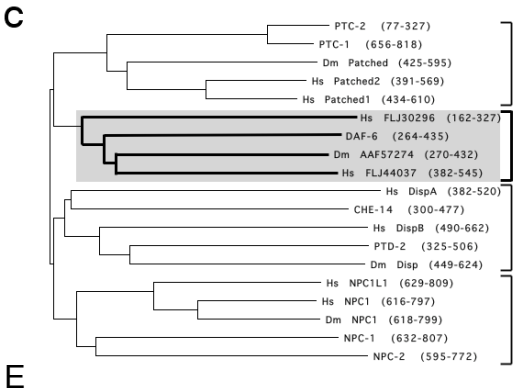

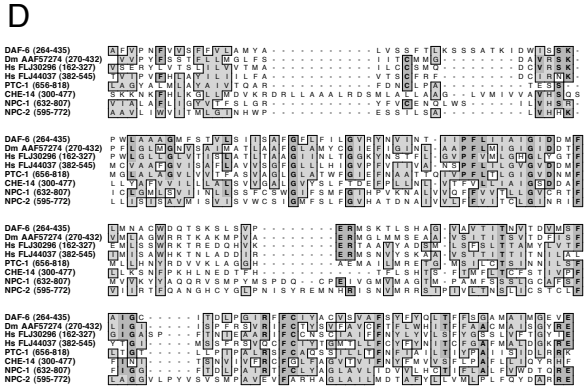

E

Relationship between DAF-6 and closely related SSD containing proteins

	overall		SSD	
	%identity	%similarity	%identity	%similarity
PTC-1	21.0%	38.7%	20.8%	43.4%
NPC-1	20.4%	37.2%	19.7%	39.3%
NPC-2	20.9%	36.8%	26.0%	42.8%
CHE-14	16.5%	32.2%	21.4%	40.5%
Dm AAF57274	29.0%	46.2%	36.4%	54.9%
Hs FLJ44037	19.5%	31.3%	33.5%	53.2%
Hs FLJ30296	18.9%	33.7%	23.7%	47.7%

Figure 2.2. *daf-6* Encodes a Patched-Related Protein. (A) *daf-6* gene structure. Boxes, exons. V-shaped lines, introns. Mutation sites and nucleotide and mRNA/protein alterations are indicated. Putative null and hypomorphic mutations are below and above the gene schematic, respectively. The putative null allele *daf-6*(*m506*) lacks most of the 5′ end of the gene, and is not shown. (B) Dye-filling defects (Dyf) per animal and molecular lesions of *daf-6* alleles. 200 animals were scored for each allele. NA, not applicable. (C) Dendogram showing sequence relationships of DAF-6 SSD to SSDs of related *C. elegans*, *Drosophila*, and human PTRs, Patched, Dispatched, and NPC1. (D) Sequence comparison of putative SSDs of DAF-6 (amino acids 264-435), *Drosophila* AAF57274 (270-432), human FLJ30296 (162-327), human FLJ44037 (382-545), *C. elegans* PTC-1 (656-818), *C. elegans* CHE-14 (300-477), *C. elegans* NPC-1 (632-807), and *C. elegans* NPC-2 (595-772). Boxes, similarities and identities. Bold letters and dark shading, identities. Light shading, similarities. (E) Identities and similarities between DAF-6 and closely related SSD-containing proteins. Percentages are shown for the entire proteins (overall) and for the SSD alone (SSD).

Figure2.3

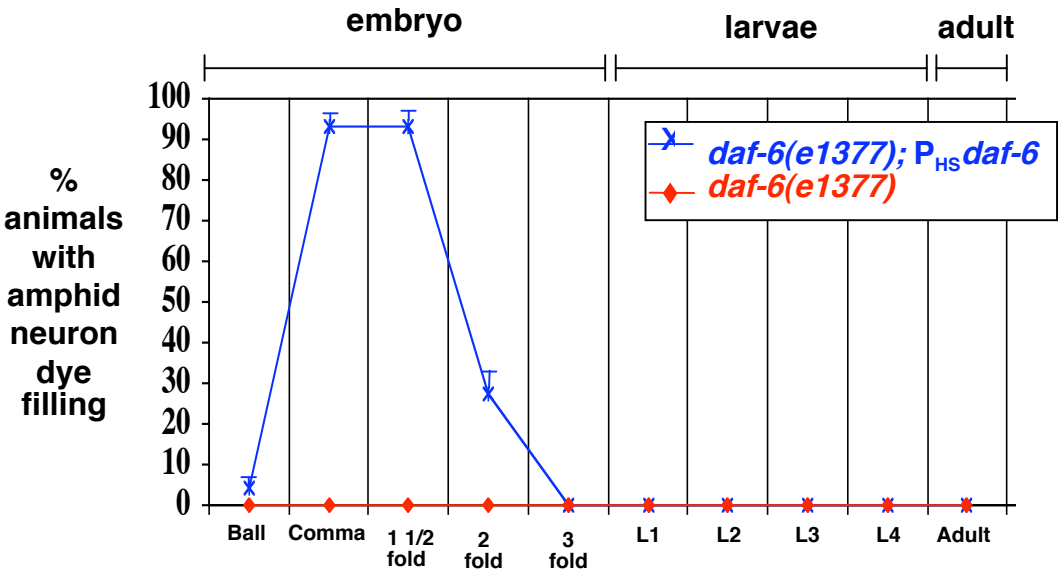

stage at time of heat

	ball	comma	1.5 fold	2 fold	3 fold	L1	L2	L3	L4	Adult
No. *daf-6(e1377); P$_{HS}$daf-6*:	75	74	53	74	42	131	115	139	126	40
No. *daf-6(e1377)*:	91	60	52	59	20	20	24	28	22	25

Figure 2.3. Heat shock rescue of *daf-6* dye-filling defect by *daf-6* cDNA. Horizontal axis, time of heat shock. Vertical axis, % animals with amphid neuron dye filling assayed four days after heat shock. Error bars, standard error of the mean (SEM). Numbers of animals observed for each time point are indicated.

Figure2.4

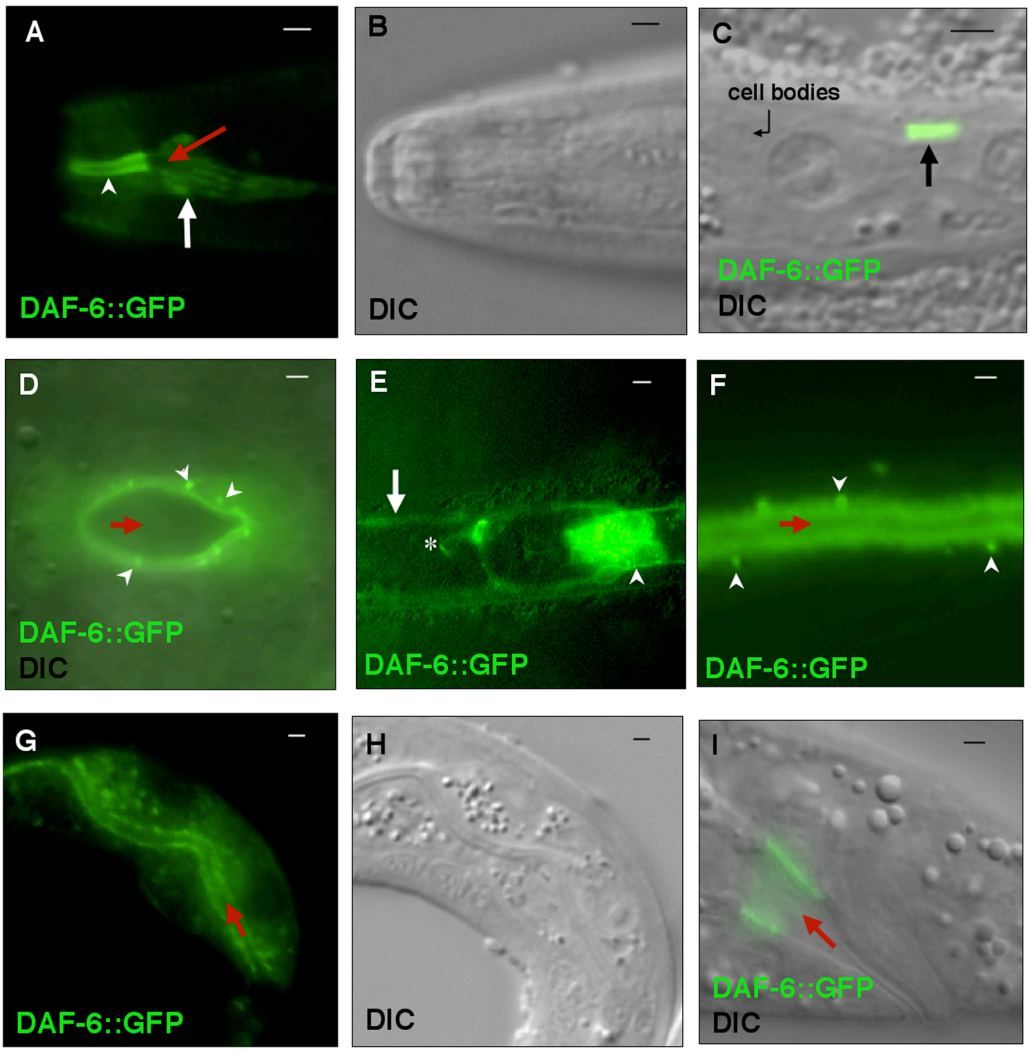
A
DAF-6::GFP
B
DIC
C
cell bodies
DAF-6::GFP
DIC
D
DAF-6::GFP
DIC
E
DAF-6::GFP
F
DAF-6::GFP
G
DAF-6::GFP
H
DIC
I
DAF-6::GFP
DIC

Figure 2.4. DAF-6 Lines the Luminal Surfaces of Tubes. All images are of wild-type animals expressing $P_{daf\text{-}6}$*daf-6*::GFP. (A) Fluorescence and (B) DIC images of DAF-6::GFP localized to the amphid channel in an L2. White arrow, luminal surfaces of amphid sheath cell. Arrowhead, amphid socket lumen. Red arrow, sheath cell lumen. (C) Merged fluorescence and DIC image. DAF-6::GFP localized to phasmid sheath and socket cell channels (straight arrow). (D) Merged ventral fluorescence and DIC images of DAF-6::GFP in the vulva. GFP lines the lumen (red arrow) and localizes to puncta (arrowheads). (E) Fluorescence image (dorsal view). DAF-6::GFP lines lumen surfaces of the excretory canal cell (arrow), duct and pore cells (asterisk), gland cells (arrowhead). (F) Fluorescence image. DAF-6::GFP lines the excretory canal lumen (red arrow) and is seen in puncta (arrowheads). (G) Fluorescence and (H) DIC images. DAF-6::GFP lines luminal surface of posterior intestine. Red arrow, lumen. (I) Merged fluorescence and DIC image. DAF-6::GFP localized to the luminal surface of K, K', F, and U cells. Red arrow, rectal lumen. In all images, except D and E, anterior is left, dorsal is up. Scale bars, 1 μm (except E, 5 μm).

Figure 2.5

	Transgene	Lesion	%Dyf (n) [Transgene in *daf-6(e1377)*]	%Dyf (n) [Transgene in WT]	Subcellular Localization	Image
A	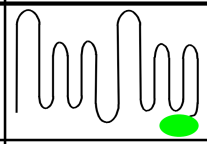	none	A: 35% (52) B: 40% (78)	A: 0% (100) B: 0% (40)	localized	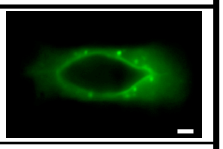
B	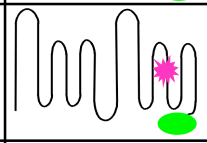	D817N	A: 32% (88) B: 45% (222) C: 56% (44)	A: 0% (80) B: 0% (80) C: 0% (40)	localized/ diffuse	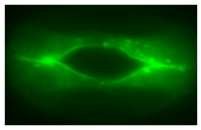
C	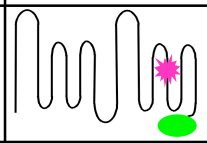	D817A	A: 100% (100) B: 77% (70) C: 78% (110)	A: 33% (92) B: 0% (36) C: 0% (36)	localized/ diffuse	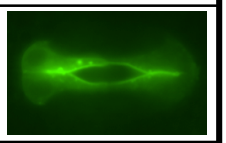
D	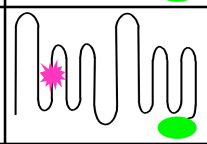	G321R	A: 52% (50) B: 44% (50) C: 32% (50)	A: 0% (50) B: 0% (22) C: 10% (100)	localized/ diffuse	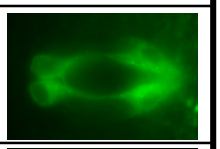
E	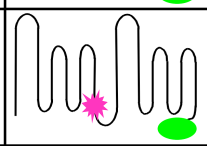	M431N	A: 13% (60) B: 44% (50) C: 46% (54)	A: 2% (50) B: 3% (80)	localized	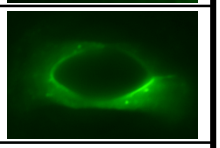
F	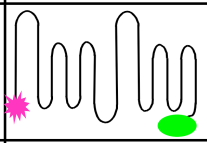	G18E	A: 50% (50)	N.D.	diffuse	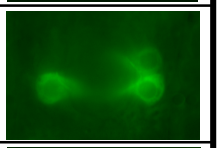
G	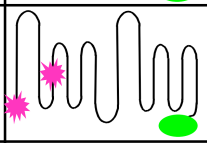	G18E G321R	A: 100% (52) B: 100% (40) C: 100% (40)	A: 0% (40) B: 3% (40) C: 0% (40)	diffuse	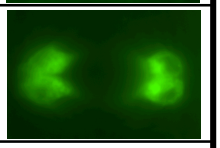
H	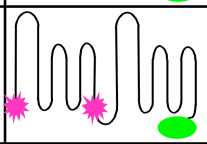	G18E M431N	A: 100% (40) B: 100% (42) C: 100% (46)	A: 0% (50) B: 2% (50) C: 0% (50)	diffuse	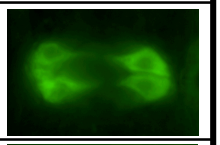
I	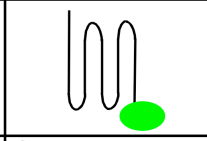	SSD alone	A: 100%(100) B: 100% (40) C: 100% (60)	A: 1% (292) B: 2% (109) C: 1% (100)	diffuse	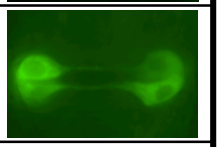
J	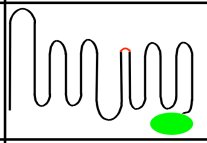	Δ Loop 2	A: 100% (70) B: 100% (140) C: 100% (80)	A: 1% (150)	diffuse	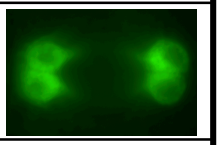
K	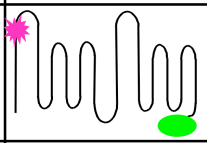	N96K	A: 97% (282) B: 100% (94) C: 99% (80)	N.D.	localized	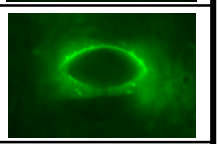
L	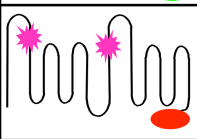	S253P F568L	N.D.	A: 81%(104)	peri-nuclear	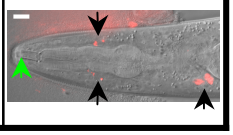

Figure 2.5. Mutations in DAF-6 Affect Function and Subcellular Localization. Indicated transgenes were injected into *daf-6*(*e1377*) or wild-type animals to establish transgenic lines. Animals were assayed for amphid dye filling defects (Dyf) per amphid to assess rescue and dominant effects of the transgenes. Subcellular locaization of transgenic proteins was assayed in vulvae of L4 animals where visualization was easiest, except in 4L. In 4L, localization is seen in amphids at the sheath and socket cell bodies (black arrows,) in contrast to wild-type localization at the anterior tip of the worm (green arrow). N.D., Not Determined. Scale bars, 1 μm (except L, 5 μm).

Figure2.6

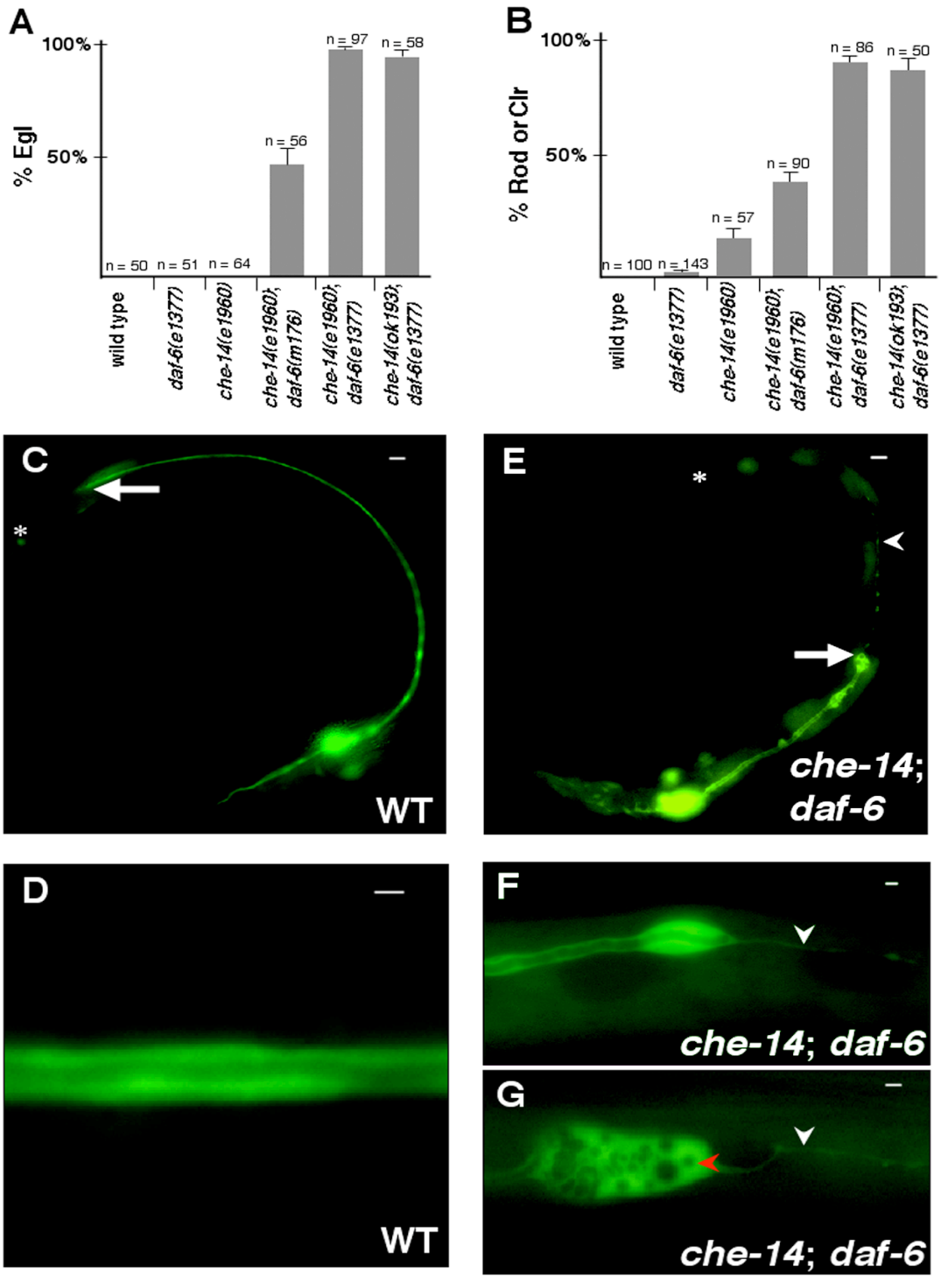
A
100%
50%
% Egl
n = 50
n = 51
n = 64
n = 56
n = 97
n = 58
wild type
daf-6(e1377)
che-14(e1960)
che-14(e1960); daf-6(m176)
che-14(e1960); daf-6(e1377)
che-14(ok193); daf-6(e1377)
B
100%
50%
% Rod or Clr
n = 100
n = 143
n = 57
n = 90
n = 86
n = 50
wild type
daf-6(e1377)
che-14(e1960)
che-14(e1960); daf-6(m176)
che-14(e1960); daf-6(e1377)
che-14(ok193); daf-6(e1377)
C
WT
E
che-14; daf-6
D
WT
F
che-14; daf-6
G
che-14; daf-6

Figure 2.6. *daf-6* and *che-14* Interact to Regulate Lumen Morphogenesis. (A) Histogram depicting egg-laying defects (Egl) of strains of the indicated genotype. Error bars, SEM. (B) Histogram depicting Rod and Clr defects (see text) of strains of the indicated genotype. Error bars, SEM. (C-G) Fluorescence images of animals expressing $P_{vha\text{-}1}$GFP. (C) Wild-type animal. Excretory cell lumen (arrow) extends towards posterior end of the animal (asterisk). (D) Wild type, note continuous lumen. (E) *che-14*(*e1960*); *daf-6*(*e1377*) mutant. Lumen fails to extend to posterior end of animal (arrow), but process does (arrowhead). Asterisk, posterior tip. (F) *che-14*(*e1960*); *daf-6*(*e1377*) mutant. Note lack of lumen in posterior region (arrowhead). (G) *che-14*(*e1960*); *daf-6*(*e1377*) mutant. Note lack of a lumen in posterior region (white arrowhead). Red arrowhead, numerous accumulated vesicles. In images D, F, and G, anterior is left, dorsal is up. Scale bars: C and E, 10 μm; D, F, G, 1 μm.

Figure2.7

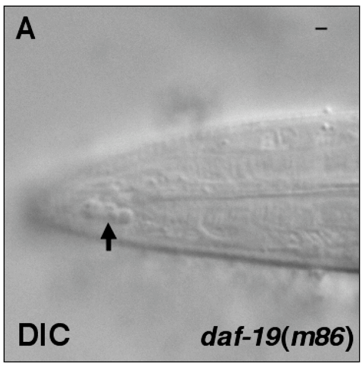

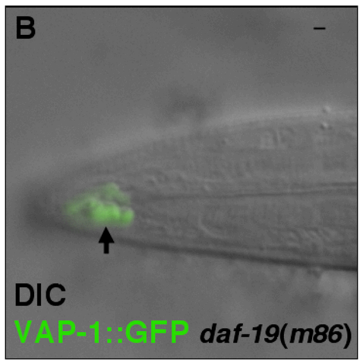

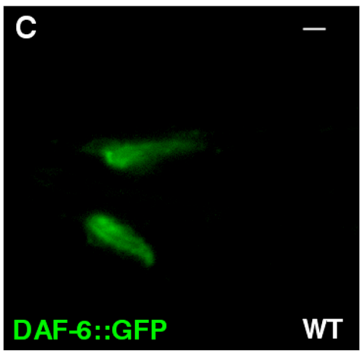

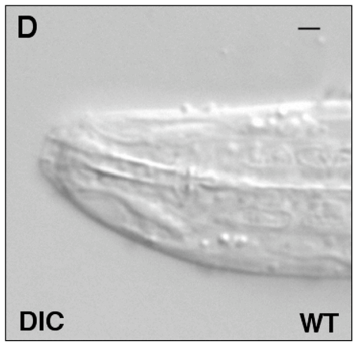

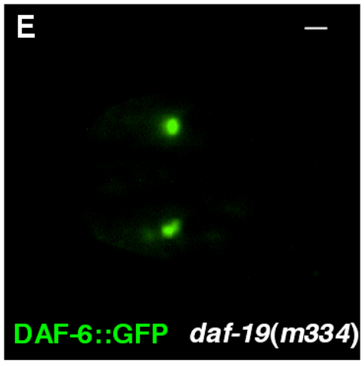

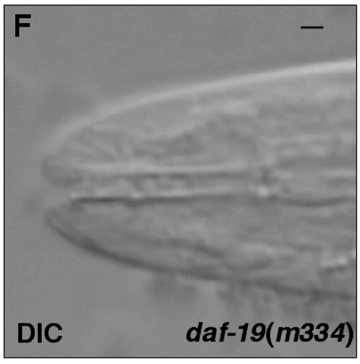

G Amphid DAF-6::GFP Appearance in Cilia Mutants

Strain	%	%	n
nsEx85	88%	12%	51
nsEx164	64%	36%	36
che-3(e1124); nsEx85	11%	89%	20
che-3(e1124); nsEx164	11%	89%	27
che-11(e1810); nsEx85	9%	91%	23
che-11(e1810); nsEx164	4%	96%	24
che-13(e1805); nsEx85	4%	96%	25
che-13(e1805); nsEx164	0%	100%	26
daf-10(e1387); nsEx85	4%	96%	25
daf-10(e1387); nsEx164	0%	100%	27
daf-19(m334); nsEx85	0%	100%	31
daf-19(m334); nsEx164	10%	90%	31
daf-19(m86); nsEx110	19%	81%	37
osm-6(p811); nsEx85	7%	93%	29
osm-6(p811); nsEx164	3%	97%	31

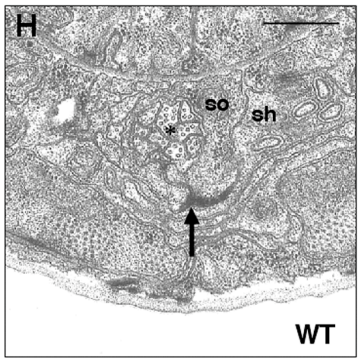

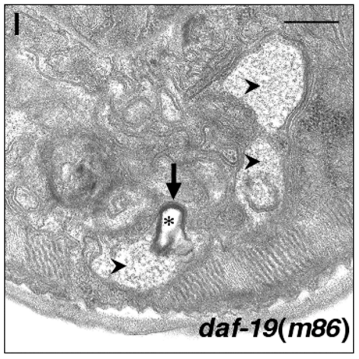

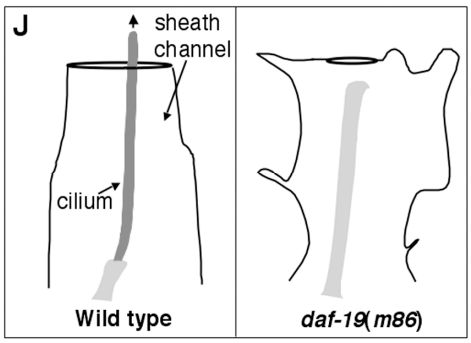

Figure 2.7. Defective Sheath Cell Lumen Morphogenesis in Cilia Formation Defective Mutants. (A) DIC and (B) merged fluorescence and DIC images of a *daf-19*(*m86*) L1 expressing P_{vap-1}*vap-1*::GFP. Arrows, matrix-filled vacoules. (C) Fluorescence and (D) DIC images of a wild-type L1 expressing P_{daf-6}*daf-6*::GFP. (E) Fluorescence and (F) DIC images of a *daf-19*(*m334*) L1 expressing P_{daf-6}*daf-6*::GFP. (G) Table charting DAF-6::GFP localization in strains of the indicated genotype. Each extrachromosomal array is an independently generated P_{daf-6}*daf-6*::GFP transgene. (H, I) Electron micrographs of the amphid sheath-socket junction (arrow) of a wildtype or *daf-19*(*m86*) L1, respectively. In I, the junction is misshapen, and matrix-filled sheath pockets (arrowheads) are seen. so, socket. sh, sheath. Asterisks, amphid channel filled with cilia (H) or empty (I). (J) Cartoons of amphid sheath channel in wild-type and *daf-19*(*m86*) animals based on electron micrographs of serially sectioned L1s. Only one dendrite is shown. In *daf-19*(*m86*) animals, the sheath-socket junction is misshapen, the amphid sheath channel is malformed, and the anterior end of the sensory dendrites are closer to the sheath-socket junction. A-F, dorsal images, anterior is left. Scale bars, 1 μm.

Figure 2.8

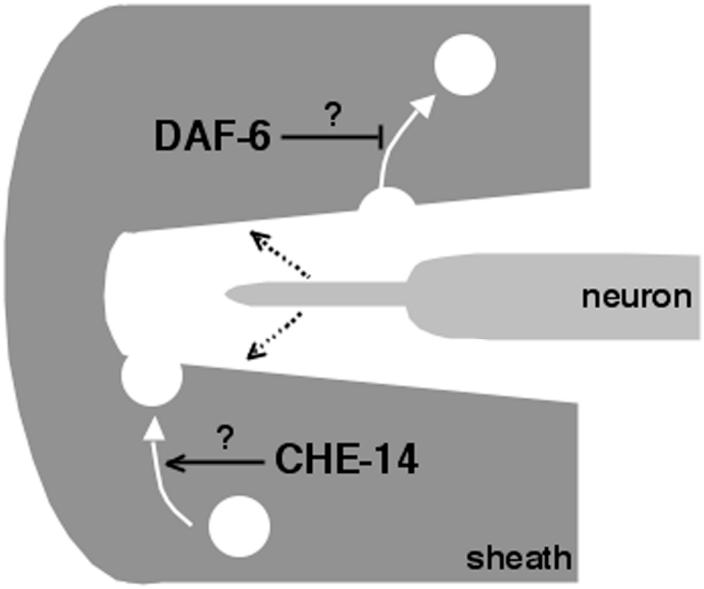

Figure 2.8. A Possible Model For Amphid Lumen Formation. A hypothetical developmental intermediate is shown. To generate the lumen, and open the sheath glia channel, DAF-6 may inhibit endocytosis, while CHE-14 may promote exocytosis. DAF-6 and CHE-14 may act similarly in other tubes, such as the excretory canal. A signal from neuronal cilia (dashed arrow) may determine the shape of the amphid channel and DAF-6 localization.

Table 2.1

Table 2.1. *daf-6* Amphid Mutant Defects

	Genotype	L1	L2	L3	L4	Adult
A. % Dye-filling defective	N2	0 (50)	0 (50)	0 (50)	0 (50)	0 (50)
	daf-6(*e1377*)	100 (50)	100 (50)	100 (50)	100 (50)	100 (50)
B. % Cilia fail to extend through sheath/socket	N2	ND	0 (20)	0 (21)	0 (22)	0 (20)
	daf-6(*e1377*)	ND	100 (20)	100 (23)	100 (23)	100 (22)
C. % Curved cilia	N2	0 (25)	0 (27)	0 (37)	0 (22)	0 (28)
	daf-6(*e1377*)	16 (44)	69 (49)	100 (39)	100 (33)	100 (20)
D. % Vacuole accumulation	N2	0 (21)	0 (30)	0 (18)	0 (34)	0 (20)
	daf-6(*e1377*)	38 (32)	66 (32)	89 (36)	92 (36)	100 (20)

Numbers in parentheses are the total number of animals scored.
ND, not determined.

Chapter 3

Identification of mutations that suppress the sensory organ morphological defects in *Caenorhabditis elegans daf-6* mutants

Elliot A. Perens, Yun Lu and Shai Shaham

Yun Lu performed the electron microscopy.

Summary

To understand lumen formation, we have been studying lumen formation in the *C. elegans* amphid sensory organ. Previously, we demonstrated that the Patched-related sterol-sensing domain containing protein DAF-6 is required for amphid lumen formation. Here, we describe a genetic screen used to identify genes that function with *daf-6*. We screened for mutations that suppressed the dauer formation and amphid neuronal dye uptake defects in *daf-6* mutants. We isolated and characterized seven mutants. Importantly, we demonstrated that these mutants also suppress the *daf-6* lumen formation defects.

Introduction

Sensory organs share a common morphology. Sensory neurons extend the specialized ending of their dendrites though a lumen formed by associated glia or epithelia. This structure found in the *C. elegans* poly-modal amphid sensory organs (Ward et al., 1975), *Drosophila* olfactory and mechanosensory organs (Hartenstein and Posakony, 1989; Shanbhag 2000), and vertebrate taste buds, retina, and olfactory epithelium (Burkitt, 1993). Thus lumen formation is an essential step during sensory organ morphogenesis.

Lumens are an important component of most organ systems, including the respiratory, excretory and digestive systems. The tubes found in these systems come in many forms. They can be multicellular, unicellular with an autocellular junction, or a seamless unicellular tube. Furthermore, some are extensively branched while others are unbranched. Despite these differences, there appears to be some common mechanisms involved in generating many lumens (Lubarsky and Krasnow, 2003). After the cells have migrated, invaginated, or extended into their correct position, they establish their polarity such that the apical surface becomes the luminal surface. Then intracellular vesicles add membrane to the luminal surface, thereby generating and expanding the luminal space.

To gain insight into the genetic basis of sensory organ lumen formation, we are studying the morphogenesis of the *C. elegans* amphid sensory organ. *C. elegans* possesses two bilaterally symmetric amphids, located at the anterior tip of the animal (Ward et al., 1975). Each amphid consists of twelve sensory neurons and two ensheathing glial cells, the sheath and socket cells. Amphid neurons have two projections: an axon that extends into the nerve ring, and a dendrite

that extends to the anterior tip of the animal. Amphid sheath and socket glia also extend anterior processes that contact amphid neuron dendritic projections (Ward et al., 1975). At the tip of the nose all neuronal sensory endings are ensheathed by the sheath glia. Four of the amphid neurons, which mediate chemotaxis to volatile chemicals and thermotaxis (Bargmann, 1997; Mori and Ohshima, 1995), have dendritic endings that are fully embedded within the amphid sheath glia. These endings are lodged within tightly fitting glial channels in which the neurons are surrounded by an undefined matrix material. The remaining eight neurons end in sensory cilia, and gain access to the outside environment by extending through the main amphid channel: a bipartite channel, formed anteriorly by the socket glia and continued posteriorly by the sheath glia (Ward et al., 1975). This matrix-filled channel is open to the outside environment and is supported by an array of cytoskeletal elements (Ward et al., 1975). We will henceforth refer to this channel as the amphid channel. Amphid channel neurons are required for avoidance of high osmolarity solutions, chemosensation of water-soluble solutes, and mechanosensation (Bargmann, 1997); Driscoll and Kaplan, 1997). They also sense dauer pheromone (Riddle, 1997).

Previously, we demonstrated that *daf-6* (for dauer formation defective), which encodes a sterol-sensing domain (SSD) containing Patched related protein, is required for amphid lumen formation (Perens and Shaham, 2005). In *daf-6* mutants, the anterior portion of the sheath cell lumen is incompletely formed, so the worms are unable to sense dauer pheremone (Daf-d), dye-filling defective (Dyf), osmosensataion defective (Osm), and chemotaxis defective (Che) (Perens and Shaham, 2005; Starich et al., 1995). Furthermore, *daf-6* is only required

during a narrow window of embryogenesis, suggesting that *daf-6* is required for lumen formation, but not maintenance. DAF-6 lines the luminal surface of the amphid and phasmid sensory organ sheath and socket cells, excretory system cells, vulva cells, and rectal epithelial cells. Interestingly, worms mutant for both *daf-6* and the closely related Dispatched homolog *che-14* have defects in all of these other lumens. Therefore lumen formation in these tubes requires both *daf-6* and *che-14*.

The mechanism of DAF-6 function in lumen formation is unknown. To gain insight into DAF-6 function and lumen formation, we screened for mutations that suppress the *daf-6*(*e1377*) amphid lumen formation defects. We identified seven mutations that suppress *daf-6*.

Results

Screening for mutations that suppress amphid morphology defects in *daf-6*(*e1377*) animals

To identify mutations that suppress the amphid morphological defects in *daf-6* mutants, we preformed a genetic screen. The amphid sheath cell lumens fail to open in *daf-6* mutants, and consequently these worms are Daf-d, Dyf, Osm, and Che. Previous attempts at screening for mutations that suppress the *daf-6* Dyf phenoptye, as a read-out of amphid sheath cell morphology, demonstrated that a *daf-6* suppressing mutation would be rare (E. Perens, S. Hinden, and S. Shaham, unpublished observation). Therefore we designed a screening strategy that would allow us to screen though a large number of genomes. This screen required several features. First, to screen though a large number of worms rapidly, the screen was semi-clonal. Second, in screening though many worms, we needed to have low background. Thus, we used the most penetrant *daf-6* mutant allele, which would rarely display the wildtype phenotype. The most penetrant *daf-6* allele is *daf-6*(*e1377*), which contains an early amber mutation (Perens and Shaham, 2005). Finally, to screen though a large number of a worms, we used a strong selection- a phenotype that could easily distinguish a *daf-6* mutant from a suppressed *daf-6* mutant. The phenotype we used was the dauer formation defect. Dauer animals exhibit prolonged life span and resistance to environmental insults, and entry into dauer is mediated by a continuously released pheromone (Riddle and Albert, 1997). Suppressed *daf-6* mutants, unlike *daf-6* mutants, would be able to undergo dauer formation. Furthermore, dauer worms can easily be distinguished from non-dauer worms;

dauer worms are resistant to 1% SDS, while 1% SDS rapidly kills non-dauer worms (Cassada and Russell, 1975).

To perform this screen, we placed 50 F1 mutagenized *daf-6*(*e1377*) on each plate (Figure 3.1A). These worms were allowed to self-fertilize for 10 days, during which time the worms would go though about two more generations. During this time, all of the food on the plate would be eaten. Thus there would be a high density of worms on the plate, and the worms would be starved. These conditions would allow a worm at the correct stage of development (late L1 first larval stage) to enter into dauer development, if they were genetically susceptible to doing so.

At this point three types of worms could be identified in the screen (Figure 3B). First, we could isolate worms that suppress the morphological defect in *daf-6* mutants- the worms desired from this screen. Secondly, even though *daf-6*(*e1377*) is a strong allele, we could isolate worms that did not have a suppressing mutation, but failed to express the Daf-6 dauer formation defect. Finally, a mutations in a number of genes can cause worms to be dauer formation constitutive (Daf-c), and epistasis experiments have demonstrated that these genes act genetically downstream of *daf-6* (Riddle, 1997). The gene products of these genes function mostly in neuro-hormonal signaling or neuron formation, and are unlikely to affect amphid lumen formation. Thus we needed to separate these last two classes worms from the desired class of suppressed worms.

To determine whether dauer worms recovered from the screen had heritable suppression of the amphid lumen formation defects, we first placed the recovered worms on NGM plates with food and determined whether these

worms could exit dauer development and resume wildtype development (Figure 3.1B). Some Daf-c worms are unable to recover from dauer, even under favorable conditions, so worms with these suppressing mutations would be revealed by this selection. Secondly, we determined whether the progeny of the worms that recovered from dauer could uptake lipophilic dye. Both worms that entered into dauer development due to incomplete penetrance of the *daf-6*(*e1377*) mutation and worms that have *daf-6* dauer suppressing mutations that suppress only the dauer formation defect but not the amphid morphology defect would have progeny that fail to uptake dye (Figure 3.1B). Only *daf-6* worms with a mutation that suppressed the amphid morphological defect should be able to recover from dauer and have non-Dyf progeny (Figure 3.1B).

Identification of mutations that suppress amphid morphology defects in *daf-6*(*e1377*) animals

We screened approximately 30,000 F1 animals, representing 60,000 mutagenized genomes. The 30,000 F1 animals were spread out over 600 NGM plates (50 F1 worms per plate). 40% of these plates produced dauer animals. Most plates had 1-5 dauer progeny, but some had 20-30 dauer progeny. Of these worms, only seven had progeny that were able to uptake dye in their amphid neurons. Thus, most dauer progeny of mutagenized *daf-6*(*e1377*) animals were either worms with incompletely penetrant Daf-d defect or worms that carried a mutation that suppressed the Daf-d defect but not the amphid lumen formation defect.

Of the seven identified mutations, we have mapped four of them to a chromosome (see Experimental Procedures). Because they map to three different chromosomes, these four mutations represent at least three different genes.

Phenotypic and genetic characterization of mutations that suppress amphid morphology defects in *daf-6*(*e1377*) animals

To confirm and characterize the suppression of the amphid defects, we examined the dye-filling defects in these strains. We scored animals homozygous for both *daf-6*(*e1377*) and a suppressor mutation at four stages of larval development and adulthood (Table 3.1A). As shown in Table 3.1A, wildtype animals were non-Dyf and *daf-6*(*e1377*) animals were 100% Dyf at all stages. *daf-6*(*e1377*); *ns122*, *daf-6*(*e1377*); *ns123*, *daf-6*(*e1377*); *ns125*, *daf-6*(*e1377*); *ns132*, *daf-6*(*e1377*); *ns133* animals were approximately 50%-75% Dyf. In other words, in these strains approximately 25%-50% of these animals had dye-uptake by neurons in at least one of the two amphid sensilla. Also, ~95% of *daf-6*(*e1377*); *ns121* animals were suppressed, and ~5% of *daf-6*(*e1377*); *ns124* animals were suppressed (Table 3.1A). The Dyf defects remained relatively unchanged for most strains as the animals aged, except for *daf-6*(*e1377*); *ns122* and *daf-6*(*e1377*); *ns133*, which decreased slightly as the animals aged (Table 3.1A).

The suppression screen was performed using *daf-6*(*e1377*), and the mutation in this strain results in an early amber stop codon. Thus, these *daf-6*(*e1377*) suppression mutations could be amber suppressor mutations in one of the 12 *C. elegans* tRNA(Trp) genes (Kondo et al., 1990). To determine whether the suppressors we identified were ambers suppressor mutations, we tested whether

the mutations could suppress other *daf-6* alleles that do not have amber stop mutations. Specifically, we used *daf-6*(*n1543*), which has a 71 base pair deletion that shifts the gene out of frame, and *daf-6*(*m176*), which has a missense mutation (Perens and Shaham, 2005). *ns122*, *ns123*, *ns124*, *ns132*, and *ns133* suppressed at least one of these other *daf-6* alleles at levels comparable to the *daf-6*(*e1377*) suppression (Table 3.2B). Therefore, these five alleles are unlikely to be amber suppressor mutations. On the other hand, we were unable to suppress *daf-6*(*e1377*); *ns121*. Thus, *ns121*may be an amber suppressor mutation. Also, we were unable to suppress *daf-6*(*e1377*); *ns124*, but this result may due to the difficulty of working with these animals; *daf-6*(*e1377*); *ns124* are sick and do not mate well.

In addition to characterizing the suppression of the Dyf phenotype, we also characterized the suppression of the Daf-d phenotype, as described in the Experimental Procedures. Using this procedure, no *daf-6*(*e1377*) dauer animals were recovered while an average of 366 ± 90 wildtype dauer animals were recovered. All *daf-6*(*e1377*) strains bearing a suppressor mutation produced dauer larvae, confirming suppression of this phenotype. Specifically, the following average number of dauer worms (± the standard error of the mean) were recovered for the corresponding strain: *daf-6*(*e1377*); *ns121* (80 ± 19),*daf-6*(*e1377*); *ns122* (39 ± 15),*daf-6*(*e1377*); *ns123* (208 ± 53),*daf-6*(*e1377*); *ns124* (6 ± 1),*daf-6*(*e1377*); *ns125* (66 ± 23),*daf-6*(*e1377*); *ns132* (8 ± 3), and *daf-6*(*e1377*); *ns133* (206 ± 36).

Finally, and most importantly, we determined whether the *daf-6*(*e1377*) amphid lumen morphogenesis defect is suppressed in these strains. As

described in Perens and Shaham, 2005, while the amphid neuronal cilia extend through the sheath and socket cells in wildtype worms, the cilia fail to extend through the sheath cell in *daf-6*(*e1377*) mutants; that is, the sheath cell is incompletely formed (Perens and Shaham, 2005). To examine in detail the structure of the amphids, we first examined animals that were homozygous for *daf-6*(*e1377*) and a suppressor allele, and that also harbored two transgenes: a P_{vap-1}DsRed transgene, expressing DsRed fluorescent protein in amphid sheath cell under the control of the *vap-1* gene promoter (*vap*, venom allergen protein); and a P_{gcy-5}GFP transgene, expressing green fluorescent protein (GFP) in the right ASE (ASER) amphid channel neuron (Yu et al., 1997).

Consistent with the variable penetrance of the Dyf suppression, we observed variable suppression of the amphid lumen morphogenesis defects in *daf-6*(*e1377*) animals bearing a suppressor allele (Figure 3.2). While the sheath cell defects were present in some of these animals, importantly the amphid appeared normal in other sensilla. Thus even though we screened for suppression of the Dyf and Daf-d defects, the morphological defects were suppressed as well.

To confirm the suppression of the amphid morphological defects, we examined electron micrograph cross-sections (Figure 3.3). In wildtype animals, neuronal cilia reside in a tight fitting channel in both the sheath and socket cells (Figure 3.3 A, B). We preformed EM on *daf-6*(*e1377*); *ns122*, *daf-6*(*e1377*); *ns132*, and *daf-6*(*e1377*); *ns132* animals in which amphid neurons in only one sensilla could uptake dye (Figure 3.3 C-I). In cross sections though the socket cell, neuronal cilia could be observed in only one amphid sensillum; amphid neuronal cilia were not present on the other side of the animal (Figure 3.3 C, E,

G). Similarly, in cross sections though the sheath cell, the cilia resided in a tight fitting channel on one side of the animal (Figure 3.3 D, F, H, I). On the other side of the animal, the channel had Daf-6 phenotypes as previous described in Perens and Shaham, 2005. Specifically, the channel was enlarged and filled with excessive amounts of matrix material, and the neuronal cilia were bent. Thus, consistent with the Dyf phenotype of the selected animals, the amphid lumen had a wildtype morphology in one of the two amphid sensilla. In conclusion, the *daf-6* lumen morphogenesis defects were suppressed in these animals, and the suppression of the Dyf phenotype corresponded with the suppression of the morphological defect.

We also determined the mode of inheritance for each suppressor as described in the Experimental Procedures. Some heterozygous cross progeny were non-Dyf, but the penetrance of the Dyf suppression was less than in worms homozygous for the suppressor mutation (Table 3.2). Therefore, each mutation is semi-dominant.

Finally, we wanted to determine the number of loci represented by these seven mutations. Because the mutations are semi-dominant, interpreting complementation tests could be difficult; when two mutations are placed in trans, the frequency of suppression could represent either the combined effect of two semi-dominant mutations or non-complementation. Therefore, we chose to determine whether these mutations could be alleles by mapping them genetically. We have determined the genetic location for four of the mutations, as described in the Experimental Procedures and Figure 3.4. *daf-6*(*e1377*); *ns125* and *daf-6*(*e1377*); *ns133* are on the X chromosome, *daf-6*(*e1377*); *ns132* is on

chromosome III, and *daf-6*(*e1377*); *ns122* is on chromosome IV. Therefore, the seven mutations identified in the screen represent at least three different loci.

Discussion

We isolated seven mutations that suppress the Daf-d, Dyf, and, most importantly, the amphid lumen formation defects of *daf-6* mutants. These mutations represent at least three different loci.

Cloning the mutated genes and determining the nature of the mutations (loss-of-function or gain-of-function) will be essential for determining the functions played by these by these genes. Theoretically, a mutation identified in this screen could fall into one of two classes. First, it could be a regulatory suppressor- a loss-of-function mutation in a negative regulator of lumen formation. Alternatively, it could be a bypass suppressor- a gain-of-function mutation in pathway parallel or downstream to *daf-6*. In fact, *che-14*, a *C. elegans* Dispatched homolog with an expression pattern, subcellular localization, and phenotype similar to *daf-6*, was shown to act in a parallel, non-functionally redundant pathway with *daf-6* (Perens and Shaham, 2005). However the four suppressors that we have mapped to a chromosome do not map to the same chromosome as *che-14*. Still, other *C. elegans patched-related* or *dispatched* genes may act in parallel to *daf-6*.

Data presented in this chapter suggests these mutations may be gain-of-function mutations. While the fact that these mutations are semi-dominant is consistent with both haploinsufficient loss-of-function and gain-of-function mutations, the rate of appearance of these mutations is more consistent with gain-of-function mutations. We identified only seven alleles for at least three and as many as seven loci in a screen of approximately 60,000 genomes. Thus, it is unlikely that null, loss-of-function mutations in many genes could suppress *daf-6*. One shortcoming with this analysis is the potentially high rate of false

negatives in this screen. Worms may have had a mutation that suppressed the *daf-6* Daf-d phenotype, but were at the wrong stage of development for entering into dauer development when the plate became excessively crowded and the worms became starved. Thus we may have effectively screen through only a fraction of the 60,000 genomes.

Experimental Procedures

General methods and strains

Strains were cultured using as described by Brenner (Brenner, 1974). All strains were maintained at 20°C. The wild-type strain used was *C. elegans* var. Bristol (N2). In addition to the mutations isolated in the screen (*ns121*, *ns122*, *ns123*, *ns124*, *ns125*, *ns132*, *ns133*), the following alleles/strains were used in this study and are listed according to linkage group (LG).

LGV: $P_{gcy\text{-}5}$GFP(*ntIs1*)

LGX: *daf-6*(*e1377*, *m506*, *n1543*) (Starich et al., 1995), *unc-3*(*e151*) (Brenner, 1974).

Extrachromosomal: $P_{vap\text{-}1}$*DsRed*; $P_{gcy\text{-}5}$*gfp* (*nsEx820*, *nsEx927*, *nsEx942*), $P_{vap\text{-}1}$ DsRed(*nsEx71*)

Hawaiian (HW) is a polymorphic mapping strain (Wicks et al., 2001).

Mutagenesis and screening

Fourth larval stage (L4) P0 *daf-6*(*e1377*) animals were mutagenized with 25 mM ethyl methanesulfonate (EMS) for four hours at 20°C. These animals were then washed five times in M9 to remove the EMS. The animals were then placed on nematode growth medium (NGM) plates seeded with *E. coli* strain OP50. F1 progeny were picked to nine centimeter diameter NGM plates seeded with OP50. 50 F1 animals were placed on each plate, and 600 plates were prepared. These worms were cultured at 20°C for 10 days. Presumably these animals self-fertilized for two generations. After 10 days, no OP50 remained on the plates, and the worms were starved out. The starved worms were washed off the plates

with M9, placed in 1.5mL eppendorff tubes, spun down briefly in a picofuge, and the supernatant was removed. 0.5mL of 1% sodium dodecyl sulfate (SDS) was added to each tube, and the tubes were inverted several times over five to 10 minutes. Then the tubes were spun down briefly in a picofuge, and the worm pellet was removed and placed on a NGM plate. Any live dauer worms were picked off the plate, and placed on a NGM plate seeded with OP50. We did not separate individual dauer progeny; we assumed that dauer progeny were siblings, rather than independent mutations. The worms were allowed to recover from dauer and self fertilize, and their progeny were analyzed for amphid neuron dye uptake ability, as described below. Progeny of 30,000 mutagenized F1 worms, representing 60,000 mutagenized genomes, were screened.

Genetic analysis of mutations

Mode of inheritance: *daf-6*(*e1377*); $P_{gcy\text{-}5}$*gfp* males were crossed to hermaphrodites homozygous for *daf-6*(*e1377*) and a suppressor mutation. The Dyf phenotype was determined for GFP positive cross progeny hermaphrodites.

X-chromosome linkage: As described above, all suppressors are either semi-dominant or recessive. Therefore, to determine whether a mutation is on the X chromosome, we compared the penetrance of the Dyf phenotype in hermaphrodite versus male cross progeny. If the mutation is on the X chromosome, then the mutation would be hemizygous in male cross progeny and heterozygous in hermaphrodites. Two mutations (*ns125* and *ns133*) appear linked to chromosome X (Table 3.2).

The following is a strategy for further genetic mapping of *ns125* and *ns133* (Figure 3.4D). Mapping these mutations is slightly more complicated because these mutations are on the same chromosome as *daf*-6 (the X chromosome). First, as shown in Figure 3.4D, one can determine the frequency of recombination between the suppressor mutation and a *daf-6* allele marked by a recessive *unc-3* allele, which is 0.3 map units from *daf-6*. Second, a similar strategy can be used to determine the location and a refine the position of these mutations (Figure 3.4D). In this case, the *daf-6 unc-3* mutations are in a HW background. (This strain was generated by crossing the HW strain with the *daf-6 unc-3* ten times before re-homozygousing the strain for *daf-6 unc-3*.) After the crosses described in Figure 3.4D, one would determine the loci that are still homozygous for the N2 SNP. Only loci linked to the suppressor mutation (as well as *daf-6 unc-3*) would remain homozygous for the N2 SNP.

Autosome linkage: Polymorphic Hawaiian strain males were crossed to *daf-6*(*n1543*) *unc-3*(*e151*); *ns122* and *daf-6*(*n1543*) *unc-3*(*e151*); *ns132* hermaphrodites (Figure 3.4). Non-Unc cross progeny hermaphrodites were picked to new plates. Individual Unc, nonDyf progeny of these animals were then picked to individual plates. These worms should be homozygous for *daf-6*(*n1543*) *unc-3*(*e151*) and homozygous or heterzygous for *ns122* or *ns132*. To determine whether they were homozygous for the *ns* mutation, we determined whether 12 progeny of these worms all had non-Dyf progeny. Once we confirmed that the *ns* mutation was homozygous, we determined linkage to single nucleotide polymorphisms (SNPs). To identify the SNPs, we prepared the DNA and performed polymerase chain reaction (PCR) and restriction digests as previously described (Wicks et al., 2001). The locations of the SNPs, primers

used for PCR, enzymes used for restriction digests, and results are listed in Figure 3.4B and C.

Dye Uptake

Animals were washed off the plates with M9 and spun down briefly in a picofuge. The supernatant was removed, and the lipophilic dye 1, 1'-dioctadecyl-3, methylindodicarbocyanine, 4-chlorobenzenesulfonate salt ("DiD" solid; DiIC18(5) solid) (Molecular Probes) was added at 10 μg/ml in M9. Animals were then soaked in dye for 2 hr in the dark and at room temperature. Animals were next placed on NGM plates seeded with OP50 and scored using a fluorescence dissecting microscope.

Dauer formation ability

Five animals were placed on a 4cm diameter NGM plate seeded with OP50. Worms were allowed to grow and self-fertilize for 10 days at 20°C. During that time, all of the OP50 was eaten, and the worms became starved and crowded. As described above for the screen, these worms were soaked in 1% SDS for 5-10 minutes. We then counted the number of surviving, dauer animals. The assay was performed for 5 separate plates per strain. Because *daf-6*(*e1377*); *ns125* grew slowly, they were allowed to grow for 16 days.

Germline Transformation

Germline transformations were carried out using standard protocols (Mello and Fire, 1995). Some constructs were injected together with plasmid pRF4, containing the dominant marker *rol-6*(*su1006*) (Mello et al., 1991).

Microscopy

Animals were examined by epifluorescence using either a fluorescence dissecting microscope (Leica) or an Axioplan II compound microscope (Zeiss). Images were captured using an AxioCam CCD camera (Zeiss) and analyzed using the Axiovision software (Zeiss).

Electron Microscopy

Animals were fixed in 0.8% glutaraldehyde, 0.7% OsO4, 0.1 M cacodylate buffer for 1 hour on ice. Samples were post-fixed in 2% OsO4, 0.1 M cacodylate buffer, mounted into agar blocks, dehydrated in a series of alcohols and propylene oxide, and embedded in a mixture of Epon-Araldite. Thin sections (50 nm) were cut on an Leica Ultracut UCT Ultramicrotome, contrasted with 2% Uranyl Acetate and 1% Lead Citrate, and pictures were taken with an FEI Teenai G2 Spirit Biotwin TEM at 80 kV equipped with a Gatan 4K x 4K digital camera.

Acknowledgements

Thank-you to Grigorios Oikonomou for constructing and characterizing the Dyf phenotype of the *daf-6*(*n1543*) ns133 strain.

References

Bargmann, C. I., Mori, I., ed. (1997). Chemotaxis and thermotaxis. (Cold Spring Harbor, NY, Cold Spring Harbor Laboratory Press).

Brenner, S. (1974). The genetics of *Caenorhabditis elegans*. Genetics *77*, 71-94.

Burkitt, H. G., Young, B., Heath, J.W. (1993). Wheater's Functional Histology (Edinburgh, UK, Churchill Livingstone Press).

Cassada, R. C., and Russell, R. L. (1975). The dauerlarva, a post-embryonic developmental variant of the nematode Caenorhabditis elegans. Dev Biol *46*, 326-342.

Hartenstein, V., and Posakony, J. W. (1989). Development of adult sensilla on the wing and notum of Drosophila melanogaster. Development *107*, 389-405.

Kondo, K., Makovec, B., Waterston, R. H., and Hodgkin, J. (1990). Genetic and molecular analysis of eight tRNA(Trp) amber suppressors in Caenorhabditis elegans. J Mol Biol *215*, 7-19.

Lubarsky, B., and Krasnow, M. A. (2003). Tube morphogenesis: making and shaping biological tubes. Cell *112*, 19-28.

Mori, I., and Ohshima, Y. (1995). Neural regulation of thermotaxis in Caenorhabditis elegans. Nature *376*, 344-348.

Perens, E. A., and Shaham, S. (2005). C. elegans daf-6 encodes a patched-related protein required for lumen formation. Dev Cell *8*, 893-906.

Riddle, D. L., Albert. P.S., ed. (1997). Genetic and environmental regulation of dauer larva development. (Cold Spring Harbor, NY, Cold Spring Harbor Laboratory Press).

Shanbhag , S. R., Müller, B., Steinbrecht, R.A (2000). Atlas of olfactory organs of Drosophila melanogaster 2. Internal organization and cellular architecture of olfactory sensilla. Arthropod Structure & Development *29*, 211-229.

Starich, T. A., Herman, R. K., Kari, C. K., Yeh, W. H., Schackwitz, W. S., Schuyler, M. W., Collet, J., Thomas, J. H., and Riddle, D. L. (1995). Mutations affecting the chemosensory neurons of Caenorhabditis elegans. Genetics *139*, 171-188.

Ward, S., Thomson, N., White, J. G., and Brenner, S. (1975). Electron microscopical reconstruction of the anterior sensory anatomy of the nematode Caenorhabditis elegans.?2UU. J Comp Neurol *160*, 313-337.

Wicks, S. R., Yeh, R. T., Gish, W. R., Waterston, R. H., and Plasterk, R. H. (2001). Rapid gene mapping in Caenorhabditis elegans using a high density polymorphism map. Nat Genet *28*, 160-164.

Yu, S., Avery, L., Baude, E., and Garbers, D. L. (1997). Guanylyl cyclase expression in specific sensory neurons: a new family of chemosensory receptors. Proc Natl Acad Sci U S A *94*, 3384-3387.

Figure 3.1

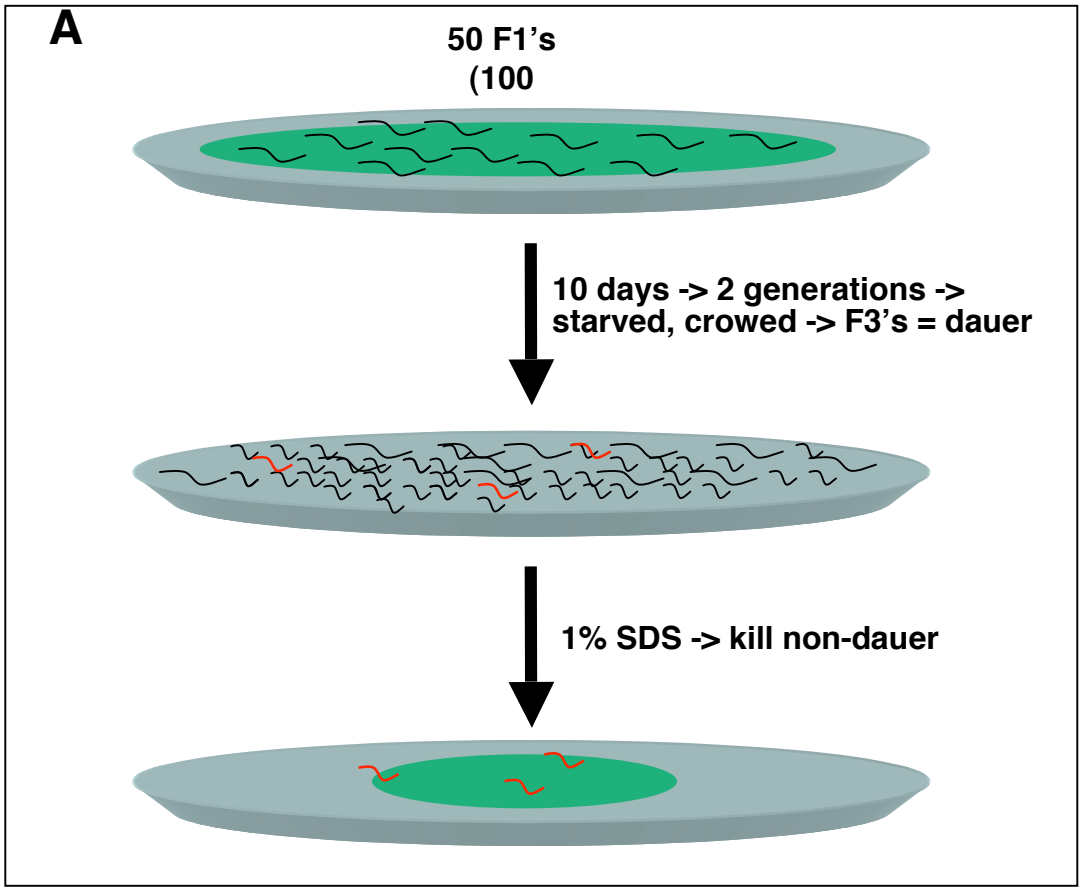
A
50 F1's
(100
10 days -> 2 generations ->
starved, crowed -> F3's = dauer
1% SDS -> kill non-dauer

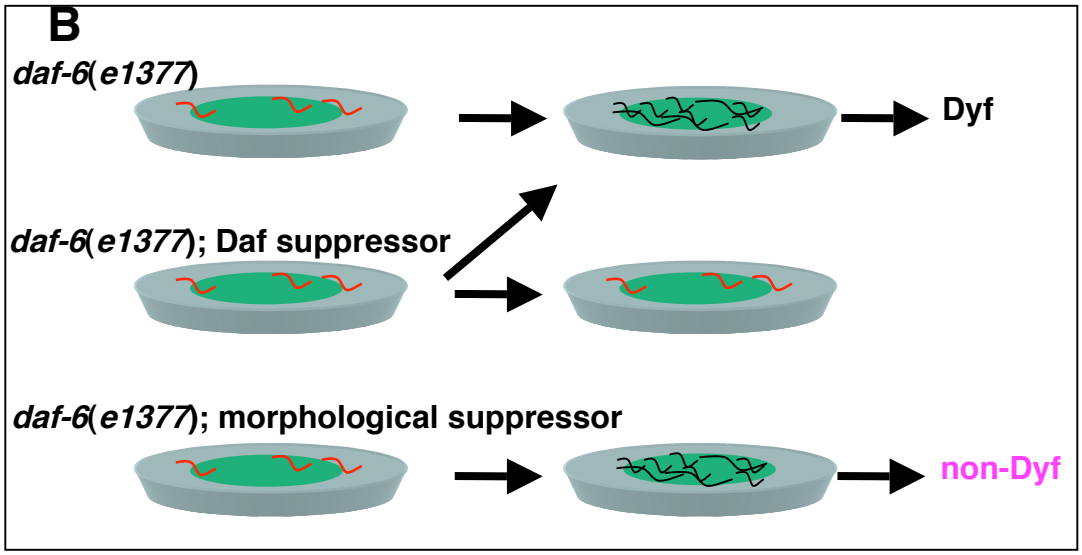
B
daf-6(e1377)
Dyf
daf-6(e1377); Daf suppressor
daf-6(e1377); morphological suppressor
non-Dyf

Figure 3.1. A screen for *daf-6* suppressors. (A) 50 mutagenized F1 *daf-6*(*e1377*) animals (curved lines) were placed on an NGM plate (gray circle) seeded with OP50 (green). Animals were allowed to self-fertilize for 10 days, during which time they would eat all of the OP50 and become starved and crowded. Some worms (red curved lines), as described in the text, may enter into dauer development. All worms were exposed to 1% SDS, which kills all non-dauer animals. (B) Live, dauer animals were placed on a separate plate, freshly seeded with OP50. Animals were allowed to recover from dauer, and their progeny were tested for dye uptake ability. Only worms with suppression of the amphid morphological defect should both recover from dauer and have non-Dyf progeny.

Figure 3.2

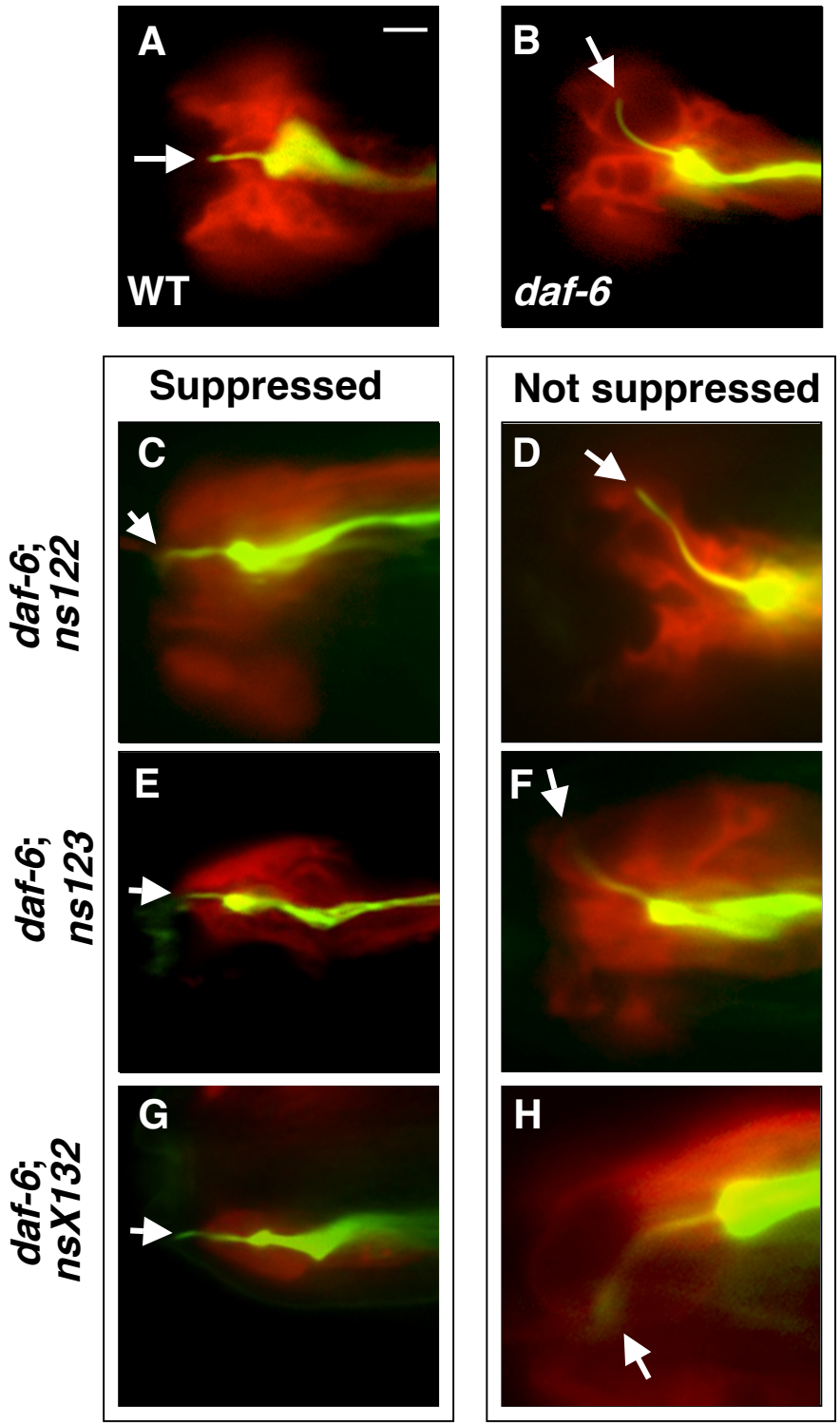
A
WT
B
daf-6
Suppressed
Not suppressed
C
D
daf-6; ns122
E
F
daf-6; ns123
G
H
daf-6; nsX132

Figure 3.2. The Amphid Sheath Cell Lumen Opens in suppressed *daf-6*(*e1377*) animals. Fluorescence images of adults containing P_{gcy-5}GFP (ASER neuron) and P_{vap-1} DsRed (sheath) reporter transgenes. (A) Image of a wild-type adult. ASE cilium (arrow) extends through sheath cell lumen. (B) Image of a *daf-6*(*e1377*) adult. ASE cilium (arrow) fails to extend through sheath cell lumen and remains embedded within the sheath cell. (C-H) Images of different *daf-6*(*e1377*) adult bearing a suppressing mutations. (C,E,G) Examples of suppressed animals in which the cilia extend through the sheath cell (arrow). (D,F,H) Examples of animals in which the Daf-6 amphid morphological defect is not suppressed and the cilia (arrow) remain embedded within the sheath cell. Anterior is left, dorsal is up. In some images (especially E and G), the sheath cell is at an angle, and as a result appears slightly smaller. Scale bar, 5 μm.

Figure3.3

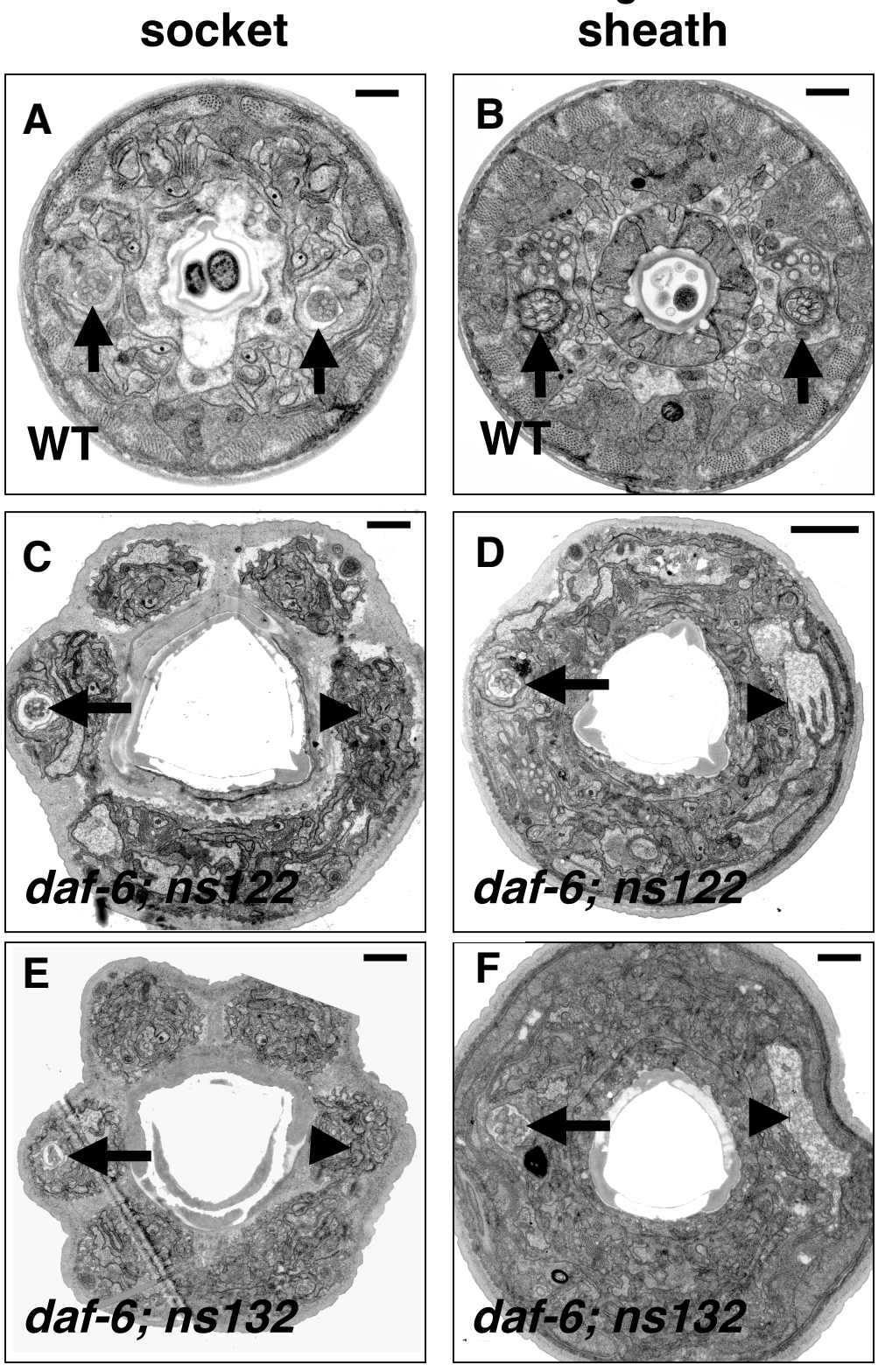
socket
sheath
A
WT
B
WT
C
daf-6; ns122
D
daf-6; ns122
E
daf-6; ns132
F
daf-6; ns132

Figure3.3

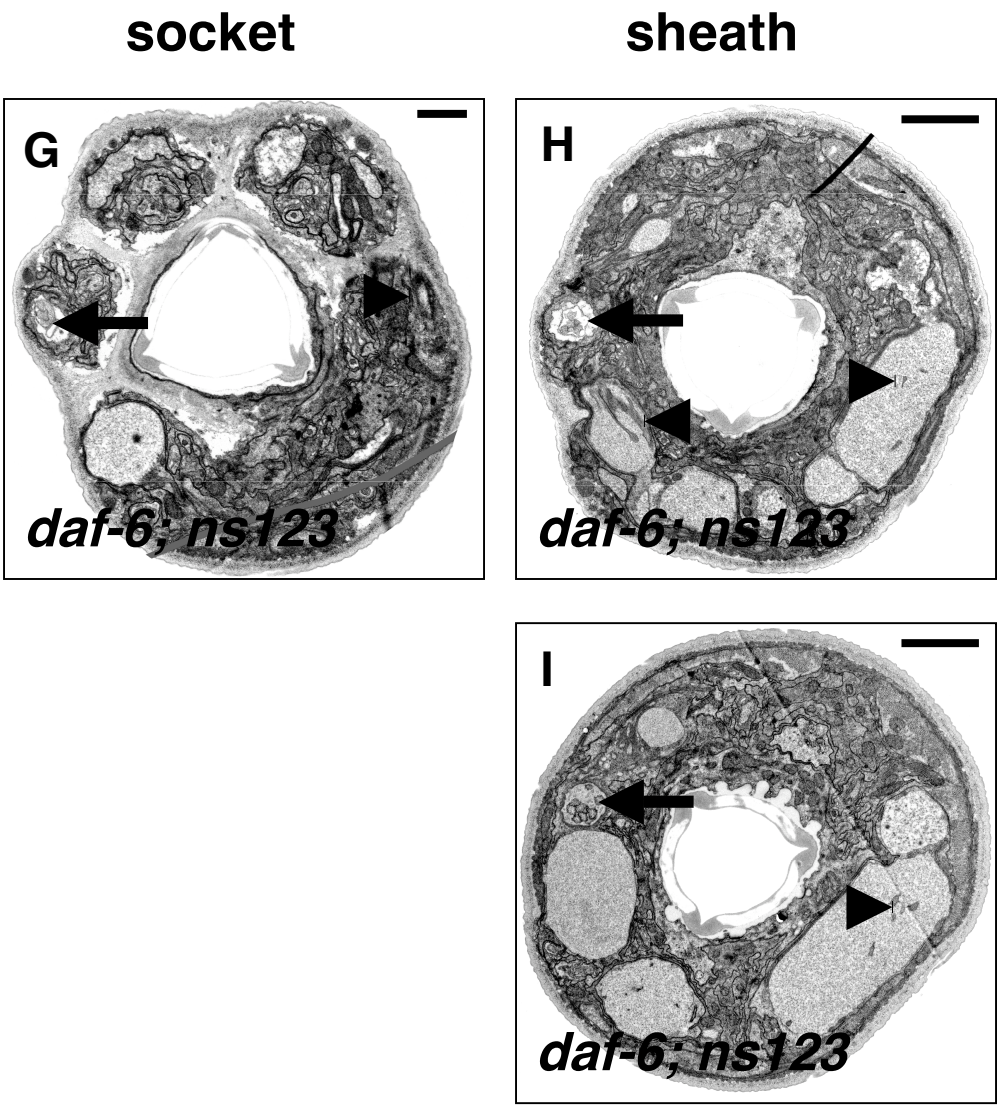

Figure 3.3. Suppressor mutations rescue amphid morphological defects. (A) Electron micrographs of a section of wild-type (A, B), *daf-6*(*e1377*); *ns122* (C, D), *daf-6*(*e1377*); *ns132* (E, F) adults, and *daf-6*(*e1377*); *ns123* (G-I) animals. (A, C, E, G) Sections at level of the socket cell. In both wild-type amphid sensilla, and one amphid of *daf-6*(*e1377*); *ns122*, *daf-6*(*e1377*); *ns132*, and *daf-6*(*e1377*); *ns123*, cilia extend through the socket cell (arrow). In one amphid of *daf-6*(*e1377*); *ns122*, *daf-6*(*e1377*); *ns132*, and *daf-6*(*e1377*); *ns123*, no cilia were identified in the socket (arrowhead). (B, D, F, H, I) Sections at level of the sheath cell. In one amphid of *daf-6*(*e1377*); *ns122*, *daf-6*(*e1377*); *ns132*, and *daf-6*(*e1377*); *ns123*, the sheath cell lumen is greatly expanded and contains electron-dense matrix and bent neuronal cilia (arrowhead), as previously seen in *daf-6*(*e1377*) animals (Perens and Shaham, 2005). In both wild-type amphid sensilla, and one amphid of both *daf-6*(*e1377*); *ns122* and *daf-6*(*e1377*); *ns132*, cilia reside in a tight fitting sheath cell lumen (arrow). In the *daf-6*(*e1377*); *ns132* animal, at a more posterior section (I) the cilia reside together in one channel (right side, arrow). More anteriorly (H), however, some cilia remain in a wild-type channel (left side, arrow), while others have spilt off into a separate channel and have a Daf-6 mutant appearance (bent cilia with accumulation of matrix) (left side, arrowhead). Scale bars, 0.5 μm (A), 1 μm (B,C,E,F, G), 2 μm (D, H, I).

Figure3.4

A

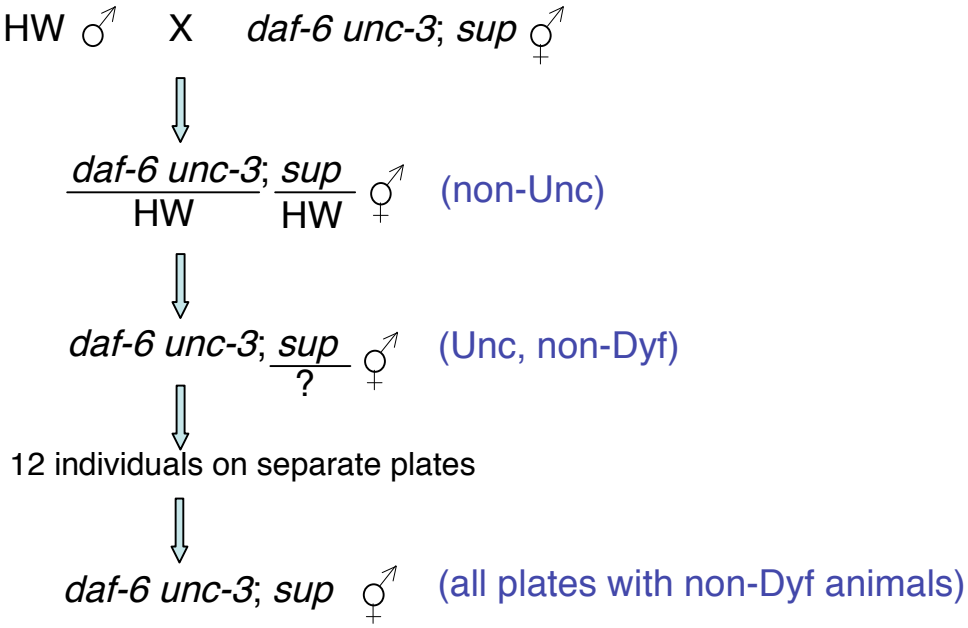
HW ♂ X daf-6 unc-3; sup ♀
daf-6 unc-3; sup / HW HW ♀ (non-Unc)
daf-6 unc-3; sup / ? ♀ (Unc, non-Dyf)
12 individuals on separate plates
daf-6 unc-3; sup ♀ (all plates with non-Dyf animals)

Figure3.4

B. *ns122* mapping data

Cosmid	Genetic Map Position	Primer Sequences, (restriction enzyme)	HW:N2 polymorphisms
Y18H1A	I: -18.6	AAGCGAACCAATCAGCAG, TCACGCCAAAATTAATGGG, (DraI)	13:13
D1007	I: -1.0	AAAATATCAGGAAAGAGTTTCGG, TTTAAAGATTAAGGGTGGAGCG, (DraI)	14:12
C37A5	I: 23.2	CTCATGCATGATTTCGAGGG, AAATCCAACAGGAGCAGGAC, (EcoRI)	15:11
Y38F1A	II: 13.9	TAGGAAAGTTGTGTCCACCTGG, TGATGACTCCTTCTTCAGCTGC, (HinfI)	8:18
T13C2	II: 0.1	TCCACACTATTTCCCTCTG, GAGCAATCAAGAACCGGATC, (DraI)	11:15
F58E1	II: -15.0	TTCAACCGTCTTGACTGCTAC, ATGGTAACCGCATGCTTTG, (XbaI)	7:19
Y71H2B	III: -12.1	GAGGAACCAAATCTGGCGTA, TGAAAACTTGGAAAATCGGTG, (DraI)	14:12
Y111B2A	III: 17.96	CTAGGCACCAATCATTACAAGC, TTTGTTGCCCTGATTTACATCC, (MseI)	13:13
F31F6	III: -0.9	CATTAGGAAGTGATGCAAGTGG, TGGATTTGAGAGGTGTCCATAG, (AvaII)	16:10
Y105C5B	IV: 14.4	GAATTTCAGGTGTTGGAAGG, TGCTCTGAAAAAATTGGCTG, (DraI)	6:20
Y45F10C	IV: 10.3	CCCAAAATGGAGTCTCTGTG, CCCAAGCTTTCATAATCGCG, (DraI)	6:20
F15E6	IV: 0.1	CCCTTCGTCAAAAATCATGCTC, TTCAGATGCAGAAAACGACAGG, (AccI)	4:22
W03D2	IV: -1.0	GGTTTTTGGGGTTACGGTAGTC, TCCCAGTTACTGTAGCTCCATG, (ApoI)	2:24
M02B7	IV: -2.2	TTAATTGGTGGAACTTTCGG, CTTGGAGTTGCCAAGAAGC, (NruI)	2:24
Y55H10A	IV: -4.1	CTCTTCCAAGATCTTCCAAGG, CTAAAAGTTGGCTGTTGACC, (AgeI)	2:24
F42A6	IV: -4.7	ACTTTCAGCTGCTCGTACTCTC, TCTGCCTTTTCACTTGCC, (DraI)	4:22
C37F5	IV: -8.3	TGTGGACACTTGAAACATTGTG, GTAGCCGCAATTACCAACTTTC, (EcoRI)	5:19
C54E4	IV: -10.2	CACAGTGTTCCCAGGTTGTAG, CCAAAATTCAAGTTGATGGC, (DraI)	5:19
K03H6	IV: -19.2	GTCATTGTCAGCAGGTTTCCC, TTCAAAGTCTTGATGGCTTCTG, (HpaII)	10:16
Y51A2D	V: 16.8	CAGGCATATTACATGGGATAGG, CAATCTCACCTCCATTCTGTG, (DraI)	15:11
Y61A9LA	V: -5.0	AAAAATCGACTACACCACTTTT, GAGATTCTAGAGAAATGGACAC, (DraI)	14:12

C. *ns132* mapping data

Cosmid	Genetic Map Position	Primer Sequences, (restriction enzyme)	HW:N2 polymorphisms
Y18H1A	I: -18.6	AAGCGAACCAATCAGCAG, TCACGCCAAAATTAATGGG, (DraI)	5:23
D1007	I: -1.0	AAAATATCAGGAAAGAGTTTCGG, TTTAAAGATTAAGGGTGGAGCG, (DraI)	6:22
C37A5	I: 23.2	CTCATGCATGATTTCGAGGG, AAATCCAACAGGAGCAGGAC, (EcoRI)	7:19
Y38F1A	II: 13.9	TAGGAAAGTTGTGTCCACCTGG, TGATGACTCCTTCTTCAGCTGC, (HinfI)	5:15
T13C2	II: 0.1	TCCACACTATTTCCCTCTG, GAGCAATCAAGAACCGGATC, (DraI)	10:18
F58E1	II: -15.0	TTCAACCGTCTTGACTGCTAC, ATGGTAACCGCATGCTTTG, (XbaI)	6:22
T25C8	III: 21.3	CGGTGGTGGTAAAAGTGTAAC, CAACATTCAGGCTGTGCTTTCC, (Hpy188III)	0:28
Y111B2A	III: 17.96	CTAGGCACCAATCATTACAAGC, TTTGTTGCCCTGATTTACATCC, (MseI)	0:28
Y75B8A	III: 15.4	AAACAGCATTGTCGACGAGC, AGCCTAAGCCCAAGCTTTAG, (HindIII)	0:28
Y47D3A	III: 9.4	CCGGATATTTTTATTCCGGC, GTCGGTTTTATTGAGAGGGG, (DraI)	6:22
T28D6	III: 8.7	TTTCGTGTACGAACGTCTCC, CATTTCTCCCACTCTTGCTG, (DraI)	6:22
Y39A1A	III: 4.4	CCCCACAGCTTTTAATCTTG, AAAGCCTTTCGGAACTTCC, (DraI)	12:14
F31F6	III: -0.9	CATTAGGAAGTGATGCAAGTGG, TGGATTTGAGAGGTGTCCATAG, (AvaII)	10:18
	III: -12.1	GAGGAACCAAATCTGGCGTA, TGAAAACTTGGAAAATCGGTG, (DraI)	13:15
Y105C5B	IV: 14.4	GAATTTCAGGTGTTGGAAGG, TGCTCTGAAAAAATTGGCTG, (DraI)	12:16
F42A6	IV: -4.7	ACTTTCAGCTGCTCGTACTCTC, TCTGCCTTTTCACTTGCC, (DraI)	13:15
K03H6	IV: -19.2	GTCATTGTCAGCAGGTTTCCC, TTCAAAGTCTTGATGGCTTCTG, (HpaII)	10:18
Y51A2D	V: 16.8	CAGGCATATTACATGGGATAGG, CAATCTCACCTCCATTCTGTG, (DraI)	10:16
Y61A9LA	V: -5.0	AAAAATCGACTACACCACTTTT, GAGATTCTAGAGAAATGGACAC, (DraI)	8:20

Figure3.4

D

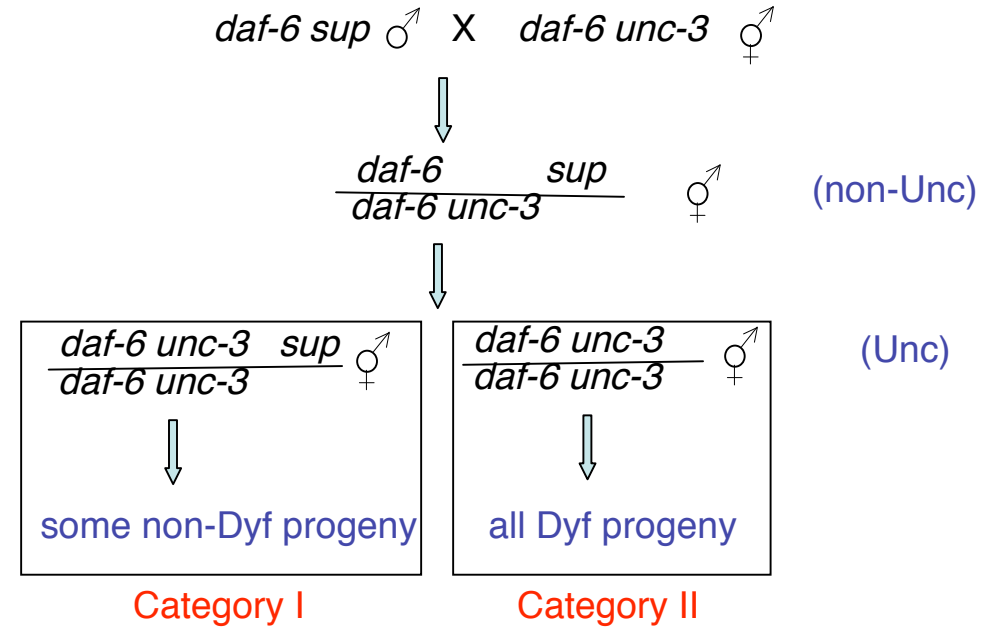
daf-6 sup ♂ X daf-6 unc-3 ♂
daf-6 sup
daf-6 unc-3
♂
(non-Unc)
daf-6 unc-3 sup
daf-6 unc-3
♂
some non-Dyf progeny
daf-6 unc-3
daf-6 unc-3
♂
all Dyf progeny
(Unc)
Category I
Category II

Figure 3.4. Mapping strategies and data. (A) Crosses for mapping *ns122* or *ns132*. Hawaiian (HW) is a polymorphic mapping strain. Hawaiian males were crossed to *daf-6*(*n1543*) *unc*-3; *sup* hermaphrodites, where *sup* was either *ns122* or *ns132*. The *daf-6*(*n1543*) *unc*-3; *sup* animals have the N2 strain genetic background. Non-Unc cross progeny were picked and allowed to have self-progeny. Unc, non-Dyf progeny were then picked to individual plates. These animals should be homozygous for *daf-6* (*daf-6* is 0.3 map units away from *unc-3*). Also, because these mutations are semi-dominant, they are either homozygous or heterozygous for the suppressor mutation. To determine whether the animals were homozygous for the suppressor mutation, we picked 12 progeny of each of these animals to separate plates and determined whether they all contained the suppressor mutation; that is, whether all of the progeny had non-Dyf progeny. (B,C) Mapping data for *ns122* and *ns132*. Single nucleotide polymorphisms, as described in Wicks et al., 2001, were identified using the listed primer sequences for PCR followed by restriction digestion with the listed restriction enzyme. Primer sequences are in the 5′ to 3′ orientation. The cosmid refers to the genomic clone containing the amplified sequence, and the genetic map position is the chromosome (roman numbers) and genetic location (as listed on www.wormbase.org) on the chromosome (arabic numbers) of the cosmid. Individual worms were obtained as described above, and we determined whether the animal was homozygous for the N2 polymorphism, homozygous for the HW polymorphism, or heterozygous for the two polymorphisms. Thus in each animal we tested two chromosomes. Listed in the "HW:N2 polymorphism" column is the total ratio of HW and N2 polymorphisms. If the mutation is linked to a loci, the frequency of the N2 polymorphism should be greater than HW

polymorphism. Conversely, if the loci is unlinked, then there should be equal numbers of N2 and HW polymorphisms. SNPs with the strongest linkage are highlighted. (D) Crosses for mapping suppressor mutations on the X chromosome (*ns123* and *ns133*). The ratio of Category I to Category II animals will reflect the recombination frequency between *daf-6 unc-3* and the suppressor mutation (*sup*). Also, when the *daf-6 unc-3* mutations are in the HW genetic background, SNPs can be characterized in the Category I worms. Loci linked to the *sup* (as well as *daf-6 unc-3*) will have the N2 SNP.

Table 3.1. Characterization of Dyf Phenotpyes

A. % Dyf defect in *daf-6*(*e1377*) animals

Strain	L1	L2	L3	L4	Adult
wild-type	0(50)	0(50)	0(50)	0(50)	0(50)
daf-6(*e1377*)	100(50)	100(50)	100(50)	100(50)	100(50)
daf-6(*e1377*); *ns121*	5(19)	4(50)	3(40)	3(45)	20(80)
daf-6(*e1377*); *ns122*	44(32)	55(29)	59(69)	54(52)	62(40)
daf-6(*e1377*); *ns123*	48(50)	52(55)	71(51)	50(50)	70(121)
daf-6(*e1377*); *ns124*	nd	100(50)	94(50)	98(50)	97(70)
daf-6(*e1377*); *ns125*	27(48)	18(50)	30(50)	26(50)	36(50)
daf-6(*e1377*); *ns132*	66(50)	62(50)	72(50)	64(70)	69(100)
daf-6(*e1377*); *ns133*	52(50)	64(50)	62(50)	75(51)	81(70)

B. % Dyf defect in *daf-6*(*n1543*) and *daf-6*(*m176*)

daf-6 allele	*daf-6*	*daf-6; ns122*	*daf-6; ns123*	*daf-6; ns124*	*daf-6; ns132*	*daf-6; ns133*
n1543	100(50)	58(50)	79(400)	97(220)	62(300)	73(104)
m176	94(50)	68(50)	64(50)	nd	76(50)	58(50)

Number in parentheses is the total number of animals scored.
ND, not determined

Table 3.2. Characterization of Dyf phenotypes in Cross Progeny

strain	**hermaphrodite**	**male**
daf-6(*e1377*); *ns121*	75(69)	43(105)
daf-6(*e1377*); *ns122*	94(80)	86(109)
daf-6(*e1377*); *ns123*	91(108)	73(206)
daf-6(*e1377*); *ns124*	98(108)	96(123)
daf-6(*e1377*); *ns125*	100(161)	81(115)
daf-6(*e1377*); *ns132*	99(76)	91(193)
daf-6(*e1377*); *ns133*	96(116)	60(183)

% Dyf animals.
Number in parentheses is the total number of animals scored.

Chapter 4

Conclusions and Future Directions

Elliot A. Perens

In this thesis, I demonstrate a requirement for *daf-6* and *che-14* in lumen morphogeneis and identify additional loci that function with *daf-6* to control amphid lumen formation. We still don't understand, however, how these lumens form and how these genes regulate lumen formation.

In this Chapter, I will discuss events that may occur to generate the amphid lumen, and I'll propose possible roles for *daf-6* in lumen formation. I will then briefly discuss a concept that may tie together three main concepts (lumen formation, glia morphogeneis, and SSD containing proteins) raised in this thesis- namely, lipid rafts. Finally, I'll propose experiments to address these questions.

Models for amphid lumen formation and *daf-6* function

daf-6 is required for lumen formation (Perens and Shaham, 2005). First, the amphid morphological and behavioral defects in *daf-6* mutants are consistent with a lumen formation defect. Second, *daf-6* is required in the amphid sheath cell when lumen formation occurs. Third, DAF-6 is expressed in and lines the luminal surface of numerous lumen forming cells in the worm, suggesting that *daf-6* is required for the formation of many tubes, not just the amphid. Consistent with this idea, *daf-6*; *che-14* double mutant worms have lumen defects in these other tubes.

Several possible steps may occur to form the lumen portion of the amphid. Presumably, the luminal surfaces must be specified. Several proteins, including DAF-6, CHE-14, and EXC-4, localize selectively to this surface, suggesting that it has unique membrane properties. The sheath and socket form junctions with each other, while the socket also forms junctions with the cuticle and the sheath

junctions with the amphid neurons. It is possible that these junctions separate the luminal surfaces from the remainder of the plasma membrane. In fact DAF-6::GFP in the amphid appears to extend posteriorly to the point of the neuron-sheath junctions. Thus, in the same way adherens junctions separate the apical surface from the basolateral surface in polarized epithelial cells, these junctions may separate the luminal from non-luminal surface. Still these junctions may only serve to maintain the different luminal surfaces, not to specify or generate them.

It is also unknown how lumen formation is initiated in the sheath and socket cells. The socket cell, which forms an autocellular junction, may wrap around the luminal space. On the other hand, lumen formation in the sheath, which has a seamless, intracellular lumen, may be initiated via invasion by the neuronal dendrites, followed by elaboration of the luminal membrane by the addition of vesicles. A similar mechanism appears to occur in *Drosophila* terminal and branch tracheal cells (Uv et al., 2003). Of course there are other possibilities. For example, in a process analogous to the formation of lumens in some fly trachea branches, the sheath and socket could initially form one multicullular lumen, with each cell initially wrapping half-way around the lumen (Ribeiro et al., 2004). Then cell migration would "pull" the cells apart, and the intercellular junctions would become the autocellular junctions for the socket and the sheath-neuron junctions for the sheath cell. As in the fly, zona-pellucida proteins would be required to maintain the integrity of the lumen as the cells change orientations relative to one another (Jazwinska et al., 2003).

As discussed in Chapter 1, vesicle addition to the luminal membrane appears to be a common feature in the formation of both unicellular and

muticellular lumens. Considering that *daf-6* is expressed and required in all types of tubes- seamless unicellular tubes (the amphid sheath cell and the excretory canal cell), unicellular tubes with autocellular junctions (the socket cell), and multicellular tubes (the vulva and rectum)- it is likely that *daf-6* plays a role in a common mechanism required for the formation of a types of tubes, such as vesicle transport. Several lines of evidence suggest that *daf-6* is involved in vesicle transport. First, DAF-6::GFP can be seen in punctate vesicle-like structures. Second, in place of an excretory canal lumen in *daf-6*; *che-14* mutants, unfused vesicles accumulate. Thus *daf-6* may regulate vesicle fusion to generate the lumen. Furthermore, DAF-6 related SSD containing proteins have all been found associated with vesicles, and the SSD may be an important regulator of subcellular localization. Perhaps most relevant, the worm Patched homolog PTC-1, which localizes to vesicles and the growing cleavage furrow, is required for germline cytokinesis. Thus *daf-6* may promote the addition (or prevent the removal) of vesicles from the growing luminal surface.

Lumen formation, glia morphogenesis, SSD containing proteins, and lipid rafts

At first glance, lumen formation, glia morphogenesis, and SSD containing proteins may appear to be random topics. In fact, perhaps the only common feature of these subjects is the role that the SSD containing protein DAF-6 plays in sensory organ lumen formation, as presented in Chapter 2. There may, however, be one underlying theme worth speculating about at this point, namely lipid rafts.

Lipid rafts are tightly packed membrane microdomains enriched in sphingolipids and cholesterol. Lipid rafts have been proposed to play roles in

processes such as signal transduction pathways, cell adhesion, cytoskeleton organization, and sorting during exocytosis and endocytosis. The rigid structure of cholesterol and sphingolipids orders membrane bilayers and reduces membrane permeability. Certain lipids and proteins prefer associating with the ordered membrane domains. Thus lipid rafts can organize membrane domains via lipid content, as opposed to protein-protein interactions.

So what does this have to do with lumens, glia, and SSD-containing proteins? First of all, as described in Chapter 1, the luminal surface of tubes corresponds to the apical surface of polarized epithelial cells. It turns out that lipid rafts may play an essential role in the biogenesis of the apical surface (while protein-protein interactions control the generation of the basolateral surface) (Schuck and Simons, 2004). While the plasma membrane, in general, has a higher cholesterol content than internal membranes, the apical surface is especially enriched in sphingolipids and cholesterol, perhaps to ensure their protective and diffusion functions (Simons and van Meer, 1988). Certainly, luminal surfaces, like in the amphid, vulva, rectum, and excretory canal (which are all exposed to substances from the outside environment), would benefit from having a membrane surface more stable and more resistant to diffusion. Sorting the lipid and protein components of the luminal surface by association with lipid rafts would ensure the enrichment of sphingolipids, cholesterol, and raft associated proteins in the luminal membranes.

Furthermore, like apical surfaces and luminal membranes, myelin is especially enriched in sphingolipids and cholesterol. In fact, some have noted the similarity in membrane composition between myelin and apical membranes (de Vries and Hoekstra, 2000). Like apical membranes, myelin is contiguous

with the rest of the plasma membrane but must acquire unique membrane characteristics. Thus, this feat may be accomplished in part by the preferential sorting of lipids and proteins via lipid rafts.

Finally, SSD-containing proteins may be a type of protein whose membrane distribution is determined by the presence of lipid rafts. In other words, the SSD may allow the protein to associate with the lipid raft. For example, SCAP and HMGCR would alter their membrane distribution depending on the level of sterols in the cell. In the presence of high sterols, lipids rafts could form, and these proteins could associate with other proteins that sort to the raft, in this case Insig 1 and 2. The association with the rafts and/ or the Insigs would ultimately determine the SSD-containing proteins subcellular sorting or degradation. Similarly, in the case of Patched, when Patched binds cholesterol-modified Hedgehog, the membrane properties may be altered. In turn, this would affect the ability of Patched to associate with lipid rafts and ultimately its ability to associate with other membrane proteins, especially Smoothened. SSD mutations, which affect the proteins' transmembrane region, may alter the proteins' ability to associate with lipid rafts.

In the case of DAF-6, its luminal surface localization may depend on the association of its SSD with luminal surface lipid rafts. In fact, evidence presented in Chapter 2 suggests that the DAF-6 SSD does play a role in targeting DAF-6 to the luminal surface.

Approaches to determining amphid lumen formation and *daf-6* function

There are several approaches to determining the *daf-6*'s role in lumen formation. Working in *C. elegans*, perhaps the most powerful approach would be

to do genetic screens, in this case *daf-6* modifier screens. Identification of genes that function with *daf-6* could provide insight into both *daf-6* function and lumen formation. One screen, a *daf-6*(*e1377*) suppression screen described in Chapter 3, has already identified loci that function with *daf-6* in amphid lumen formation. Of course, cloning the mutated genes is essential. Additionally, determining the nature of the mutations (gain-of-function versus loss-of-function) will provide insight into the role of these genes relative to *daf-6*. It will also be interesting to determine whether the mutations also suppress *che-14* mutations. This experiment would determine whether these loci function downstream or in parallel to just *daf-6* or both *daf-6* and *che-14*. Also, it would be interesting to determine whether these suppressor mutations could suppress the excretory canal and vulva defects in *daf-6*; *che-14* double mutant worms. This experiment would determine whether these genes, like *daf-6* and *che-14*, function in multiple lumen forming cells.

Other modifier screens could identify additional genes that function with *daf-6*. As described in Chapter 2, *daf-6*(*m176*) is a missense mutation in the first DAF-6 extracellular loop, and while the mutant protein is non-functional, it still properly localizes to the luminal surface. This mutation may disrupt the interaction between DAF-6 and an extracellular ligand. Thus a *daf-6*(*m176*) suppressor screen could identify an interaction suppressor. Because the *daf-6*(*m176*) phenotype is not fully penetrant, this screen would have to be performed clonally. Furthermore, a *daf-6* enhancer screen could identify additional factors like *che-14*. A technical problem with this screen is that *daf-6*; *che-14* mutants are very sick and fail to produce many progeny due to the Clr

and Elg phenotypes. Thus it could be difficult to identify worms with *che-14*-like enhancement of *daf-6* mutants.

Some evidence suggests that DAF-6 interacts with other proteins. As mentioned above, the *daf-6(m176)* allele is a missense allele. This mutation is in the first extracellular loop, and the mutant protein is still properly localized. These findings suggest that DAF-6 function may depend on an interaction with other proteins binding to the extracellular loop. Furthermore, a DAF-6::DsRed fusion protein, which was restricted to a perinuclear structure, caused Daf-6 phenotypes. These defects may have been caused by DsRed-induced aggregation of DAF-6, titrating proteins with which DAF-6 normally interacts. These factors could possibly be determined by identifying proteins that co-immunoprecipitate with DAF-6. More specifically, to identify proteins that interact with the first extracellular loop, one could look for proteins that co-IP with wildtype DAF-6 but not DAF-6(M176).

An additional approach to gaining insight into *daf-6* would be to examine *daf-6* homologs in other experimental organisms. For example, where are these genes expressed- lumen forming cells, glia, sensory organs? These experiments could reveal the evolutionarily conserved function of DAF-6.

Some experiments could be based on models for *daf-6* function and lumen formation. As described above and in Chapter 2, we propose that DAF-6 regulates vesicle transport during lumen formation. More specifically, as discussed in Chapter 2, DAF-6 could inhibit endocytosis during lumen formation. To test this idea, DAF-6 could be misexpressed in cells that normally undergo endocytosis. DAF-6 expression in HeLa cells, which undergo constitutive endocytosis, failed to inhibit this endocytosis (E. Perens, J.

Rappaport, and S. Shaham, unpublished observations). However, this result may be due to the inability of a worm protein to function in vertebrate cells. This difficulty could be overcome by using a vertebrate *daf-6* homolog or different cells. Alternatively, *daf-6* could be misexpressed in C. *elegans* ceolomocytes, which endocytosis material from the worm's body cavity. An assay for ceolomoctye function has been created and could be used to test *daf-6* ability to inhibit endocytosis (Fares and Greenwald, 2001). Taking a step back, one could determine whether, as described in Chapter 1, exocytosis is necessary for lumen formation. To test whether this is true, one could determine whether dominant negative forms of exocytosis factors expressed in the sheath and socket cells disrupt lumen formation.

Finally, one could determine the identity of the DAF-6::GFP positive vesicles seen in Figure 5 of Chapter 2. For example, is DAF-6 found in endosomes or lysosomes, like Patched (Capdevila et al., 1994; Denef et al., 2000; Incardona et al., 2002)? Alternatively, do these vesicles contain apical cell surface markers, like the *C. elegans* Crumbs homolog CRB-1, as seen in vesicles in the developing Drosophila salivary gland (Myat and Andrew, 2002)? In addition to identifying the nature of these vesicles, one could determine the identity of the different plasma membrane regions in the sheath and socket cells, as well as the other *daf-6* expressing, lumen forming cells. As discussed in Chapter 1, the luminal surface of various tubes contains apical surface markers. Is this property conserved by the sheath and socket lumens? In other words, does an apical surface marker, such as CRB-1, localize to the luminal surfaces of the sheath and socket cells? If this property of lumen forming cell is conserved, additional features of lumen formation in these other systems may be true for the sheath

and socket lumens.

References

Capdevila, J., Pariente, F., Sampedro, J., Alonso, J. L., and Guerrero, I. (1994). Subcellular localization of the segment polarity protein patched suggests an interaction with the wingless reception complex in *Drosophila* embryos. Development *120*, 987-998.

de Vries, H., and Hoekstra, D. (2000). On the biogenesis of the myelin sheath: cognate polarized trafficking pathways in oligodendrocytes. Glycoconj J *17*, 181-190.

Denef, N., Neubuser, D., Perez, L., and Cohen, S. M. (2000). Hedgehog induces opposite changes in turnover and subcellular localization of patched and smoothened. Cell *102*, 521-531.

Fares, H., and Greenwald, I. (2001). Genetic analysis of endocytosis in *Caenorhabditis elegans*: coelomocyte uptake defective mutants. Genetics *159*, 133-145.

Incardona, J. P., Gruenberg, J., and Roelink, H. (2002). Sonic hedgehog induces the segregation of patched and smoothened in endosomes. Curr Biol *12*, 983-995.

Jazwinska, A., Ribeiro, C., and Affolter, M. (2003). Epithelial tube morphogenesis during *Drosophila* tracheal development requires Piopio, a luminal ZP protein. Nat Cell Biol *5*, 895-901.

Myat, M. M., and Andrew, D. J. (2002). Epithelial tube morphology is determined by the polarized growth and delivery of apical membrane. Cell *111*, 879-891.

Perens, E. A., and Shaham, S. (2005). *C. elegans daf-6* encodes a patched-related protein required for lumen formation. Dev Cell *8*, 893-906.

Ribeiro, C., Neumann, M., and Affolter, M. (2004). Genetic control of cell intercalation during tracheal morphogenesis in *Drosophila*. Curr Biol *14*, 2197-2207.

Schuck, S., and Simons, K. (2004). Polarized sorting in epithelial cells: raft clustering and the biogenesis of the apical membrane. J Cell Sci *117*, 5955-5964.

Simons, K., and van Meer, G. (1988). Lipid sorting in epithelial cells. Biochemistry *27*, 6197-6202.

Uv, A., Cantera, R., and Samakovlis, C. (2003). *Drosophila* tracheal morphogenesis: intricate cellular solutions to basic plumbing problems. Trends Cell Biol *13*, 301-309.

Appendix I

Functional Genomics of the Cilium, a Sensory Organelle

Oliver E. Blacque[1], Elliot A. Perens[2], Keith A. Boroevich[1], Peter N. Inglis[1], Chunmei Li[1], Adam Warner[3], Jaswinder Khattra[3], Rob A. Holt[3], Guangshuo Ou[4], Allan K. Mah[1], Sheldon J. McKay[3], Peter Huang[3], Peter Swoboda[5], Steve J.M. Jones[3], Marco A. Marra[3], David L. Baillie[1], Donald G. Moerman[6], Shai Shaham[2] and Michel R. Leroux[1]

[1] Department of Molecular Biology and Biochemistry, Simon Fraser University, 8888 University Drive, Burnaby, British Columbia V5A 1S6, Canada, [2] Laboratory of Developmental Genetics, The Rockefeller University, 1230 York Avenue, New York, New York 10021, [3] Genome Sciences Centre, British Columbia Cancer Agency, Vancouver, British Columbia V5Z 4E6, Canada, [4] Section of Molecular and Cellular Biology, Center for Genetics and Development, University of California, Davis, Davis, California 95616, [5] Department of Biosciences, Section of Natural Sciences, Karolinska Institute, Södertörn University College, S-14189 Huddinge, Sweden, [6] Department of Zoology, University of British Columbia, Vancouver, British Columbia V6T 1Z4, Canada

I showed that C27H5.7a is *dyf-13* and characterized the *dyf-13* mutant phenotype.

For Supplemental Figures and Tables, see Blacque et al., 2005

Summary

Cilia and flagella play important roles in many physiological processes, including cell and fluid movement, sensory perception, and development (Scholey, 2003). The biogenesis and maintenance of cilia depend on intraflagellar transport (IFT), a motility process that operates bidirectionally along the ciliary axoneme (Scholey, 2003 and Rosenbaum and Witman, 2002). Disruption in IFT and cilia function causes several human disorders, including polycystic kidneys, retinal dystrophy, neurosensory impairment, and Bardet-Biedl syndrome (BBS) (Pazour and Rosenbaum, 2002; Katsanis et al., 2001; Ansley et al., 2003). To uncover new ciliary components, including IFT proteins, we compared *C. elegans* ciliated neuronal and nonciliated cells through serial analysis of gene expression (SAGE) and screened for genes potentially regulated by the ciliogenic transcription factor, DAF-19 (Swoboda et al., 2000). Using these complementary approaches, we identified numerous candidate ciliary genes and confirmed the ciliated-cell-specific expression of 14 novel genes. One of these, C27H5.7a, encodes a ciliary protein that undergoes IFT. As with other IFT proteins, its ciliary localization and transport is disrupted by mutations in IFT and *bbs* genes. Furthermore, we demonstrate that the ciliary structural defect of *C. elegans dyf-13(mn396)* mutants is caused by a mutation in C27H5.7a. Together, our findings help define a ciliary transcriptome and suggest that DYF-13, an evolutionarily conserved protein, is a novel core IFT component required for cilia function.

Results and Discussion

Identification of Candidate Ciliary Genes through SAGE and a Bioinformatic Screen for Genes Potentially Regulated by X Box Promoter Elements

In the first approach, we used LongSAGE to obtain a *C. elegans* ciliated-cell transcriptome. Ciliated neurons expressing GFP from the ciliated-cell-specific *bbs-1* gene promoter (Ansley et al., 2003) were isolated and used to construct a LongSAGE library as described (Shah et al., 2002 and McKay et al., 2003). To identify candidate ciliary genes, we compared our ciliated-cell SAGE transcriptome to pan-neural-, muscle-, and gut-specific transcriptomes, all normalized to 50,000 tags (available at http://www.bcgsc.ca). Because ciliated neurons account for only 20% of all embryonic neurons, genes expressed predominantly in ciliated neurons should be represented by more SAGE tags in the ciliated-cell (C) transcriptome than in the pan-neural (P) transcriptome. Similarly, ciliated-cell-specific transcripts should be underrepresented in the nonciliated muscle (M) and gut (G) transcriptomes. Table S1 (in the Supplemental Data available with Blacque et al., 2005) presents the SAGE data, sorted by genes with the most favorable ciliated-cell SAGE tag enrichment factors across all three comparison groups (C/P, C/M, and C/G). As expected, the top-ranked genes from Table S1 contain numerous cilia-related genes, including IFT-related genes (*daf-19*, *bbs-1*, *che-2*, *che-13*, and *osm-6*), structural components (*tba-9*, *tba-6*, and *mec-12)* and motor components (F41G4.1, axonemal dynein; *dli-1*, cytoplasmic dynein; and *klp-11*, kinesin). To assess the specificity of

our SAGE approach in detecting ciliated-cell-specific genes, we screened Table S1 for genes known to be expressed predominantly in ciliated cells; 25 of 42 such genes found (60%) were enriched for SAGE tags in the ciliated-cell transcriptome versus the pan-neural, muscle, and gut transcriptomes (Table S2). These data suggest that Table S1 likely contains many excellent candidate ciliary genes. To estimate the proportion of false positives in Table S1, we investigated the top 200 genes and found 51 genes with known expression data; 34 of these genes (67%) are expressed in nonciliated cells, indicating a relatively high but acceptable false-positive rate. On the basis of these findings, we sought to further refine our search for candidate cilia-related genes with a complementary approach.

We performed a genome-wide bioinformatic screen for genes potentially regulated by X boxes. In *C. elegans*, these conserved 14 bp regulatory elements (usually 50–150 bp upstream of start codons) are bound by DAF-19, the RFX-type transcription factor that regulates ciliary gene (IFT and *bbs*) expression (Ansley et al., 2003; Swoboda et al., 2000; Fan et al., 2004; and Li et al., 2004). We derived an improved X box consensus sequence for our screen by confirming the ciliated-cell-specific expression of several candidate X-box-containing genes identified in a previous, more preliminary study (Fan et al., 2004). Using transcriptional-GFP reporters, we observed ciliated-cell-specific expression for five novel genes, namely K03E6.4, C48B6.8, C47E8.6, ZK328.7a, and F19H8.3 (Figure S1; data not shown for F19H8.3). Figure S1 also shows the ciliated-cell-specific pattern for Y110A7A.20 and K08D12.2, which were not shown in our previous study (Fan et al., 2004). Importantly, the expression of ZK328.7a, Y110A7A.20, and C48B6.8 was found to be dependent on DAF-19 (Figure S2). Using an updated Hidden

Markov Model X box profile based on 22 sequences, including the novel X-box-containing genes discussed above (Table S3), we scanned the *C. elegans* genome for X boxes within 1500 bp upstream of start codons. A total of 1572 putative X-box-containing genes with human homologs were identified (Table S4). As expected, the greatest number of high-scoring (>16.0) X boxes occurred between -60 and -120 bp (Figure S3A), which coincides with the canonical position (Swoboda et al, 2000).

As described above for the SAGE data, we found that the number of false positives in Table S4 is relatively high, but the dataset still contains a large proportion of bona fide ciliary genes. Of the top 200 ranked candidate X box genes with known anatomic expression data (64 genes), 27 (or 42%) are expressed in ciliated cells.

To identify our best candidate ciliary genes, we considered genes with enrichment of SAGE tags in the ciliated SAGE dataset versus the pan-neural, muscle, and intestine datasets (Table S1), *and* with putative X boxes within 250 bp of start codons (Table S4). Using these criteria, we present 46 such genes in Table 5.1. Also included are seven additional genes (at the bottom of Table 5.1), which rank highly in *either* the SAGE *or* X box datasets. As expected, Table 5.1 contains many known IFT-related genes, including *che-2*, *che-13*, *osm-1*, *osm-5*, *osm-6*, F32A6.2 (IFT81), *bbs* genes, and *daf-19*. Other excellent candidate and known ciliary genes include K08D12.2 (homolog of retinitis pigmentosa 2), which is expressed predominantly in ciliated neurons (Figure S1), and Y32G9A.6, an ankyrin-repeat-containing protein that is homologous to inversin, which is

linked to cilia-associated *situs inversus* and cystic-kidney phenotypes (Otto et al., 2003). Table 1 also includes uncharacterized genes identified as candidate ciliary genes in other genomic and proteomic screens (Li et al., 2004; Avidor-Reiss et al., 2004; and Ostrowski et al., 2002); these genes include C27H5.7a (TPR containing), C54G7.4 (WD repeat containing), K07G5.3 (Ca2+ binding domain containing), and two B9-protein-domain-containing genes (Y38F2AL.2 and K03E6.4), as well as several genes not previously associated with a ciliary function. C27H5.7a is particularly interesting because it was also recently found by Colosimi et al. (Colosimo et al., 2004) to be expressed in the AWB ciliated olfactory neuron. Importantly, the number of false-positive genes in Table 5.1 is relatively low; 13 of the 20 genes from Table 5.1 with known anatomic expression data (WormBase [http://www.wormbase.org] and Figure S1) are expressed in ciliated cells. Along with GFP-expression data presented below, we estimate the false-positive rate for the top 46 genes in Table 5.1 to be approximately 26% (7 of 27 genes), which is significantly lower than that found for the individual SAGE (67%) and X box (58%) analyses.

Expression Analysis of Candidate Ciliated-Cell-Specific Genes

Nine new candidate ciliated-cell-specific genes were chosen for expression analysis on the basis of strong SAGE *and* X box data (Table 5.1; seven genes) or a high ranking in the individual X box table (Table S4; two genes). Using transgenic worms bearing promoter-GFP reporters, we found that all nine genes demonstrated a ciliated-cell-specific expression pattern (Figure 5.1; data not shown for C02H7.1). Transcriptional *gfp* reporters for C27H5.7a (unknown

function), Y38F2AL.2 (B9 domain containing), H01G02.2 (serine/threonine kinase), C54G7.4 (WD domain containing), D1009.5 (dynein light chain), and Y32G9A.6 (inversin-like) produced strong GFP signals in most ciliated cells, including amphid, phasmid, and labial-quadrant neurons. Similarly, F54C1.5a (TPR domain containing) and K07G5.3 (Ca2+ binding domain containing) expressed in most amphid, both phasmid, and several labial-quadrant neurons. That the expression of the *gfp* reporters was not detected in nonciliated cells suggests that these novel genes have ciliary functions. It is notable that all of the genes selected from Table 5.1 for expression analysis demonstrated a ciliated-cell expression pattern. This is a very strong indication that Table 5.1 is highly enriched for novel cilia-related genes.

Cellular Localization of Candidate Ciliary Proteins

To investigate the possible functions of some of the ciliated-cell-specific proteins identified above, namely C27H5.7a, Y37E3.5, K08D12.2, and F19H8.3, we examined their cellular localization with translational *gfp* reporters (Figure S4A). Interestingly, GFP-tagged C27H5.7a (unknown function) and Y37E3.5 (GTP binding protein, ARL2-like-1) associate with ciliary axonemes in both head (amphids, labials) and tail (phasmids) neurons, with relatively little localization to cell bodies, axons, or dendrites. In addition, C27H5.7a::GFP localizes to the transition zones (basal bodies at the base of cilia). GFP-tagged Retinitis Pigmentosa 2 homolog K02D12.2 appears to envelop the transition zones in a ring-like fashion (Figure S4A), indicating a possible role at the base of cilia. GFP-

tagged ARL-3 (F19H8.3) is found throughout the cell, with little ciliary localization even though its expression is limited to ciliated cells.

C27H5.7a Is a Novel IFT-Associated Protein

A major focus of our functional genomic studies is to uncover novel core ciliary proteins, including IFT components. First described in *Chlamydomonas* (Kozminski et al., 1993), IFT involves the kinesin- and dynein-dependent bidirectional movement of IFT particles and associated cargo along ciliary axonemes (Scholey, 2003; Rosenbaum and Witman, 2002; Pazour and Rosenbaum, 2002; Kozminski et al., 1993). In *C. elegans*, anterograde transport of IFT particles along the middle segment of cilia is driven cooperatively by two Kinesin-2 motors (heterotrimeric Kinesin-2 and homodimeric OSM-3) and by OSM-3 alone along the distal segments (Snow et al., 2004). IFT particles have been shown biochemically to be composed of two large protein complexes (A and B) containing at least 16 proteins in total (Piperno and Mead, 1997; Cole et al., 1998).

Using time-lapse microscopy, we examined animals expressing C27H5.7a::*gfp* and found that the GFP-tagged protein exhibited IFT along ciliary axonemes of head and tail neurons (Figure S4B; Document S2; Movies S1 and S4). Anterograde transport rates along the middle and distal segments were determined to be 0.70 ± 0.11 É m/s (n = 245) and 1.25 ± 0.15 μm/s (n = 255), respectively, with the retrograde transport rate estimated to be 1.32 ± 0.2 μm/s (n

= 5). Remarkably, these transport rates for C27H5.7a::GFP are almost identical to those previously reported for the Kinesin-2 motors and IFT particle components (Scholey, 2003; Snow et al., 2004), indicating that C27H5.7a is transported with IFT particles by heterotrimeric Kinesin-2 and OSM-3 within the middle segments of ciliary axonemes and by OSM-3 kinesin alone within the distal segments.

We then examined the behavior of C27H5.7a::GFP in two IFT mutant strains, namely *osm-5(p813)* and *che-11(e1810)*, both of which possess truncated cilia and display abrogated IFT. In these mutants, C27H5.7a::GFP displayed little or no detectable IFT and accumulated in the dendrite and transition zones of the *osm-5* mutant, as well as within the transition zones and along the ciliary axonemes in the *che-11* background (Figure 5.2A; Document S2; Movies S2, S3, S5, and S6). The dependence of C27H5.7a on *osm-5* and *che-11* for its normal localization and motility strongly suggests that C27H5.7a is part of the motor-IFT particle-cargo complex. To provide further evidence that C27H5.7a is likely a core component (and not cargo) of IFT particles, we studied its behavior in *bbs* mutant backgrounds. Previously, we observed that GFP-tagged CHE-2 often accumulated near the midpoint and distal segments of ciliary axonemes in *bbs* mutants [Blacque et al., 2004]. We now show that three other GFP-tagged IFT components, namely CHE-13, OSM-1, and OSM-6, demonstrate the same phenotype in a *bbs-7* mutant (*osm-12(n1606)*) (Figure 5.2B; data for CHE-2 and OSM-6 shown in Figure S5). Interestingly, when expressed in the *bbs-7* or *bbs-8*mutant backgrounds, C27H5.7a::GFP displays the same mislocalization phenotype as OSM-1, OSM-6, CHE-2, and CHE-13 (Figure 5.2B; Document S2;

Movies S7–S16; data not shown for *bbs-8* mutant), suggesting that C27H5.7a is closely associated with IFT particle components and does not represent cargo.

The *dyf-13* Mutant Contains a Mutation in C27H5.7a and Possesses Abnormal Cilia

To provide additional evidence that C27H5.7a is a core ciliary component, we searched existing sensory mutants for mutations in this gene. Using this approach, we found that *dyf-13(mn396)* animals contained a guanine-to-adenine mutation in the acceptor site of intron 7 of C27H5.7a (Figure 5.3A). *dyf-13* mutants are defective in sensory neuron dye filling and chemosensation (Starich et al., 1995). Specifically, only 18% of amphid and 4% of phasmid sensory organs displayed wild-type dye filling (Figure 5.3B). This phenotype, comparable to that of IFT and *bbs* mutants (Blacque et al., 2004; Starich et al., 1995; Perkins et al., 1986), suggests that ciliary structures are compromised. Using a *ceh*-23 promoter::*gfp* reporter (gift of G. Garriga) that illuminates the cell bodies, dendrites, transition zones, and cilia of the phasmid neurons, we found that the cilia of *dyf-13* animals were indeed malformed (Figures 5.3C and 3D). Specifically, the average length of the cilium in *dyf-13*(*mn396*) animals was 6.7 ± 0.8 μm (n = 20) in comparison to 8.6 ± 1.6 μm (n = 20) in wild-type animals, and the neurons appeared to lack the distal portion of the cilia. This cilia defect is similar to that observed in animals harboring mutations in *osm-3*, an IFT-specific kinesin required to build the distal segment (Snow et al., 2004; Perkins et al., 1986). Importantly, the dye-filling defect of *dyf-13(mn396)* mutants was similarly rescued in three independent lines expressing either the C27H5 cosmid or a

transgene bearing the wild-type C27H5.7 gene (Figure 5.3B; data shown for one rescued line in each case).

On the whole, our findings provide strong evidence that DYF-13 (C27H5.7a) is an IFT protein that is important for the formation and function of cilia. Consistent with this conclusion, an uncharacterized human homolog (FLJ12571) with 37% amino acid identity and 59% similarity throughout its length exists, and counterparts are found in all ciliated organisms (including *Chlamydomonas reinhardtii*), but not in nonciliated organisms such as *Arabidopsis thaliana* or *Saccharomyces cerevisiae*.

Experimental Procedures

Strains

All strains were cultured and maintained at 20ºC with standard techniques. Strains used were N2 (Bristol), KR3532: *dpy-5(e907)*, CB3330: *che-11(e1810)*, PR813: *osm-5(p813)*, MT3645: *osm-12(n1606)*, SP1678: *dyf-13(mn396)*, PT47: *N2;Ex[che-2::gfp + rol-6(su1006)]* (donated by M. Barr, University of Wisconsin), MX47:*osm-12(n1606);Ex[che-2::gfp + rol-6(su1006)]*, MX14: *N2;Ex[che-13::gfp + rol-6(su1006)]* (donated by B. Yoder, University of Alabama), *N2;Ex[osm-1::gfp + rol-6(su1006)]* (donated by J. Scholey, University of California), *osm-12(n1606);Ex[osm-1::gfp + rol-6(su1006)]* (J. Scholey), *N2;Is[osm-6::gfp + rol-6(su1006)]* (donated by R. Herman, University of Minnesota), *osm-12(n1606);Is[osm-6::gfp + rol-6(su1006)]* (J. Scholey), MX92: *osm-12(n1606);Ex[che-13::*
Gfp + rol-*6(su1006)]*, MX9: *dpy-5(e907);nxIs11[dpy-5(+) + bbs-1p::gfp]*, JT204: *daf-12(sa204)X*, and JT6924: *daf-19(m86)II; daf-12(sa204)X*.

RNA Extraction for SAGE Analysis

To isolate a population of ciliated neuronal cells for SAGE analysis, we first generated a stable line expressing a previously described transcriptional *gfp* reporter for *bbs-1* 9 (Ansley et al., 2003). This reporter is expressed exclusively within the ciliated cells of the nematode, beginning at the onset of ciliogenesis between the comma and 1.5-fold stages of embryogenesis (Ansley et al., 2003).

According to standard protocols (McKay et al., 2003), midstage embryos from *dpy-5(e907);nxIs[dpy-5(+) + bbs-1p::gfp]* were digested, and ciliated cells expressing *bbs-1p::gfp* were isolated from the resulting total embryonic cell population via FACS sorting. The *gfp*-expressing neurons in the final sorted population were assessed to be greater than >95% of the total cell population. Total RNAwas isolated with TRIzol reagent (Invitrogen, Mississauga, ON), a monophasic solution of phenol and guanidine isothiocyanate, in conjunction with Eppendorf brand phase lock gel tubes (Fisher Scientific). The latter enable clean and quantitative recovery of the RNA-containing phase. RNAwas assessed for quality and quantified with an Agilent 2100 Bioanalyzer (Agilent Technologies, Mountain View, CA) and RNA 6000 Nano LabChip kit (Caliper Technologies, Mountain View, CA).

LongSAGE Library Construction

LongSAGE (Saha et al., 2002) library construction was performed with 5 μg of Dnase-I-treated (DNA-*free* reagent, Ambion, Austin, TX) total RNA and the Invitrogen I-SAGE Long kit. In brief, total RNA was converted to cDNA with oligo (dT) magnetic beads. After cleavage with the anchoring enzyme NlaIII, the 3′ cDNA restriction fragments were divided into two tubes and ligated to one of two linkers containing the type IIS MmeI restriction-enzyme site. The linker-cDNA molecules were released from the beads by digestion with MmeI. After ligation of the two linker-cDNA tag pools and subsequent scale-up PCR amplification, cDNA ditags were produced by cleaving with the anchoring enzyme NlaIII. The resulting ditags with CATG overhangs were ligated to form

concatemers. Different concatemer size fractions were cloned into pZErO-1 vector, and transformations were done with One Shot TOP10 Electrocomp *E. coli*. After screening of transformants by colony PCR, the best concatemer size fraction was chosen for sequencing.

Colony picking was performed with a Q-Pix robot (Genetix, Beaverton, OR), and inoculations were made into 2x YT media with 50g/ml Zeocin and 7.5% glycerol. After overnight culture, glycerol stocks were used to inoculate larger volume cultures for plasmid preparation with a standard alkaline lysis procedure adapted for high-throughput processing with microtiter plates. DNA sequencing was performed with BigDye v3.1 dye terminator cycle sequencing reactions run on Tetrad thermal cyclers (MJ Research, Waltham, MA). Sequencing reaction products were purified by isopropanol precipitation and then run on model 3730xl capillary DNA sequencers (Applied Biosystems, Foster City, CA).

Resulting DNA sequence data were collected automatically with a custom DNA sequencing Laboratory Management Information System (LIMS) and processed by trimming of reads for sequence quality and removal of nonrecombinant clones, linker-derived tags, and duplicate ditags. Although first-position SAGE tags (as defined by the NlaIII restriction site nearest the 3' poly A tail) account for >95% of all tags for a given gene transcript, we noted a small number of genes for which the tag counts were unusually high at the more 5' SAGE tag positions, indicating alternatively spliced transcripts or errors in that particular gene model. Therefore, for

each gene, we included all of the SAGE tags that fall within the predicted gene model open reading frame (WormBase version WS120). Our final dataset of 51,086 SAGE tags (of which 16,468 were unique) corresponded to 6,726 nematode

gene transcripts. Of the gene transcripts, 3,819 (or 57%) were represented by two tags or less, with only 538 (or 8%) being represented by more than 10 tags. These abundant transcripts (>10 tags) account for 32% of all tags. When comparing the relative abundance of a particular gene transcript in two SAGE libraries, we determined statistical significance values according to the method of Audic and Claverie (Audic and Claverie, 1997) and then normalized the total tag count of both libraries.

HMM Profiling

To scan the *C. elegans* genome for genes containing an X box in their upstream promoter regions, a profile Hidden Markov Model (HMM) of this regulatory DNA sequence was created with HMMER version 1.8.4 (Eddy, 1998). The profile HMM was constructed from a training set of 22 X-box-containing genes whose expression has been shown to be restricted to the ciliated neurons of *C. elegans* (Table S3). With this profile HMM, the complete *C. elegans* genome (WormBase version WS120) was scanned, resulting in the identification of 3,406 putative X box sequences (raw homology score >10.0) within 1.5 kb of the start codon. Of these putative X-box-containing genes, 1,572 of them possess significant homology to a human gene (Blast E-value $<e^{-10}$).

GFP Expression Analysis

Transcriptional and translational *gfp* fusion constructs for genes of interest were constructed via fusion PCR as described previously (Ansley et al., 2003; Blacque

et al., 2004; Hobert, 2002). For the transcriptional *gfp* fusion constructs, varying 5″UTR fragment lengths were fused to the coding sequence of *gfp*. Specifically, the 5″UTRs consisted of 507 bp for C47E8.6, 513 bp for ZK328.7a, 1047 bp for C48B6.8, 2869 bp for K03E6.4, 1121 bp for Y110A7A.20, 503 bp for K08D12.2, 669 bp for C27H5.7a, 503 bp for F54C1.5a, 511 bp for C54G7.4, 506 bp for F19H8.3, 508 bp for Y32G9A.6, 538 bp for H01G02.2, 1144 bp for D1009.5, 270 bp for K07G5.3, and 623 bp for H01G02.2. For the translational *gfp* fusion constructs (C27H5.7a, Y37E3.5, K08D12.2, and F19H8.3), the entire exonic and intronic sequences of the gene of interest, along with a segment of its 5″UTR (described above and in (Fan et al., 2004) for Y37E3.5), was fused in-frame with *gfp*. Transgenic animals expressing the transcriptional or translational *gfp* transgenes as extrachromosomal arrays in *dpy-5(e907);Ex[dpy-5(+)]* animals were generated as described previously (Ansley et al., 2003). For analysis of candidate ciliary gene expression in a *daf-19(m86)* mutant background, transcriptional *gfp* transgene expression was examined in *daf-19(m86);daf-12(sa204)* and *daf-12(sa204)* mutants as described previously (Li et al., 2004).

Dye Uptake

Animals were washed off nematode growth medium (NGM) plates with M9 medium (Sulston and Hodgkin, 1998) and spun down briefly in a picofuge. The supernatant was removed, and the lipophilic dye 1, 1″-dioctadecyl-3, methylindodicarbocyanine, 4-chlorobenzenesulfonate salt (“DiD” solid; DiIC18[5] solid) (Molecular Probes) was added at 10 μg/ml in M9. Animals were then soaked in dye for 2 hr in the dark and at room temperature. Animals were

next placed on NGM plates seeded with *E. coli* strain OP50 and were scored with a fluorescence compound microscope.

Rescue of *dyf-13(mn396)* Dyf Phenotype

dyf-13(mn396) mutants were transformed under standard protocols (Mello and Fire, 1995) with either the C27H5 cosmid or a genomic construct con-sisting of the wild-type C27H5.7 gene (i.e., the entire open reading frame of C27H5.7 along with 983 bp of 5″UTR and 60 bp of 3″UTR). Constructs were injected together with plasmid pRF4, containing the dominant marker *rol-6*(*su1006*) (Mello et al., 1991). Transgenic animals were assessed for dye-fill capacity as described above.

***dyf-13* Allele Sequence Determination**

The coding region and intron/exon boundaries of *dyf-13* were amplified by PCR from mutant animals with Amplitaq DNA polymerase (Roche) and appropriate primers. Amplicons were sequenced with an ABI sequencer.

Microscopy

For live imaging, worms were mounted on agarose pads, immobilized with 20 mM sodium azide or 15 mM levamisole, and examined on Axioskop 2+ (Zeiss) or Axioplan II (Zeiss) compound microscopes, or on an Olympus microscope equipped with a 100x, 1.35 NA objective and an Ultraview spinning-disc confocal head at 0.3 s/ frame for 2–3 min. Captured images were analyzed with Northern

Eclipse version 6.0 or Axiovision (Zeiss) software. For production of movies, individual frames were captured at 250 ms intervals, and the resulting stacked TIFF images were converted into .avi movies, with a frame rate of 4 frames/s (i.e., real time). The middle and distal anterograde IFT rates for GFP-tagged C27H5.7a-associated particles were determined along the amphid cilia as described previously (Snow et al., 2004). The retrograde IFT rate for C27H5.7a::GFP was determined along the phasmid ciliary axonemes by measuring the distance traveled by an individual particle over a minimum of three consecutive frames.

Acknowledgments

This work was funded by the Heart and Stroke Foundation of British Columbia and Yukon and the Canadian Institutes for Health Research (CIHR; CBM134736) (M.R.L.), the Patterson Trust and National Institutes of Health Medical Scientist Training Program (MSTP) grant GM07739 (S.S. and E.P.), Genome British Columbia and Genome Canada (D.G.M., D.L.B., M.A.M., and S.J.J.), and the Swedish Foundation for Strategic Research (SSF) (P.S.). M.R.L. acknowledges scholar awards from the CIHR and the Michael Smith Foundation for Health Research (MSFHR). D.L.B. holds a Canada Research Chair. O.E.B. acknowledges fellowships from the CIHR and the MSFHR. The work by G.O. was supported by a grant (NIH GM 50718) to Jonathan M. Scholey. We thank Kenta Asahina for sequencing of the *dyf-13(mn396)* allele. Correspondence relating to *dyf-13(mn396)* (phenotypic characterization and cloning of the mutation) should be addressed to S.S.

References

Ansley, S.J., Badano, J.L., Blacque, O.E., Hill, J., Hoskins, B.E., Leitch, C.C., Kim, J.C., Ross, A.J., Eichers, E.R., Teslovich, T.M., et al. (2003). Basal body dysfunction is a likely cause of pleiotropic Bardet-Biedl syndrome. *Nature 425*, 628–633.

Audic, S., and Claverie, J.M. (1997). The significance of digital gene expression profiles. *Genome Res. 7*, 986–995.

Avidor-Reiss, T., Maer, A.M., Koundakjian, E., Polyanovsky, A., Keil, T., Subramaniam, S. and Zuker, C.S. (2004). Decoding cilia function: Defining specialized genes required for compartmentalized cilia biogenesis, *Cell 117,* 527–539.

Blacque, O.E.,. Reardon, M.J, Li, C., McCarthy, J., Mahjoub, M.R., Ansley, S.J., Badano, J.L., Mah, A.K., Beales, P.L. and Davidson, W.S. *et al.* (2004), Loss of *C. elegans* BBS-7 and BBS-8 protein function results in cilia defects and compromised intraflagellar transport, *Genes Dev. 18,*1630–1642.

Blacque, O.E., Perens, E.A., Boroevich, K.A., Inglis, P.N., Li, C., Warner A., Khattra J., Holt, R.A., Ou, G., Mah, A.K., et al. (2005). Functional genomics of the cilium, a sensory organelle. *Curr Biol. 15*, 935-941

Cole, D.G., Diener, D.R., Himelblau, A.L., Beech, P.L., Fuster, J.C. and Rosenbaum, J.L. (1998). *Chlamydomonas* kinesin-II-dependent intraflagellar transport (IFT): IFT particles contain proteins required for ciliary assembly in *Caenorhabditis elegans* sensory neurons, *J. Cell Biol. 141,* 993–1008.

Collet, J., Spike, C.A., Lundquist, E.A., Shaw, J.E., and Herman, R.K. (1998). Analysis of *osm-6,* a gene that affects sensory cilium structure and sensory neuron function in *Caenorhabditis elegans*. *Genetics 148*, 187–200.

Colosimo, M.E., Brown, A., Mukhopadhyay, S., Gabel, C., Lanjuin, A.E., Samuel, A.D. and Sengupta, P. (2004). Identification of thermosensory and olfactory neuron-specific genes via expression profiling of single neuron types, *Curr. Biol. 14,* 2245–2251.

Eddy, S.R. (1998). Profile hidden Markov models. *Bioinformatics 14*, 755–763.

Fan, Y., Esmail, M.A., Ansley, S.J., Blacque, O.E., Boroevich, K., Ross, A.J., Moore, S.J., Badano, J.L., May-Simera, H. and Compton, D.S. *et al.* (2001). Mutations in a member of the Ras superfamily of small GTP-binding proteins causes Bardet-Biedl syndrome, *Nat. Genet. 36,* 989–993.

Fujiwara, M., Ishihara, T., and Katsura, I. (1999). A novel WD40 protein, CHE-2, acts cell-autonomously in the formation of *C. elegans* sensory cilia. *Development 126*, 4839–4848.

Haycraft, C.J., Schafer, J.C., Zhang, Q., Taulman, P.D., and Yoder, B.K. (2003). Identification of CHE-13, a novel intraflagellar transport protein required for cilia formation. *Exp. Cell Res. 284*, 251–263.

Haycraft, C.J., Swoboda, P., Taulman, P.D., Thomas, J.H., and Yoder, B.K. (2001). The *C. elegans* homolog of the murine cystic kidney disease gene Tg737 functions in a ciliogenic pathway and is disrupted in *osm-5* mutant worms. *Development 128*, 1493–1505.

Hobert, O. (2002). PCR fusion-based approach to create reporter gene constructs for expression analysis in transgenic *C. elegans*. *Biotechniques 32*, 728–730.

Katsanis, N., Lupski, J. R. and Beales, P. L. (2001). Exploring the molecular basis of Bardet-Biedl syndrome, *Hum. Mol. Genet. 10.* 2293–2299.

Kozminski, K.G., Johnson, K.A., Forscher, P. and Rosenbaum, J.L. (1993). A motility in the eukaryotic flagellum unrelated to flagellar beating, *Proc. Natl. Acad. Sci. USA 90,* 5519–5523.

Li, J.B., Gerdes, J.M., Haycraft, C.J., Fan, Y., Teslovich, T.M., May-Simera, H., Li, H., Blacque, O.E., Li, L. and Leitch, C.C. *et al.* (2004). Comparative genomics identifies a flagellar and basal body proteome that includes the BBS5 human disease gene, *Cell 117,* 541–552.

McKay, S.J., Johnsen, R., Khattra, J., Asano, J., Baillie, D.L., Chan, S., Dube, N., Fang, L., Goszczynski, B., Ha, E., *et al*. (2003). Gene expression profiling of cells, tissues, and developmental stages of the nematode *C. elegans*. Cold Spring Harb. Symp. Quant. Biol. *68*, 159–169.

Mello, C., and Fire, A. (1995). DNA transformation. *Methods Cell Biol*. *48*, 451–482.

Mello, C.C., Kramer, J.M., Stinchcomb, D., and Ambros, V. (1991). Efficient gene transfer in *C. elegans*: Extrachromosomal maintenance and integration of transforming sequences. *EMBO J. 10*, 3959–3970.

Orozco, J.T., Wedaman, K.P., Signor, D., Brown, H., Rose, L., and Scholey, J.M. (1999). Movement of motor and cargo along cilia. *Nature 398*, 674.

Ostrowski, L.E., Blackburn, K., Radde, K.M., Moyer, M.B., Schlatzer, D.M., Moseley, A. and Boucher, R.C. (2002). A proteomic analysis of human cilia: Identification of novel components, *Mol. Cell. Proteomics 1,* 451–465.

Otto, E.A., Schermer, B., Obara, T., O'Toole, J.F., Hiller, K.S., Mueller, A.M., Ruf, R.G., Hoefele, J., Beekmann, F. and Landau, D. *et al.* (2003). Mutations in INVS encoding inversin cause nephronophthisis type 2, linking renal cystic disease to the function of primary cilia and left-right axis determination, *Nat. Genet. 34.* 413–420.

Pazour, G. J. and Rosenbaum, J. L. (2002). Intraflagellar transport and cilia-

dependent diseases, *Trends Cell Biol. 12,* 551–555.

Perkins, L.A., Hedgecock, E.M., Thomson, J.N. and Culotti, J.G. (1986). Mutant sensory cilia in the nematode *Caenorhabditis elegans*, *Dev. Biol. 117,* 456–487.

Piperno, G. and Mead, K. (1997). Transport of a novel complex in the cytoplasmic matrix of *Chlamydomonas* flagella, *Proc. Natl. Acad. Sci. USA 94,* 4457–4462.

Qin, H., Rosenbaum, J.L., and Barr, M.M. (2001). An autosomal recessive polycystic kidney disease gene homolog is involvedin intraflagellar transport in *C. elegans* ciliated sensory neurons. *Curr. Biol*. *11*, 457–461.

Rosenbaum, J. L. and Witman, G. B. (2002). Intraflagellar transport, *Nat. Rev. Mol. Cell Biol. 3,* 813–825.

Saha, S., Sparks, A.B., Rago, C., Akmaev, V., Wang, C.J., Vogelstein, B., Kinzler, K.W., and Velculescu, V.E. (2002). Using the transcriptome to annotate the genome. *Nat. Biotechnol*. *20*, 508–512.

Schafer, J.C., Haycraft, C.J., Thomas, J.H., Yoder, B.K., and Swoboda, P. (2003). XBX-1 encodes a dynein light intermediate chain required for retrograde intraflagellar transport and cilia assembly in *Caenorhabditis elegans*. *Mol. Biol. Cell 14*, 2057–2070.

Scholey, J. M., Intraflagellar transport, *Annu. Rev. Cell Dev. Biol.* **19** (2003), pp. 423–443.

Signor, D., Wedaman, K.P., Orozco, J.T., Dwyer, N.D., Bargmann, C.I., Rose, L.S., and Scholey, J.M. (1999). Role of a class DHC1b dynein in retrograde transport of IFT motors and IFT raft particles along cilia, but not dendrites, in chemosensory neurons of living *Caenorhabditis elegans. J. Cell Biol. 147*, 519–530.

Snow, J.J., Ou, G., Gunnarson, A.L., Walker, M.R., Zhou, H.M., Brust-Mascher, I., and Scholey, J.M. (2004). Two anterograde intraflagellar transport motors cooperate to build sensory cilia on *C. elegans* neurons. *Nat. Cell Biol. 6*, 1109–1113.

Starich, T.A., Herman, R.K., Kari, C.K., Yeh, W.H., Schackwitz, W.S., Schuyler, M.W., Collet, J., Thomas, J.H. and Riddle, D.L. (1995). Mutations affecting the chemosensory neurons of *Caenorhabditis elegans*, *Genetics 139,*171–188.

Sulston, J., and Hodgkin, J. (1988). Methods. In The Nematode *Caenorhabditis elegans*, W.B. Wood, ed. (Cold Spring Harbor, NY: Cold Spring Harbor Laboratory Press.), pp. 587–606.

Swoboda, P., Adler, H.T., and Thomas, J.H. (2000). The RFX type transcription factor DAF-19 regulates sensory neuron cilium formation in *C. elegans*. *Mol. Cell 5*, 411–421.

Figure 5.1

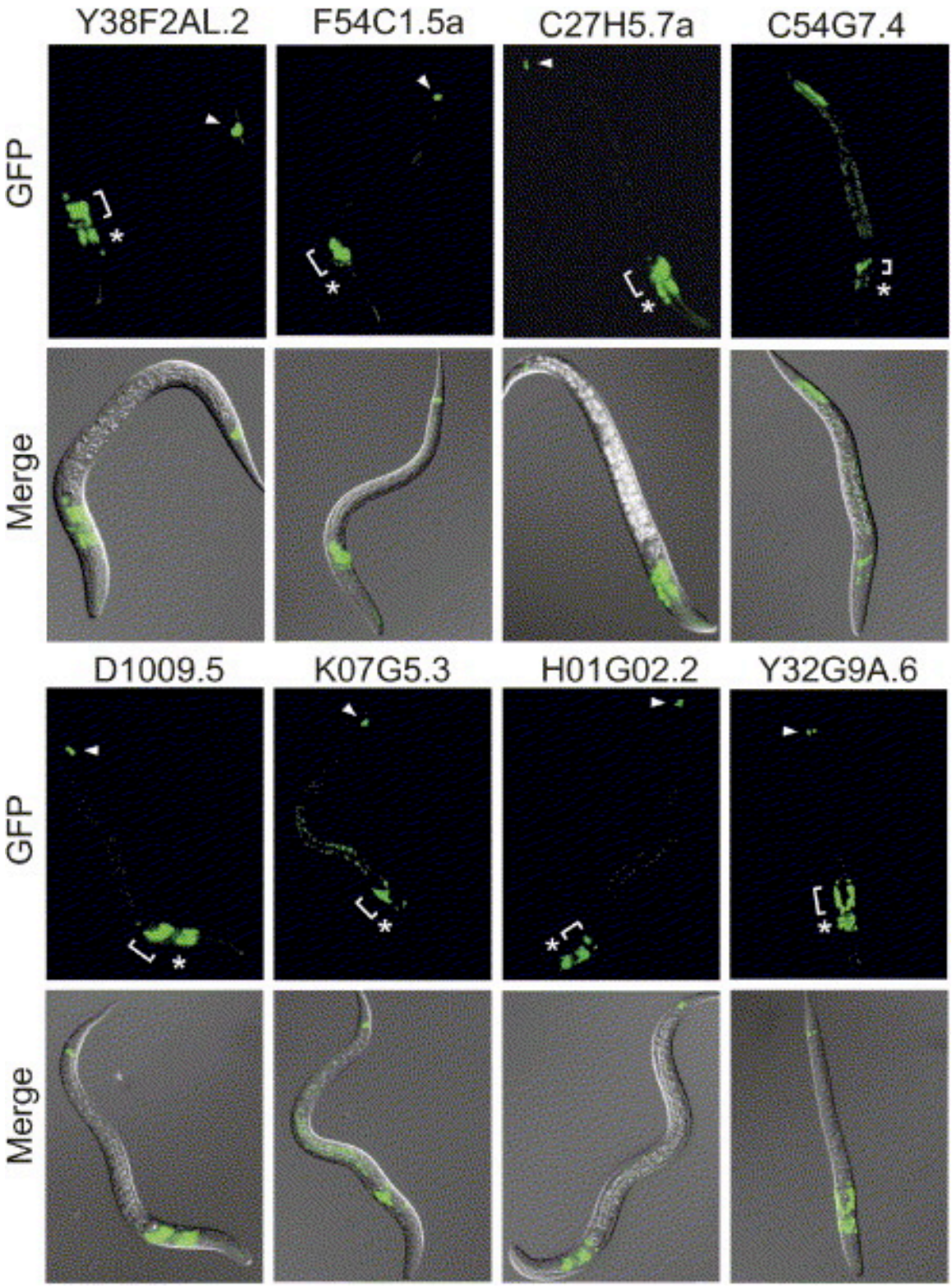
Y38F2AL.2
F54C1.5a
C27H5.7a
C54G7.4
GFP
Merge
D1009.5
K07G5.3
H01G02.2
Y32G9A.6
GFP
Merge

Figure 5.1. Expression Analysis of Candidate Cilia-Related Genes Identifies New Genes Expressed Exclusively in Ciliated Cells

Shown are whole-worm GFP and GFP/DIC merged images of transgenic animals expressing the indicated transcriptional *gfp* reporter. Expression is restricted to ciliated cells such as the amphid neurons (bracket), the labial-quadrant neurons (asterisk), and the phasmid-tail neurons (arrowhead). Note that for some markers (e.g., C54G7.4 and K07G5.3), the weak signals along the midbody are due to the nonspecific autofluorescence of gut granules.

Figure 5.2

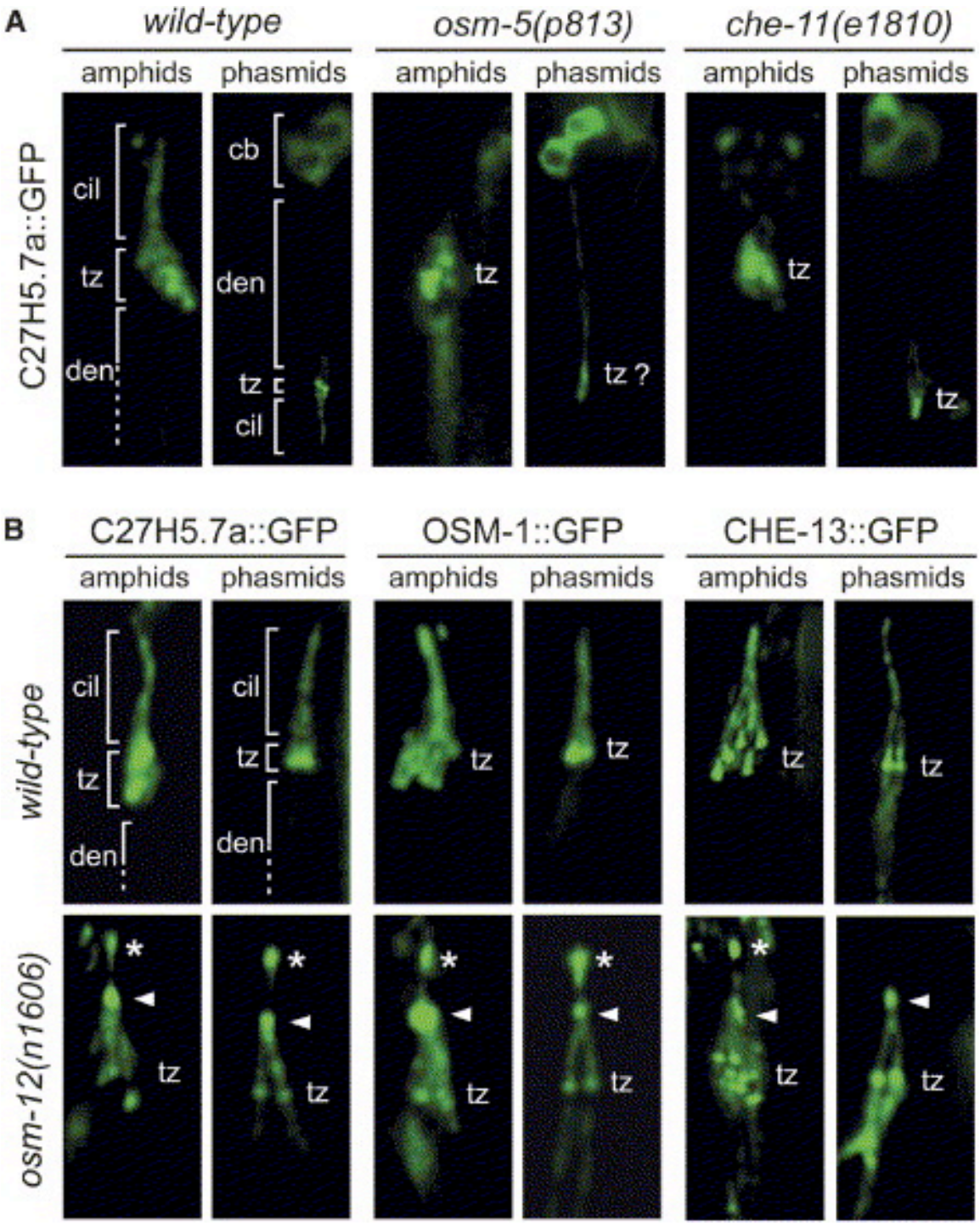
A
wild-type
osm-5(p813)
che-11(e1810)
amphids
phasmids
amphids
phasmids
amphids
phasmids
C27H5.7a::GFP
cil
tz
den
cb
den
tz
cil
tz
tz ?
tz
tz
B
C27H5.7a::GFP
OSM-1::GFP
CHE-13::GFP
amphids
phasmids
amphids
phasmids
amphids
phasmids
wild-type
cil
tz
den
cil
tz
den
tz
tz
tz
tz
osm-12(n1606)
*
tz
*
tz
*
tz
*
tz
*
tz
tz

Figure 5.2. The Ciliary Localization of C27H5.7a Is Disrupted by Mutations in IFT and *bbs* Genes

Shown are one set of amphid and phasmid cilia, with the ciliary axonemes (cil), transition zones (tz), dendrites (den), and cell bodies (cb) indicated in the left-hand panels. All images are similarly sized and oriented, with the tz positions indicated in all panels. (A) Localization of GFP-tagged C27H5.7a in wild-type, *osm-5(p813)*, and *che-11(e1810)* mutant backgrounds. In the wild-type, C27H5.7a::GFP localizes at the transition zones and along ciliary axonemes, whereas in *osm-5(p813)* and *che-11(e1810)* mutants, C27H5.7a::GFP accumulates at transition zones in *osm-5* mutants and along the stunted ciliary axonemes of *che-11* mutants. The question mark indicates that the tz position cannot be accurately identified. (B) C27H5.7a::GFP mislocalizes along *bbs-7* (*osm-12(n1606)*) mutant cilia, displaying accumulation at the midpoint of the ciliary axonemes (arrowhead) and within the distal segment (asterisk). Similar mislocalization along *bbs-7* mutant cilia is also observed for four GFP-tagged IFT proteins, namely OSM-1, CHE-13, OSM-6, and CHE-2 (see Figure S5 for OSM-6::GFP and CHE-2::GFP images).

Figure 5.3

A

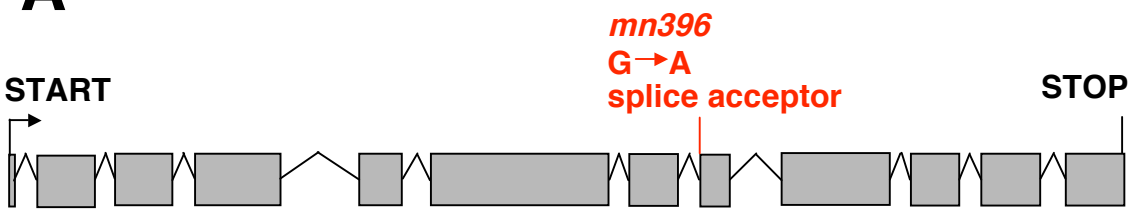

B

***dyf-13* dye-filling defects**

strain	No. dye filled neurons/ phasmid 2	1	0	n	No. dye filled neurons/ amphid 5-6	2-4	0-1	n
wildtype	100%	0%	0%	40	99%	1%	0%	72
dyf-13(*mn396*)	4%	6%	90%	50	18%	61%	21%	92
dyf-13(*mn396*); *Ex[C27H5]*	69%	13%	18%	60	65%	35%	0%	20
dyf-13(*mn396*); *Ex[C27H5.7]*	60%	6%	34%	68	nd	nd	nd	nd

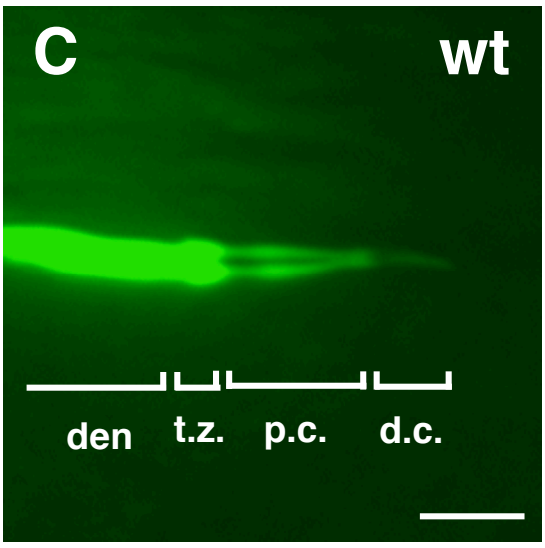

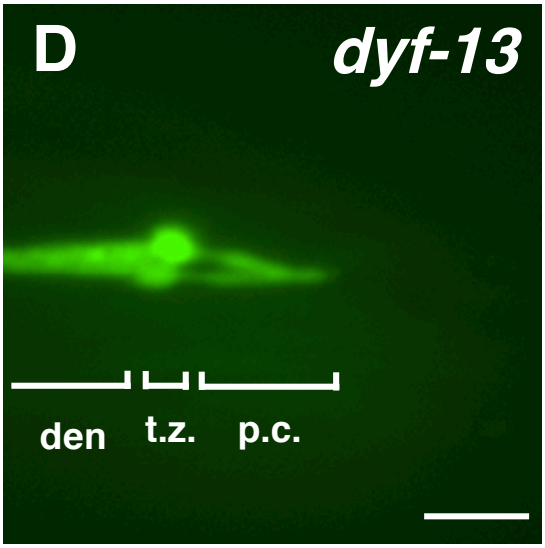

Figure 5.3. Mutation in C27H5.7a Causes the Structural Cilia Defect in *dyf-13(mn396)* Mutants

(A) A schematic of the putative exon/intron structure of C27H5.7a shows the guanine-to-adenine splice acceptor mutation in *dyf-13(mn396)*. (B) The dye-uptake-defective phenotype (Dyf) of *dyf-13(mn396)* mutants is rescued by the C27H5 cosmid and by a transgene containing the wild-type C27H5.7a gene. Shown are the percentages of sensory organs with normal dye-fill in the indicated number of amphid and phasmid neurons. "n" denotes number of sensory organs scored and "nd" denotes not determined. (C and D) The cilia of *dyf-13(mn396)* mutants are short, lacking distal portions. Shown are GFP images of animals expressing a *ceh-23* promoter*::gfp* transgene in the phasmid neurons. Anterior is to the left. Note that the phasmid cilia of *dyf-13* mutants are shorter than those of wild-type animals. The following abbreviations were used: den, dendrite; tz, transition zone; ms, middle segment; and ds, distal segment. The scale bar represents 5 μm.

Table 5.1

Table 1. SAGE and X Box Data Identify a Set of Strong Candidate Cilia-Related Genes

Gene		SAGE Data				Xbox Data			Other Studies				Annotation /
Model	Name	C	P	M	G	Sequence	Pos.	Score	A	B	C	D	Description
Y105E8A.5	*bbs-1*	19	1	0	0	GTTCCCATAGCAAC	98	19.29	✓	✓			BBS1
F59C6.7	*che-13*	26	3	1	1	GTTGCTATAGCAAC	73	17.70	✓	✓	✓		IFT57
C27H5.7a		8	0	0	1	GTCTCCATAGCAAC	102	19.07	✓	✓	✓	✓	Uncharacterized
T06G6.3		7	1	0	0	GTTGCCATGGCAAA	59	16.11					Myosin heavy chain-like
Y38F2AL.2		6	1	0	0	GTTGCCGTGGCAAC	65	16.11	✓	✓			B9 domain containing
R31.3	*osm-6*	6	1	0	0	GTTACCATAGTAAC	99	18.68	✓	✓			IFT52
F32A6.2		5	1	0	0	GTTGCCCTGGTAAC	71	16.85	✓		✓		IFT81
F38G1.1	*che-2*	5	1	1	1	GTTGTCATGGTGAC	129	16.30	✓	✓	✓		IFT80
R13G10.2	*amx-1*	5	1	0	1	GCTACCATGACAAC	144	14.52					Monoamine oxidase
F35D2.4		5	1	0	0	ATCACCATGACAAC	158	12.85					Uncharacterized
M04G12.3	*gcy-34*	4	0	1	0	GTCTTCACAGCAAC	122	11.09		✓			Guanylate cyclase
K10G6.4		4	1	0	0	GTCACCATGCCAAT	139	12.85					Uncharacterized
Y41G9A.1	*osm-5*	8	2	1	0	GTTACTATGGCAAC	114	19.79	✓	✓	✓		IFT88
W02B12.3c	*rsp-1*	7	0	2	1	GTTGTCATGGCTAC	131	15.18					Splicing factor
F33H1.1b	*daf-19*	28	8	6	7	GTTTCCATGGAAAC	108	19.61					RFX transcription factor
F08C6.4	*sto-1*	30	9	8	6	TTTTCCTTGGTAAC	201	12.69					Stomatin
K03E6.4		3	1	0	0	GTTCCCTTGGCAAC	83	17.11	✓				B9 domain containing
F13B9.5	*ksr-1*	3	1	1	0	TTTTTCTTGGCAAC	104	10.65					Kinase regulator of Ras
Y32G9A.6		3	1	0	0	GTTGTCAGGGTAAC	186	13.52					Inversin-like
Y41D4A.4		6	1	0	2	GTTGCCACGTTAAC	140	12.46					EMP70
F32A6.5	*sto-2*	6	1	2	1	GTTTCCTTAAAAAC	181	11.48					Stomatin
F28E10.1c		11	4	0	2	GTCGCCAGAGCAAC	80	13.09					Titin/Connectin
F20D12.3	*bbs-2*	8	3	0	1	GTATCCATGGCAAC	93	20.02	✓				BBS2
ZC84.6		5	2	1	0	GTTTATTTGGTAAC	99	11.11					Serine protease inhibitor
Y37A1A.3		2	0	0	0	GTCAATATGACAAC	178	10.26					Glucose transporter
B0228.5a		2	1	0	1	GTTACCATATCAGC	16	11.18					Thioredoxin
B0432.5a	*cat-2*	2	1	0	0	GTCCCCACGCCAAC	36	10.97		✓			Tyrosine hydroxylase
F56H11.1c	*fbl-1*	2	1	1	0	GTTTCCGTTACAAC	76	10.09		✓			Fibulin
K08D12.2		2	1	0	0	GTTTCCATAGCAAC	83	20.74	✓				Retinitis pigmentosa 2
C27F2.1		2	1	1	0	GTCACCATAGCAAC	83	18.41					Uncharacterized
T27B1.1	*osm-1*	2	0	0	1	GCTACCATGGCAAC	85	17.91	✓	✓	✓		IFT172
C09E10.2b	*dgk-1*	2	1	0	0	GTACTCATGCTAAC	131	10.30					Diacylglycerol kinase
H01G02.2		2	1	1	0	GTCTCCATGACAAC	159	16.96					Serine/Threonine kinase
C26B9.5		2	0	0	1	GTTTGCATAGTCAC	174	10.41					Serine protease
T01D1.6	*abu-11*	2	0	0	0	GTCAACATAACAAC	229	10.56					Keratin associated
K07G5.3		6	3	1	1	GTTGCCATAGCGAC	70	17.30		✓			Uncharacterized
K06H7.3		6	3	1	1	TTTTCCATAATAAC	238	11.48					Ankyrin repeat protein
R166.3		6	3	2	3	ATCTCCTTGGCAAC	248	13.43					AMME Syndrome 1
R11A8.2		7	4	0	0	GTTTCCATATTAAT	225	11.48					G patch and KOW motifs
ZK1151.1c	*vab-10*	7	4	1	0	GTTTTTATGGCAAA	235	12.52					MACF1
R01H10.6	*bbs-5*	19	11	2	3	GTCTCCATGGCAAC	64	20.35	✓	✓			BBS5
T24D1.1b	*sqv-5*	5	3	0	0	GTTCCTTCGGCAAC	33	11.00					Chodroitin synthase 2
F59D12.1		3	2	1	0	ATTACCATAGTTAC	170	12.92					Transmembrane protein
C02H7.1		3	2	0	0	GTCTCCATGACAAC	194	16.96	✓	✓			Uncharacterized
D1009.5		6	4	2	2	GTTGCCATGACAAC	76	17.18	✓	✓			Dynein light chain
C48B6.8		6	4	2	0	GTTTCCATGACAAC	80	18.63					B1 protein
F08B12.1		13	1	1	1								Prominin 1
ZK520.1		8	2	1	2				✓	✓			WD-repeat domain 19
C54G7.4		4	4	0	0	GTTGCCATGGCAAT	172	17.11	✓	✓			WD-repeat protein 35
F54C1.5a		3	3	1	2	GTTACCATGGATAT	105	15.50	✓	✓			TPR repeat containing
ZK328.7a		1	1	1	0	GTTACCATGGCAAT	88	17.91	✓				TPR repeat containing
F19H8.3		1	6	2	1	GTCTCTATGGTAAC	150	17.35		✓			ARL3
C47E8.6		0	0	0	0	GTTACCATGCCAAC	108	17.98					Uncharacterized

Shown are all genes (46 in total) that are enriched for SAGE tags in the ciliated-cell transcriptome (C), with ≥1.5-fold enrichment versus the pan-neural transcriptome (P) and ≥2.0-fold enrichment versus the muscle (M) and gut (G) transcriptomes, *and* with a canonically-positioned
(Pos) putative X box (i.e., within 250 bp of the start codon). Only genes with homology to a human gene (Blast E-value < e^{-10}) are represented.
Genes are sorted according to the level of SAGE tag enrichment in the ciliated-cell transcriptome versus the other three transcriptomes. The seven candidate cilia-related genes at the bottom of the table are included on the basis of their high ranking in the individual SAGE *or* X box
tables (Tables S1 and S4, respectively). Check marks indicate genes identified as candidate ciliary genes in three previous genomics and proteomics studies, namely (A) Li et al., (B) Avidor-Reiss et al., and (C) Ostrowski et al., or as a sensory-neuron-type-specific gene ([D] Colosimo et al.).